LBL-30795

Center for Advanced Materials

CAM

Surface Science Studies of Catalyzed Methanol Synthesis on Model Copper and Cu-Zn-O Surfaces

S.S.-B. Fu
(Ph.D. Thesis)

June 1991

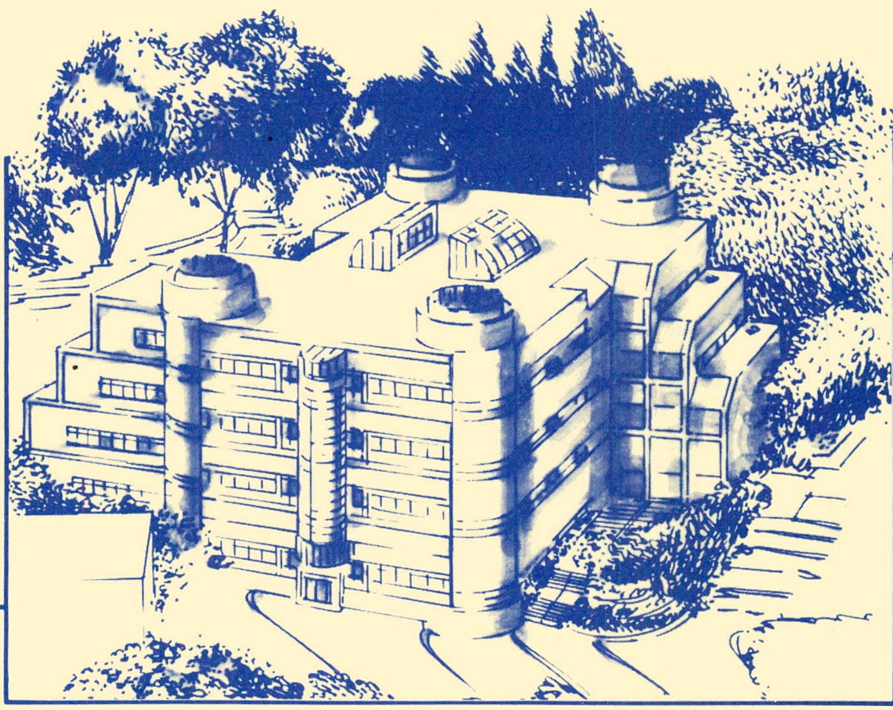

Materials and Chemical Sciences Division

Lawrence Berkeley Laboratory • University of California

ONE CYCLOTRON ROAD, BERKELEY, CA 94720 • (415) 486-4755

Prepared for the U.S. Department of Energy under Contract DE-AC03-76SF00098

LBL--30795
DE91 016425

Surface Science Studies of Catalyzed Methanol Synthesis on Model Copper and Cu-Zn-O Surfaces

Sabrina Su-Bin Fu

Ph.D. Thesis

Department of Chemistry
University of California

and

Materials Sciences Division
Lawrence Berkeley Laboratory
University of California
Berkeley, CA 94720

June 1991

This work was supported by the Director, Office of Energy Research, Office of Basic Energy Sciences, Materials Sciences Division, of the U.S. Department of Energy under Contract No. DE-AC03-76SF00098.

Surface Science Studies of Catalyzed Methanol Synthesis on Model Copper and Cu-Zn-O Surfaces

by

Sabrina Su-Bin Fu

Abstract

Cu-Zn-O surfaces that are catalysts for methanol synthesis from CO, CO_2, and H_2 are modeled using zinc oxide overlayers on copper single crystals. These studies were performed in ultra-high vacuum (UHV) utilizing Temperature Programmed Desorption, Auger Electron Spectroscopy, and Low Energy Electron Diffraction techniques.

The chemisorption of O_2, CO, CO_2, and D_2 were compared on a stepped Cu(311), and a flat Cu(110). At low pressures ($\sim 10^{-6}$ Torr), Cu(311) was found to be much more reactive than Cu(110) for the dissociative adsorption of CO_2 and D_2, and the formation of CO_2 from surface oxygen and CO. Since these reactions are important in methanol synthesis, these results suggest that methanol synthesis over copper may be a structure sensitive reaction.

The interaction of copper, zinc, and oxygen were examined by the deposition of submonolayers to multilayers of zinc and oxygen in UHV on Cu(110). Carbon monoxide adsorbs well on copper at 150 K and low pressures ($<10^{-6}$ Torr), but only poorly on the oxides of copper and zinc. Carbon dioxide adsorbs on ZnO at 150 K and low pressures ($<10^{-6}$ Torr), but not on copper or oxidized copper. We used a combination of CO and CO_2 adsorption to follow the initial growth of two-dimensional ZnO_x islands and the effects of heat and oxygen treatments on these islands. Heating above 300 K leads irreversibly to three-dimensional island

formation. In addition, the behavior of ZnO_x overlayers on Cu(311) and a high defect concentration Cu(111) were compared to ZnO_x overlayers on Cu(110).

The interaction of methanol with these model Cu-Zn-O surfaces was also studied. Oxygen was adsorbed onto the exposed copper part of the surface to form ZnO_x/y ML O/Cu(110) surfaces. The rôles of ZnO_x islands and chemisorbed oxygen on copper were investigated by monitoring methanol decomposition, into surface formate and methoxy species, on these ZnO_x/y ML O/Cu(110) surfaces. The rôle of chemisorbed oxygen on Cu(110) in the ZnO_x/y ML O/Cu(110) system is to keep the zinc oxidized and to increase the amount of formate formed on the ZnO_x component of the surface. The presence of ZnO_x increases the surface formate to methoxy ratio from that of O/Cu(110).

Acknowledgements

I would like to thank my advisor, Gabor Somorjai, for his patience and support during my time at Berkeley. Also, I would like to thank Miquel Salmeron for always making time to answer my questions. I don't think I will ever be able to thank him enough for his kindness and support.

My experiments could not have existed without the always friendly cooperation of the technical staff at Lawrence Berkeley Laboratory. Bob Wright and Dan Colomb always managed to understand what I wanted built or fixed and always found time for it. Jim Severns understood what research meant to me and was always there for moral support as well as fixing electronics that no one else could. My thanks to Sandy Stewart and Dana Pope for understanding what the various purchases mean to me and for always doing their best to get what I need when I need it.

I must thank Thomas Rucker and Daniel Strongin for introducing me to surface science and catalysis, and I thank José Carrazza for encouragement to a first year who really needed it. I will always be grateful for the support and friendship of Colette Knight, Michael Quinlan, Robert Hwang, Gerard Vurens, Roger Nix, and Marie-Paule Delplancke. They bring a smile to my face and are a pleasure to discuss science with. Special thanks to Colette Knight for listening to both my ideas and complaints about society and science, and for the many stimulating discussions. Thanks to Michael Quinlan for proof-reading this thesis and for answering my many questions.

Finally, I would like to thank my family, without whom none of this would have been possible. Thanks to my parents, sister, brother, and grandmother for their understanding and support. Special thanks to Philip who has patiently brought out the better part of me for the past three years. He understood when experiments took longer than expected and I came home very tired and very late. He encouraged and helped me through each part of graduate school, including the writing of this thesis. Thank you, Philip, for believing in me, even in the darkest of moments. It is to you, Philip James Rous, and to my parents, Stephen Shin and Siok Hoon Fu,

that this thesis is dedicated to.

This work was supported by the Director, Office of Energy Research, Office of Basic Energy Sciences, Materials Sciences Division, of the U.S. Department of Energy under Contract No. DE-AC03-76SF00098.

To Philip:

You have shown me love

Beyond all that I have imagined

and

To my parents:

When I behold the sacred *liao wo** my thoughts return
To those who begot me, raised me, and now are tired.
I would repay the bounty they have given me,
But it is as the sky: it can never be approached.

From Huston Smith's *The Religions of Man*

* A species of grass symbolizing parenthood

Contents

List of Figures

Chapter 1

Introduction

Catalyzed methanol synthesis is performed predominantly over Cu-Zn-O catalysts from CO, CO_2, and H_2. The production of methanol from CO, CO_2, and H_2 is defined by the following three reactions:

$$CO + 2H_2 \leftrightarrow CH_3OH \qquad \Delta G^o_{500K} = 19 \text{ kJ/mole} \tag{1.1}$$

$$CO_2 + 3H_2 \leftrightarrow CH_3OH + H_2O \qquad \Delta G^o_{500K} = 40 \text{ kJ/mole} \tag{1.2}$$

$$CO + H_2O \leftrightarrow CO_2 + H_2 \qquad \Delta G^o_{500K} = \text{-}20 \text{ kJ/mole} \tag{1.3}$$

Only two of these pathways are independent. Methanol may be produced from both CO_2 and H_2 or from CO and H_2, with the water-gas shift reaction ($CO + H_2O \leftrightarrow CO_2 + H_2$) controlling the availability of each route. Hence, it is important to understand the water-gas-shift reaction in studying methanol synthesis from CO, CO_2, and H_2. We will see in chapter 3 that the water-gas shift can be observed on Cu(311) surfaces in vacuum, but not on Cu(110) surfaces.

Of the three reactions written above, the water-gas shift reaction is the most thermodynamically favorable at 500 K. Because of thermodynamic constraints, high pressure is used for methanol synthesis in order to obtain reasonable amounts of product. Above 500 K, methanol synthesis is even less thermodynamically favorable due to a negative ΔS. Hence, it is desirable to perform methanol synthesis at low temperatures. To date, Cu-Zn-O based catalysts have been found to be the lowest temperature methanol synthesis catalysts with high activity and selectivity. Typically, these catalysts work at temperatures of 500-570 K at a $CO:CO_2:H_2$ ratio of 1:1:8, adding to a total pressure of 40-100 atm.

In their simplest form, industrial Cu-Zn-O based catalysts are produced from a mixture of copper, zinc, and aluminium nitrates by coprecipitation with sodium carbonate followed by filtration, washing, drying, and calcination of the purified precipitate. This produces a catalyst containing many different surface species with a surface area of approximately 30 m^2/g.

Numerous attempts have been made to characterize these catalysts. Some of the major findings are:

1. Cu^+ species in ZnO interstitial sites are the active centers for methanol synthesis. Methanol is made from CO and H_2, with CO_2 needed to stabilize Cu^+ centers in the ZnO lattice [1,2].

2. The more active catalysts have 30-60% of their copper surface area covered with oxygen after methanol synthesis reaction [3,4].

3. There is a direct correlation between the $\frac{CO_2}{CO}$ feed ratio and the amount of chemisorbed oxygen on the copper component after reaction [5].

4. The specific activity of Cu/ZnO catalysts are at least 10^3 times greater than unsupported copper [6].

5. There is no correlation between copper surface area and methanol synthesis activity among various copper/metal oxide catalysts, and Cu-Zn-O catalysts have higher activity per copper surface area than copper catalysts supported on other oxides [7,8]. This suggests that there is a synergistic behavior between the copper and the zinc oxide.

6. Chinchen and co-workers found comparable activity per unit copper surface area for unsupported copper and copper supported on various oxides [5,9].

Pan and co-workers found a direct correlation between copper surface area and methanol synthesis rate for Cu/ZnO catalysts [10].

7. Formate is the intermediate for methanol synthesis from CO_2 and H_2 [4].

8. Isotope labelling of the carbon in CO_2 shows CO_2 as the carbon source for methanol [11,12].

These conflicting results in the literature may be due to different catalyst preparations. All of the various catalyst preparations produce high surface area catalysts containing a wide variety of active sites. In order to reduce the number of surface species, several investigators have modeled Cu-Zn-O synthesis catalysts using single crystal materials. Work on ZnO single crystals has shown that methanol decomposition is a structure sensitive reaction on ZnO [13], and by the principle of micro-reversibility, methanol synthesis is therefore structure sensitive on ZnO. Relevant reactions over various copper single crystals have been examined, but of particular interest are studies demonstrating the effect of oxygen upon methanol decomposition over Cu(110). Wachs and Madix have found that, for a given methanol exposure, surface formate and methoxy production is maximized when 0.2-0.3 monolayers (ML) of oxygen is chemisorbed on Cu(110) [14]. We will see in chapter 5 how this effect changes upon adding ZnO_x islands to Cu(110) and oxygen covered Cu(110) surfaces.

In addition, a few three-component systems have been examined. Campbell and co-workers [15] have characterized the growth of copper deposited on ZnO(000$\bar{1}$) by X-ray photoelectron spectroscopy (XPS), ion scattering spectroscopy (ISS), and low energy electron diffraction (LEED). By decomposing a droplet of ZnO-saturated water solution, these same researchers formed ZnO_x on Cu(111) which they analyzed by XPS before performing catalytic studies. Chan and Griffin [16] examined the decomposition of methanol over copper deposited on oriented ZnO thin films, and found the properties of Cu/ZnO to be primarily a superposition of the separate copper and zinc oxide components. Didziulis and co-workers [17] performed a detailed surface science study of copper overlayers on ZnO(0001), (000$\bar{1}$), and (10$\bar{1}$0).

Heating in UHV resulted in loss of copper XPS intensity which they interpreted as being due to three-dimensional clustering of the copper. They also found that copper deposited on Zn^{2+} terminated ZnO(0001) surfaces is most easily oxidized.

Although a number of studies have been done on modelling Cu-Zn-O catalysts, no one has examined the interaction of submonolayers to multilayers of zinc with oxygen on copper single crystals. In this thesis, I have used copper single crystals and ZnO_x overlayers on copper single crystals to model Cu-Zn-O methanol synthesis catalysts.

We will see in chapter 3 that Cu(311) surfaces are much more reactive than Cu(110) surfaces to the dissociative adsorption of CO_2 and D_2, to the formation of CO_2 from CO plus surface oxygen, and to the water-gas shift reaction. In chapter 4, we will see how zinc oxide overlayers on Cu(110) can be formed and characterized by a combination of CO and CO_2 temperature programmed desorption (TPD), Auger electron spectroscopy (AES), and low energy electron diffraction (LEED). In chapter 5, we will compare the formation and decomposition of ZnO_x islands on Cu(311), Cu(110), and a high defect concentration Cu(111). And finally, in chapter 6, we will use the most well-characterized of these surfaces – ZnO_x on Cu(110) – as a model catalyst to examine the rôles of zinc oxide and chemisorbed oxygen on copper for methanol synthesis.

References

1. R.G. Herman, K. Klier, G.W. Simmons, B.P. Finn, and J.B. Bulko, J. Catal. 56 (1979) 407.

2. K. Klier, V. Chatikavanij, R.G. Herman, and G.W. Simmons, J. Catal. 74 (1982) 343.

3. B. Denise, R.P.A. Sneeden, and O. Cherifi, Applied Catal. 30 (1987) 353.

4. M. Bowker, R.A. Hadden, H. Houghton, J.N.K. Hyland, and K.C. Waugh, J. Catal. 109 (1988) 263.

5. G.C. Chinchen, M.S. Spencer, K.C. Waugh, and D.A. Whan, J. Chem. Soc. Faraday Trans. I 83 (1987) 2193.

6. K. Klier, Adv. Catal. 31 (1982) 243.

7. G.J.J. Bartley and R. Burch, Appl. Catal. 43 (1988) 141.

8. R. Burch and R.J. Chappell, Appl. Catal. 45 (1988) 131.

9. G.C. Chinchen, K.C. Waugh, and D.A. Whan, Appl. Catal. 25 (1986) 101.

10. W.X. Pan, R. Cao, D.L. Roberts, and G.L. Griffin, J. Catal. 114 (1988) 440.

11. G.C. Chinchen, P.J. Denny, D.G. Parker, M.S. Spencer, and D.A. Whan, Appl. Catal. 30 (1987) 333.

12. Y.B. Kagan, L.G. Liberov, E.V. Slivinskii, S.M. Loktev, G.I. Lin, A.Y. Rozoskii, and A.N. Bashkirov, Dokl. Akad. Nauk. SSSR 221 (1975) 1093.

13. W.H. Cheng, S. Akhter, and H.H. Kung, J. Catal. 82 (1983) 341.

14. I. Wachs and R. Madix, J. Catal. 53 (1978) 208.

15. C.T. Campbell, R.A. Daube, and J.M. White, Surface Sci. 182 (1987) 458.

16. L. Chan and G.L. Griffin, Surface Sci. 173 (1986) 160.

17. S.V. Didziulis, K.D. Butcher, S.L. Cohen, and E.I. Solomon, J. Am. Chem. Soc. 111 (1989) 7110.

Chapter 2

Experimental Techniques and Apparatus

2.1 Surface Analysis Techniques

Overview

Many surface analysis techniques have been developed over the past 25 years. A summary of these techniques, classified according to the nature of the probe and the mode of detection is shown in table 2.1. Many of these experimental methods, including the techniques used in this thesis (Auger Electron Spectroscopy and Low Energy Electron Diffraction), involve the detection of electrons in the energy range of 20-1000 eV. This range of energies is selected for surface studies because the mean-free path of the electron is then only a few interatomic spacings (see figure 2.1). Thus, surface sensitivity is maximized.

In order to perform well controlled studies of any surface phenomenon, one must begin with well characterized surfaces. Hence, the use of single crystal substrates for the work described in this thesis. In addition, the environment in which the surface is studied must not change the nature of the surface during the course of the experiment. At an ambient pressure of 10^{-6} Torr, each second, a monolayer of unwanted material can form on the surface by adsorption of background gases (assuming a sticking probability of unity). Hence, all the experiments described in this thesis where performed under ultra-high vacuum (UHV) conditions; an ambient pressure of less than 10^{-9} Torr. In this well controlled environment, a surface can

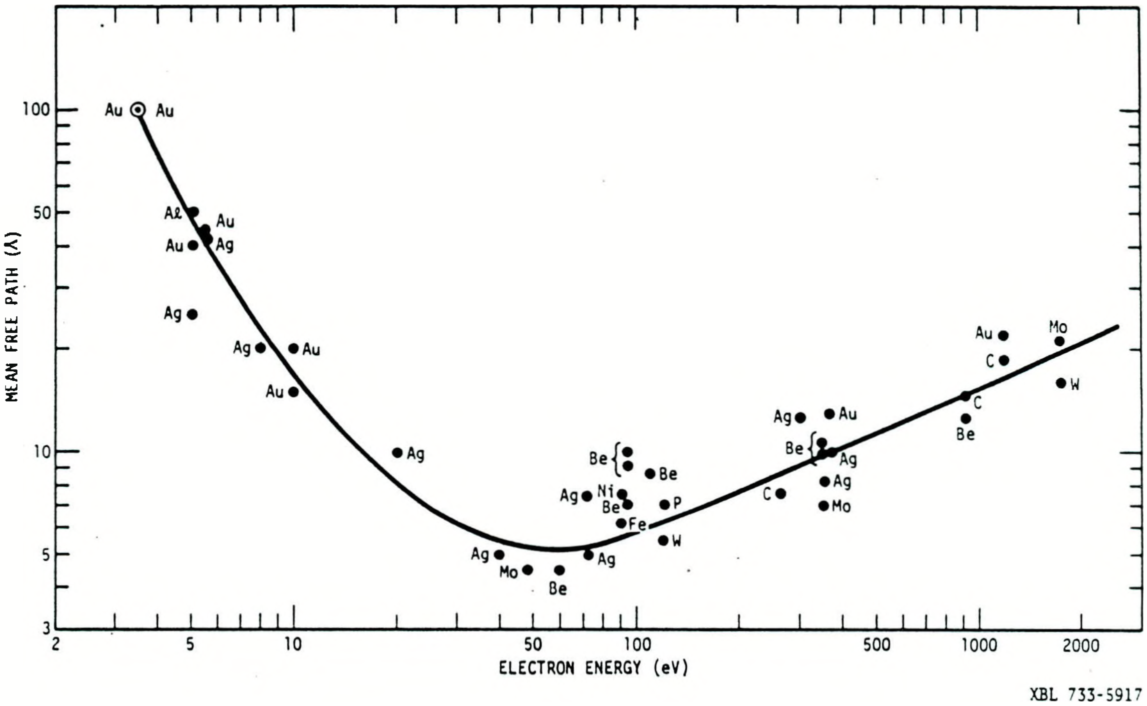

Figure 2.1: The mean free path of electrons as a function of their kinetic energy.

Table 2.1: Surface Analysis Techniques

Technique	Probe Particle	Detected Particle	Information Obtained
Ultra-Violet Photoemission Spectroscopy (UPS)	electrons	electrons	valence band structure of first few atomic layers
X-Ray Photoemission Spectroscopy (XPS)	photons	electrons	oxidation state of top $\approx 20 \AA$
Photoemission of Adsorbed Xenon (PAX)	electrons or photons	electrons	local work function
Inverse Photoemission (IPES)	electrons	photons	unoccupied electronic states
Work Function	electrons	electrons	work function
Surface-Sensitive Extended X-Ray Adsorption Fine Structure (SEXAFS)	photons	electrons	local geometry of adsorbates
Reflection High Energy Electron Diffraction (RHEED)	electrons	electrons	surface morphology
Medium Energy Electron Diffraction (MEED)	electrons	electrons	structure of top 10-20$\AA$
Low Energy Electron Diffraction (LEED)	electrons	electrons	structure of top 5-10$\AA$
High, Medium, and Low Energy Ion Scattering (HEIS), (MEIS), and (LEIS)	ions	ions	structure of top few layers
Ion Scattering Spectroscopy (ISS)	ions	ions	composition of top-most layer
Surface Penning Ionization (SPI)	metastable helium	electrons	electronic structure
High-Resolution Electron Energy Loss Spectroscopy (HREELS)			vibrational modes
Transmission Electron Microscopy (TEM)	electrons	electrons	structure of ultra-thin films
Scanning Electron Microscopy (SEM)	electrons	electrons	surface topography
Scanning Tunneling Microscopy (STM)	electrons	electrons	local electronic structure & morphology
Atomic Force Microscopy (AFM)	sensitive to forces in the 1nm range		
Field-Ion Microscopy (FIM)	ions	ions	surface structure of top-most layer
Auger Electron Spectroscopy (AES)	electrons, photons, or atoms	electrons	composition of top 5-20$\AA$
Secondary-Ion Mass Spectroscopy (SIMS)	ions	clusters	chemical state & composition of first few atomic layers
Temperature Programmed Desorption (TPD)	molecules or atoms	molecules or atoms	binding energy, composition, and reactivity of top-most layer

be characterized without appreciable changes in surface composition during the course of the experiment.

The following sections will summarize the three surface analysis techniques employed in the experiments described in this thesis. These techniques are: Auger Electron Spectroscopy (AES), Temperature Programmed Desorption (TPD), and Low Energy Electron Diffraction (LEED). For a more comprehensive description of each of these techniques, the reader is referred to [1] for AES, [2-5] for TPD, and [6,7] for LEED.

Auger Electron Spectroscopy (AES)

Fundamentals

Auger electron spectroscopy is one of the most widely used methods of surface analysis. In this technique, the surface is excited by impact with electrons, photons, or atoms which have sufficiently high energies to eject core level electrons from atoms within the surface. The Auger process begins when the core hole is filled by the de-excitation of a valence electron; the excess energy being transferred to a second electron which is emitted from the surface. It is this electron, the Auger electron, which is detected. The kinetic energy of the Auger electron is characteristic of the element from which it was ejected because the energy of the Auger electron is dependent only upon the relative energy levels of the hole and the two electrons. Hence, when an electron in energy level E_{v1} is de-excited to fill the core-hole in energy level E_c, an electron from energy level E_{v2} is ejected with kinetic energy E_c-E_{v1}-E_{v2}. The Auger process is shown schematically in figure 2.2A.

Auger electrons have kinetic energies in the range of 20-1000 eV. Due to the limited mean free path of electrons in this energy range within solids (see figure 2.1), only those Auger electrons ejected from the first 15 monolayers or less are detected.

In addition to providing the elemental composition of the near-surface region, AES can also be used to distinguish the local electronic states, if the resolution of the analyzer is sufficient. In this thesis work, the simplest of Auger electronics was used in which the energy of the electrons is selected with a retarding field. However, the reader is referred to reference [1] for a discussion of more complete AES analyses which can be performed with more sophisticated energy analyzers.

Technique

To obtain the AES spectra shown in this thesis, the surface atoms were ionized using a 2.0 KeV electron beam incident at about 70^o from the surface normal. The energies of the emitted Auger electrons were determined using a four-grid LEED optics as a retarding field analyzer [8]. The AES spectra were recorded in the derivative mode by modulating the retarding field voltage on the 2^{nd} and 3^{rd} LEED grids at 10 eV and 5000 Hz. The second harmonic of the modulated signal was detected with an Ortec Brookdeal precision lock-in amplifier. A schematic illustration of the AES experimental set-up is shown in figure 2.2B.

AES spectra may be plotted simply as intensity of the detected Auger electrons versus energy. But often, AES spectra are plotted as the derivative of the intensity with respect to the energy (dN/dE) versus energy, especially when a retarding field energy analyzer is used. By differentiating the AES peaks, it is easier to distinguish between the small Auger peaks from the rising background of secondary electrons in the low energy region. This approach also increases the signal to noise ratio, especially needed in the high energy region. Therefore, all AES spectra shown in this thesis were obtained in the derivative mode. Needham, Driscoll, and Rao [9] have shown that if the Auger peaks in the intensity (N) vs. kinetic energy plot are Gaussian, then the peak-to-peak height in the dN/dE vs. kinetic energy plot is proportional to coverage. Thus, AES peak ratios were used to determine ZnO_x coverage, after having used CO_2 TPD to determine the monolayer point of ZnO_x.

A typical Auger spectrum for clean Cu(110) and 2.0 ML ZnO_x on Cu(110) are shown in figure 2.3A and 2.3B. Copper and zinc both have Auger peaks at around 60 eV, 100 eV, and the 700-900 eV region. Because zinc and copper differ in atomic number only by one, they have many of their Auger peaks overlapping.

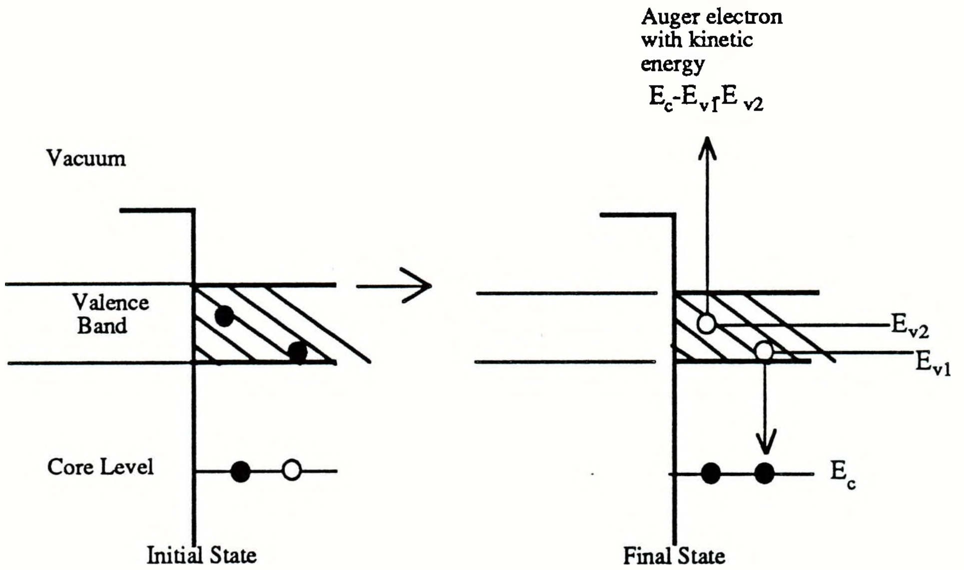

Figure 2.2A: Schematic of the Auger process.

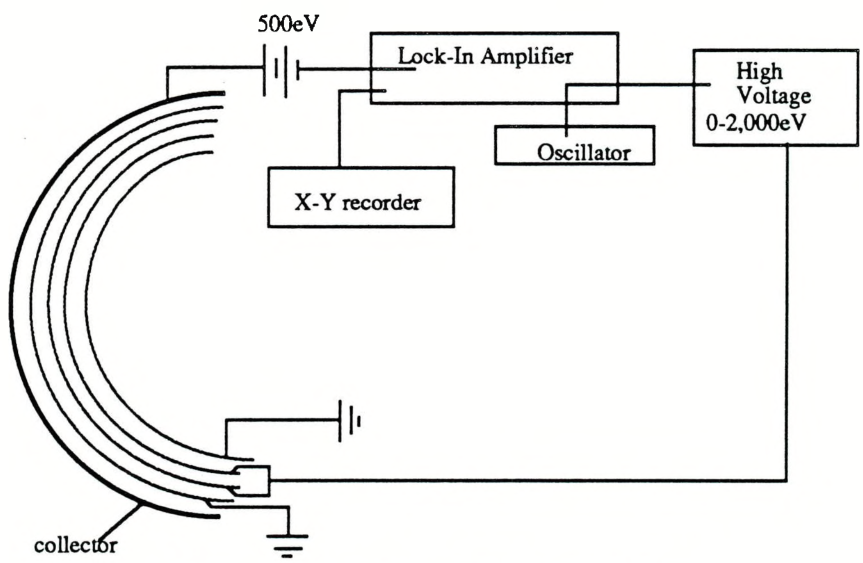

Figure 2.2B: Schematic of Auger experimental set-up.

Figure 2.2: (A) The Auger process. A valence electron, from energy level E_{v1}, is de-excited to fill a core-hole in energy level E_c, with the energy from the de-excitation used to eject an electron from energy level E_{v2}. This ejected electron leaves the surface with kinetic energy E_c-E_{v1}-E_{v2}. (B) A schematic of the Auger experimental set-up using a retarding field analyzer.

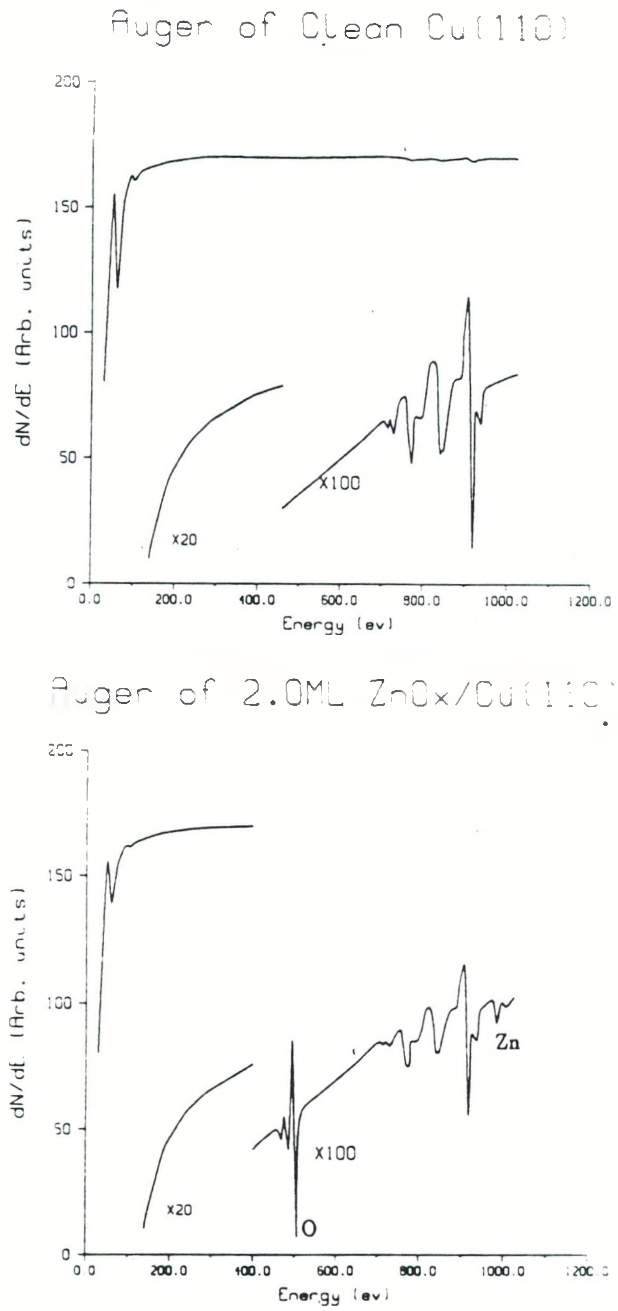

Figure 2.3: (A) Auger spectrum of clean Cu(110) and (B) 2.0 ML ZnO_x on Cu(110).

The only non-overlapping peaks have energies >900 eV, and those are the least surface sensitive of the possible AES peaks. Thus, in order to determine the surface composition of the Cu-Zn-O systems studied in this thesis, it was crucial to employ a more surface sensitive probe in tandem with AES. That probe was temperature programmed desorption (TPD), and will be discussed in the next section.

Calibrations

The AES spectra obtained during the course of the experiments described in this thesis were compared to the standard spectra of elements in reference [10] in order to determine the elements present in the near surface region. In the case of Auger emission from atomic overlayers, an estimate of the coverage can be obtained from the Auger peak heights once sensitivity factors and probabilities for transitions are taken into account. However, to obtain a quantitative measure of the coverage, calibrations need to be made. A LEED pattern corresponding to a well-ordered p(2×1) surface structure was used to define 0.5 ML coverage of oxygen on Cu(110), as this surface structure is associated with half monolayer of oxygen on Cu(110) [11]. The resulting $\frac{O}{Cu}$ AES ratio was then used to define 0.5 ML oxygen on Cu(111) and Cu(311).

To obtain quantitative coverages of ZnO_x, CO_2 titration was used to determine the monolayer point on Cu(110), and related to AES peak ratios. These calibrated AES peak ratios of zinc, oxygen, and copper for ZnO_x/Cu(110) were then used for ZnO_x overlayers on Cu(311) and Cu(111).

Temperature Programmed Desorption (TPD)

Fundamentals

In a temperature programmed desorption (TPD) or thermal desorption spectroscopy (TDS) experiment, the surface is held at a well defined temperature and exposed to a controlled amount of gas. After adsorption and/or reaction of the gas with the surface, the temperature of the surface is increased, causing desorption of molecules from the surface. These molecules are detected with the mass spectrometer, which is held in front of the sample monitoring a single or several $\frac{m}{e}$ ratios.

As adsorption on clean metal surfaces is generally a non-activated process, the desorption activation energy is approximately equal to the differential heat of adsorption. Hence, TPD is one of the simplest experimental methods available for obtaining a measure of the bond energy in adsorption. The relation between bond energy and the temperature of desorption depends upon three factors; the heating rate, the pre-exponential factor, and the desorption order.

The rate of desorption from a unit surface area may be written as

$$N(t) = -\frac{d\sigma}{dt} = \nu_n \sigma^n exp(-E/RT) \tag{2.1}$$

where

n is the order of the desorption reaction,

σ is the surface coverage in molecules/cm^2,

ν=the rate constant for the particular desorption process,

and E the activation energy of desorption.

If we assume E is independent of σ and use a linear change of sample temperature ($T=T_o+\beta t$), where β is the heating rate, then we can solve equation (2.1) for various desorption orders:

$$ln(\frac{d\sigma_p}{dT_p}) = ln(\frac{\nu\sigma_o}{\beta}) - \frac{E}{RT_p} \qquad \text{(zero order desorption)} \tag{2.2}$$

$$ln(\frac{E}{RT_p}) = ln(\frac{c\nu}{2\beta})\sqrt{\sigma_o} + ln(\frac{T_p}{\sqrt{\sigma_p}}) - \frac{E}{RT_p} \qquad \text{(half order desorption)} \tag{2.3}$$

$$\frac{E}{RT_p^2} = (\frac{\nu}{\beta})exp(\frac{-E}{RT_p}) \qquad \text{(first order desorption)} \tag{2.4}$$

$$\frac{E}{RT_p^2} = (\frac{\sigma_o\nu}{\beta})exp(\frac{-E}{RT_p}) \qquad \text{(second order desorption)} \tag{2.5}$$

where

T_p=the temperature at peak rate of desorption,

σ_p is the coverage at the temperature of peak desorption,

σ_o is the initial coverage,

and c is a constant.

The desorption order can be determined by fitting the observed desorption spectra to the equations for zero, half, first, and second order desorption. Once the order is known, the binding energy can be determined. For example, if we plot $\frac{1}{T_p}$ vs $\ln(\frac{d\sigma_p}{dT_p})$ and obtain a straight line, the desorption is zero-order with the slope of the line equal to $\frac{-E}{R}$. We will see an example of this in chapter 4.

In addition to determining coverage and bond energies, TPD can also be used to determine the reactivity of the surface. For example, by exposing oxygen covered copper surfaces to a known amount of CO, we can determine if the reaction $CO+O_{(surface)} \rightarrow CO_2$ can occur on copper surfaces under our experimental conditions by monitoring for CO_2 with the mass spectrometer. The reactivity of surface oxygen can be confirmed by AES (and for certain surfaces, by LEED) after TPD experiments. Hence, by a combination of TPD, LEED, and AES, we can determine the reactivity and changes which occur on the surface under various conditions, as we have a mass balance of what has left the surface and what remains behind.

This thesis uses TPD to determine the reactivity of the surface, the surface bond energies, and the coverage of the surface. More detailed information on the kinetics and interaction of surface species can be obtained from TPD, as described in references [2] through [5].

Techniques

In order to minimize the background contribution to the measured TPD spectra from molecules desorbed from the manipulator parts, the 0.8 cm^2 sample was placed 2 mm in front of the 1 cm^2 mass spectrometer orifice. The mass spectrometer had a

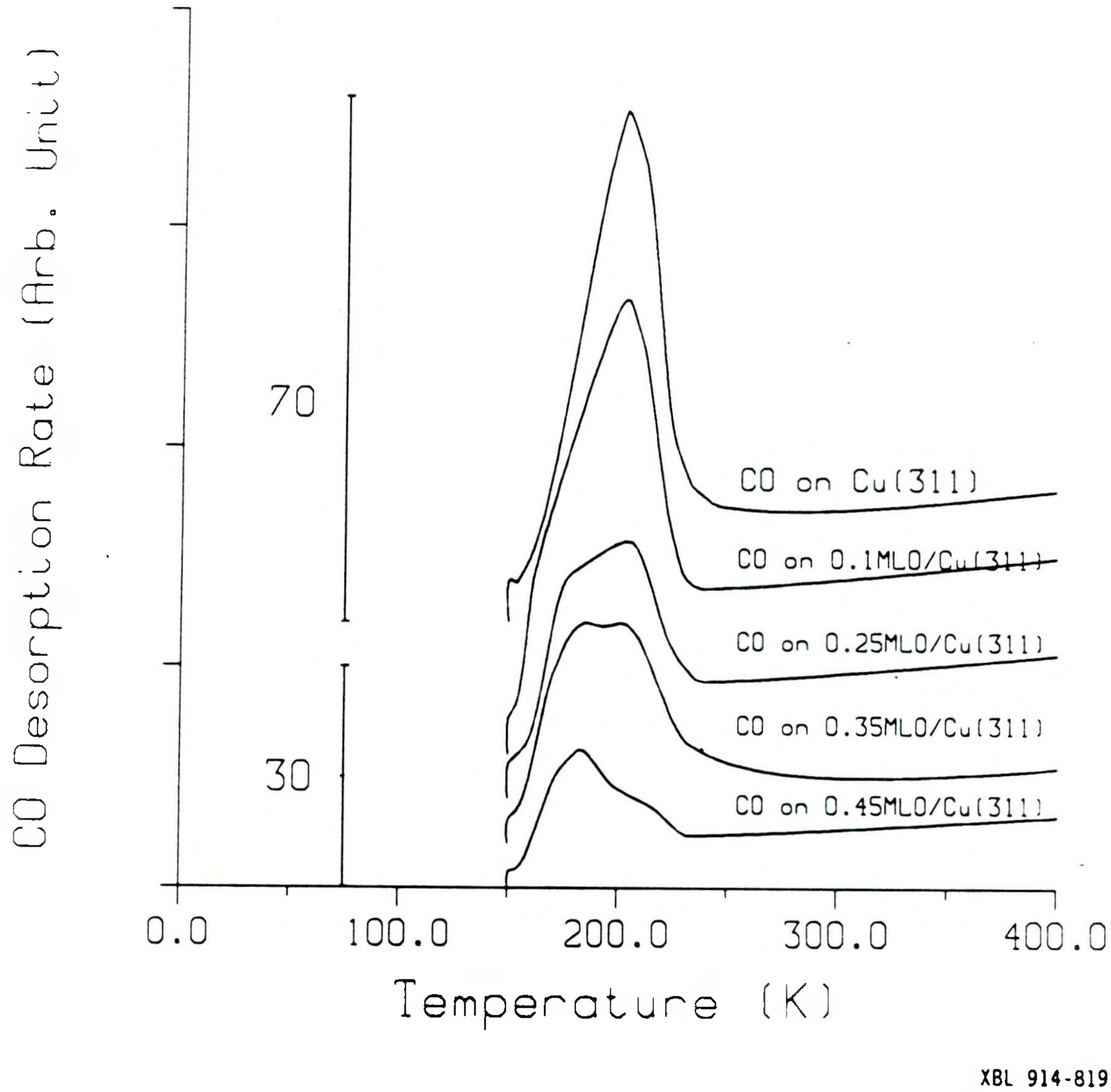

Figure 2.4: CO desorption from Cu(311) surfaces covered with various amounts of oxygen. Each surface was exposed to enough CO (20 L) to produce saturation coverages. As in all TPD spectra presented in this thesis, each TPD curve is offset for better viewing.

stainless steel shield surrounding this orifice, which shielded the spectrometer from molecules desorbed from the manipulator parts.

For the TPD experiments described in this thesis, all gases were dosed with the sample in front of the mass spectrometer, and the exposures reported were not corrected for ion gauge sensitivities. After the desired gas exposure, Cu(110) and Cu(111) crystals were heated at a linear rate of 30 K/s and Cu(311) was heated at 10 K/s. All of the TPD spectra shown in this thesis have been referenced to a common scale (in arbitrary units), with the multiplication factor given either on the graph or in the figure caption. When no multiplication factors are reported, the scale is that of the reference scale.

An illustration of some TPD spectra are shown in figure 2.4. From this plot of temperature versus CO desorption rate for various oxygen coverages on Cu(311), one can see that oxygen blocks the CO adsorption site whose desorption peak is centered at 203 K. In addition, information such as activation energy of desorption and surface coverage can be obtained from such plots, as was discussed above.

Calibrations

The mass spectrometer's sensitivity was monitored prior to each day of TPD experiments by measuring the intensity of the $\frac{m}{e}$=28 peak when 1×10^{-8} Torr of CO was admitted into the UHV chamber. This signal fluctuated as much as 50% over the two year period during which the experiments described in this thesis were performed. Quantitative comparisons of the amount of desorbed gases were made only after accounting for the changes for mass spectrometer sensitivity.

As was mentioned earlier, one advantage that TPD has over AES is its superior surface sensitivity. Since most molecules and atoms are adsorbed directly upon the surface and usually cannot penetrate the top-most atomic layer, TPD is inherently more surface sensitive than AES. Furthermore, it has been shown that if the pumping speed is fast enough (so that readsorption is negligible), the mass spectrometer signal is proportional to ambient pressure [2], and hence to the surface coverage prior to desorption. Thus, once a calibration is made to relate the number of molecules to a particular area under TPD spectra (with known mass spectrometer conditions), the number of molecules desorbed can be determined. For the work described in this thesis, this calibration was done by determining the area under the CO desorption peak obtained from a CO overlayer on Cu(110), which, prior to desorption displayed a p(2×1) surface structure. Since this surface structure is associated with a 0.5ML coverage of CO on Cu(110) [12], the mass spectrometer could be calibrated by assuming that the area under the CO desorption peak corresponded to 4.4×10^{14} molecules of CO; half of the number of copper surface atoms on the 0.8 cm^2 Cu(110) crystal. To obtain the number of CO_2 molecules per unit area, the relative mass spectrometer sensitivity for CO and CO_2 was determined using equal fluxes of both gases. The relative sensitivity of the mass spectrometer varied from 1.0 to 1.5 over the two year period of these experiments, and the variations have been accounted for in each set of experiments when the area under CO_2 TPD spectra was converted to molecules of CO_2.

Low Energy Electron Diffraction (LEED)

In low energy electron diffraction (LEED), electrons with kinetic energies between 20 to 300 eV are directed at a surface and the diffracted electrons observed with a fluorescent screen. A schematic diagram of a LEED experiment is shown in figure 2.5. Diffraction occurs because of the wave-like nature of electrons as postulated by deBroglie [13]. Electrons with kinetic energy E have a deBroglie wavelength: $\lambda(\AA) = \frac{h}{p} = \sqrt{\frac{150.4}{E(eV)}}$. Thus electrons with kinetic energies of 20 to 300 eV have wavelengths of 1-3 $\AA$; a value which is comparable to interatomic distances within solids. Therefore electron diffraction is anticipated. If the atoms are in an ordered array, such as in a crystalline solid, then constructive interference implies that the electrons are reflected from the surface within discreet Bragg beams, which, when observed on a fluorescent screen, appear as diffraction spots. The diffraction patterns for Cu(110), Cu(311), and Cu(111) are shown in figure 2.6, along with their real space lattice. These diffraction patterns are reciprocal space mappings of the real space lattice parallel to the surface. Hence, LEED can be used

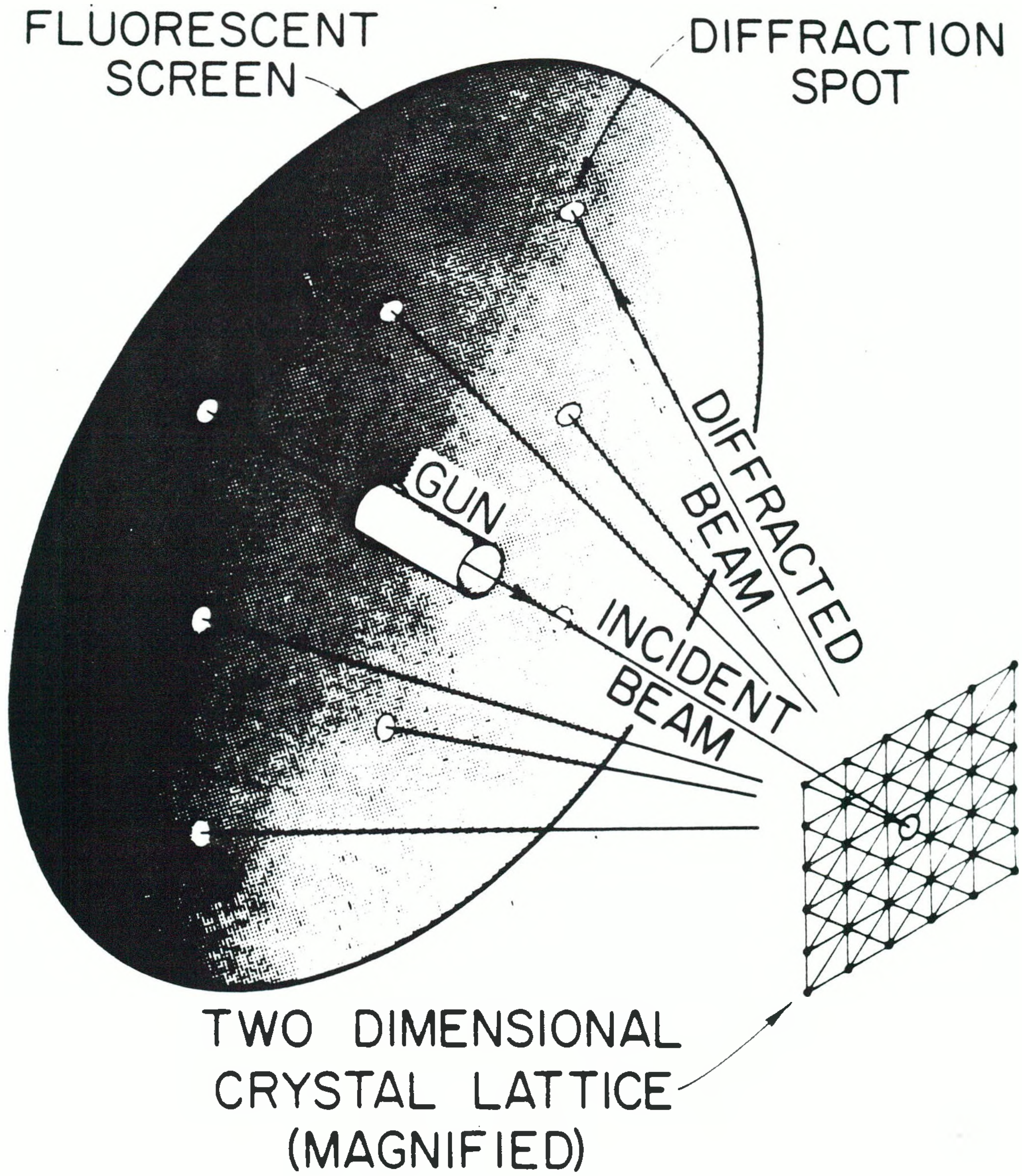

Figure 2.5: Schematic diagram of a low energy electron diffraction (LEED) experiment from an idealized two-dimensional crystal lattice.

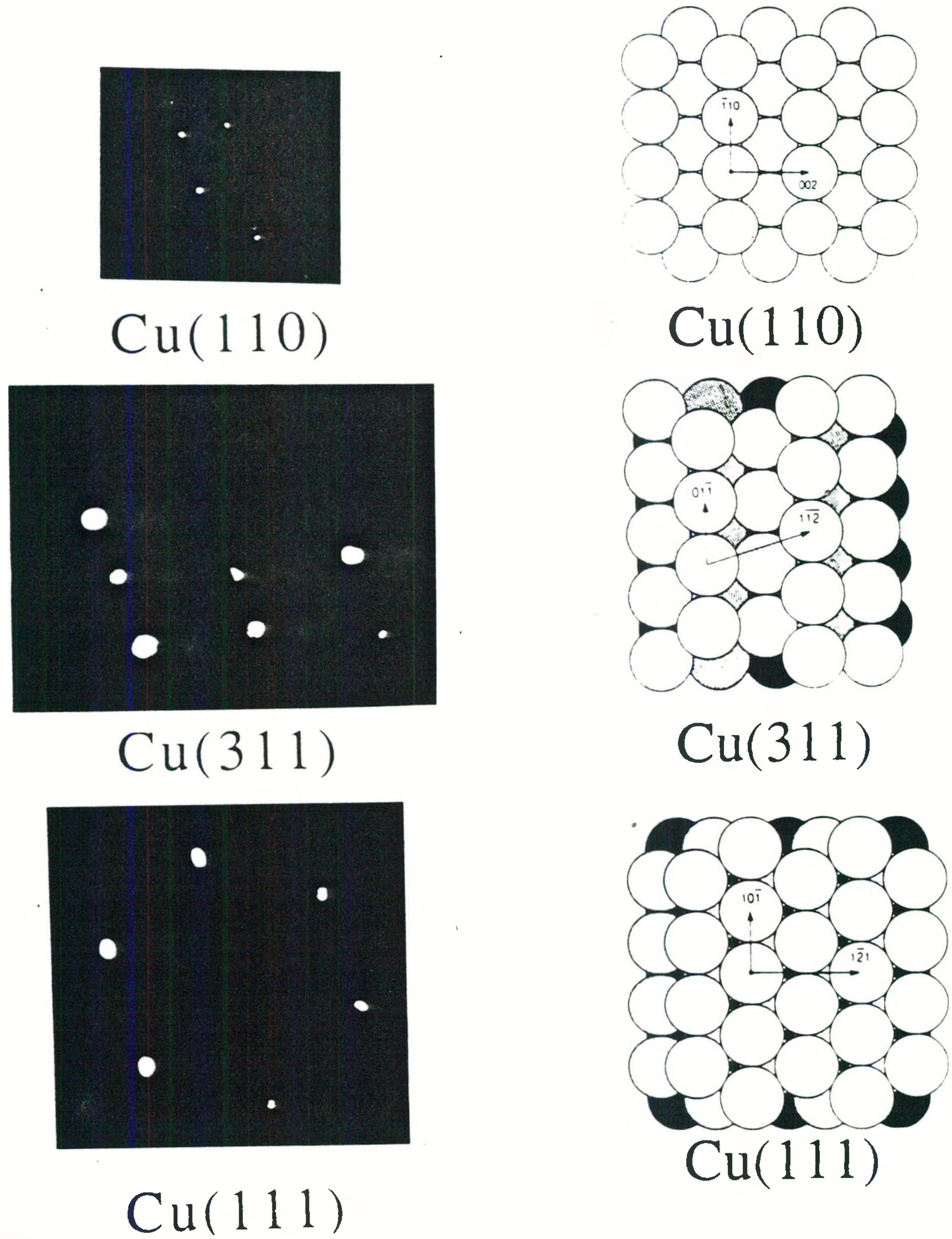

Figure 2.6: LEED patterns of Cu(110) (at 151 eV), Cu(311) (at 100 eV), and Cu(111) (at 118 eV) used in this thesis, along with their idealized real space schematics.

to characterize the long range order of the surface. This is predominantly the mode in which LEED has been used in this work.

If an ordered overlayer is deposited onto the single crystal, the LEED diffraction pattern of the new unit cell, in reciprocal space, can be seen on the fluorescent screen. The 2D lattice formed by the overlayer atoms and molecules is superimposed on the substrate unit cell in reciprocal space. These patterns reveal the shape, and size of the overlayer unit cells with respect to the reference cell. However, the diffraction pattern cannot be used to determine the nature of the atoms/molecules within the surface unit cell; in particular, the adsorption site or number of molecules contained within the overlayer unit cell are usually inaccessible from the LEED pattern alone.

Much more complete structural information can be obtained from LEED by analysis of spot intensities as a function of energy; so called IV spectra. These IV spectra can be interpreted within the framework of multiple scattering theory to determine bond lengths and angles in the near-surface region, both parallel and perpendicular to the surface. For further details of the use of LEED as a complete structural tool, the reader is referred to [6,7]. Although no such analysis was performed in the work described in this thesis, we have compared IV spectra to determine if two different surfaces which produce the same diffraction pattern have the same surface structure. We employed LEED in this "fingerprint" mode to determine if the ordered (1×1) pattern is due to the ZnO_x overlayer or the copper substrate.

2.2 Apparatus

The experiments described in this thesis were performed in a stainless-steel ultrahigh vacuum (UHV) chamber operating at a base pressure less than 2×10^{-10} Torr, pumped with a Varian ion pump at 500 liters/sec. The residual background gases consisted of water, carbon monoxide, methane, helium, hydrogen, and argon, (usually in that order of abundance) adding to a total pressure of 2×10^{-10} Torr or less.

The chamber was equipped with the following:

- An off-axis Varian manipulator
- A retarding field analyzer (RFA) for low-energy electron diffraction (LEED) and Auger electron spectroscopy (AES)
- A glancing incidence electron gun for AES mounted 70° from surface normal
- A normal incidence electron gun for LEED
- An ion gun for argon sputtering
- A zinc source for zinc deposition
- Leak valves
- A UTI-100C quadrupole mass spectrometer for residual gas analysis and temperature programmed desorption (TPD)
- A Pfeiffer TSU 170 turbomolecular pump (50 liters/sec) with roughening pump DUO 1.5A, used during argon sputtering
- A pumping well consisting of a Varian ion pump and titanium sublimation pump

A schematic diagram of the chamber is shown in figure 2.7.

Everything mounted on the UHV chamber was obtained commercially except the zinc source which was designed specifically for the experiments described in this thesis. The zinc source consisted of 99.999% pure zinc wires (Aldrich) enclosed in a ceramic effusive source, built by Robert Wright of the LBL technical staff. This effusive source was mounted in a stainless steel casing equipped with bellows and a shutter. In addition, the zinc source was equipped with water cooling capabilities and chromel-alumel thermocouples to monitor the temperature of the zinc. A schematic diagram of the zinc source is shown in figure 2.8.

The zinc source requires three hours to equilibrate as indicated by a plateau in the temperature versus time and zinc signal (as measured by the mass spectrometer) versus time graphs. Typically, a current of 3.9 amps is used to heat the zinc. With this current, the thermocouples glued to the back of the inner ceramic indicate 110°C. This produces a monolayer of zinc oxide every 120 seconds when dosed in an ambient of $\geq 1\times10^{-7}$ Torr O_2.

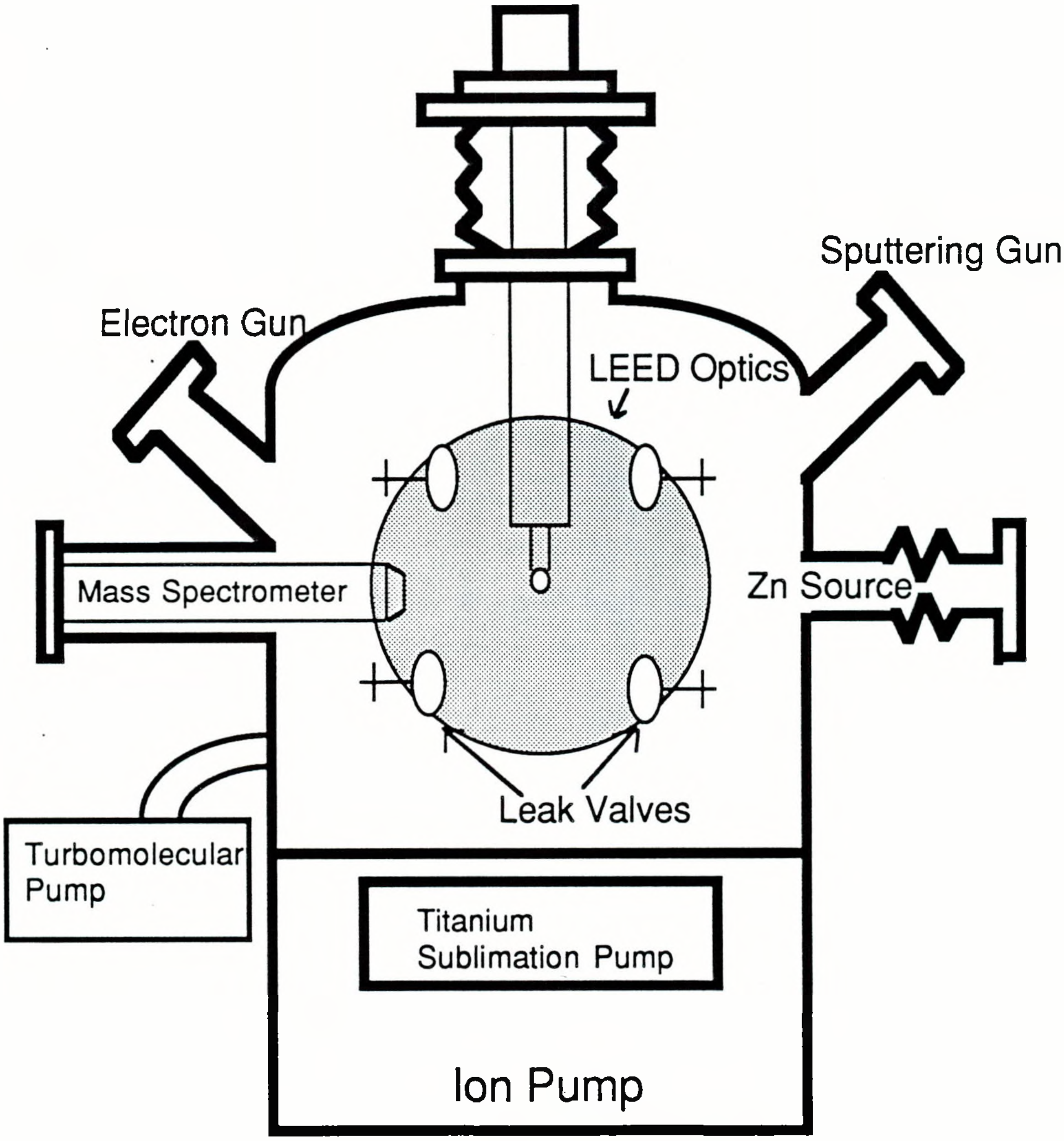

Figure 2.7: Schematic of the surface analysis chamber used for this thesis.

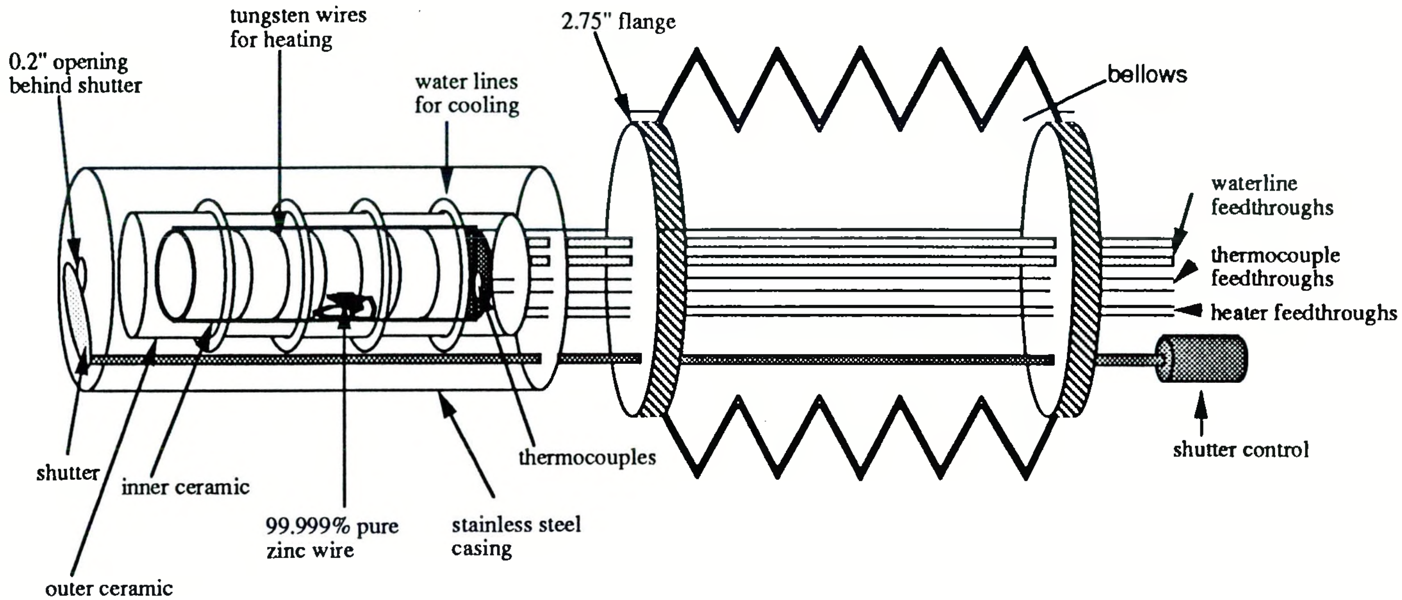

Figure 2.8: Diagram of the zinc source.

2.3 Experimental Procedure

Preparation of Single Crystals

The single crystals used for the experiments described in this thesis were obtained from three different sources:

1. One of the Cu(110) crystals was cut by Wini Heppler of the LBL technical staff.

2. Two of the Cu(110) crystals used were purchased from a commercial source (Monocrystals).

3. The Cu(311) and Cu(111) single crystals were obtained from the Université Libre de Bruxelles, Chimie Analytique, through Marie-Paule Delplancke.

All the crystals were 99.999% pure, and cut using standard metallurgical techniques. Four 21 mil (one thousandth of an inch) holes at the edge and one 10 mil hole on the bottom of the 0.8 cm^2 disks were spark-eroded (see sample mounting section). The single crystals were then polished, beginning with 20 micron Al_2O_3, and finishing mechanically with 0.3 micron α-alumina. The copper single crystals were then electropolished in a phosphoric acid bath by the application of a $^{+}1.8$ eV potential between the crystal and the cathode. After electropolishing, the crystal was rinsed with 10% phosphoric acid in water solution, followed by high purity ethanol and acetone rinses, ending by drying with a heat gun. One must be careful to wash off all the phosphoric acid before placing the single crystal in vacuum. Sonicating the copper single crystal in ethanol destroys its surface order. Hence, careful washing in ethanol and acetone with a squirt bottle was used.

Once the copper single crystals were electropolished, they were mounted using 20 mil platinum wires, and 5 mil chromel-alumel thermocouples were attached to the 10 mil hole on the bottom of the crystal. This produced even heating in UHV as seen by a uniform glow across the crystal when it was heated to 790 K and above.

The copper single crystals were cleaned in UHV by argon bombardment in 5×10^{-5} Torr of argon with an ion gun voltage of 500 eV and emission current of 20 mA. This produced a current of 10 μA between the crystal and the ground. The different single crystals contained various amounts of impurities, which segregated to the surface upon heating due to their endothermic heats of segregation. The main contaminants were carbon and sulfur, and the extent of sputtering needed to remove all bulk impurities from the crystal varied from 5 hours to 50 hours, depending on the source of the crystal. The temperature was cycled from 300 K to 910 K during sputtering. The crystals were then annealed in vacuum. The final annealing conditions for Cu(111) and Cu(110) crystals were 910 K for 15 minutes, and for the Cu(311) crystals, at 770 K for 60 minutes.

Sample Mounting and Manipulator

Each copper single crystal was mounted onto the manipulator by spark eroding four 21 mil holes at the edge of the crystal and one 10 mil hole on the bottom of the crystal before polishing. After mechanical and electropolishing the crystal, 20 mil platinum wires were physically attached to the copper through the holes as shown in figure 2.9. The 20 mil platinum supports are attached by screws onto copper blocks, which then are accessible to liquid nitrogen cooling and resistive heating through copper braids attached to the copper blocks of the cold fingers. The 10 mil hole on the bottom is used to attach the thermocouples to the copper crystal. The mounting of the crystal to the manipulator is also shown in figure 2.9. With this set-up, the temperature of the crystal could be brought down to 150 K routinely. For the experiments using a Cu(111) substrate, thicker copper braids were installed between the cold fingers and the copper blocks which enabled us to achieve a sample temperature of 130 K routinely.

Reagents

The reagents used in this thesis are given in table 2.2. All gases except the ^{18}O enriched isotopes were obtained from metal gas cylinders. The ^{18}O enriched gases were obtained in break-seal glass flasks which were fitted with o-ring-sealed, teflon stopcocks. Cajon ultra-torr fittings were used for glass to metal connection to the

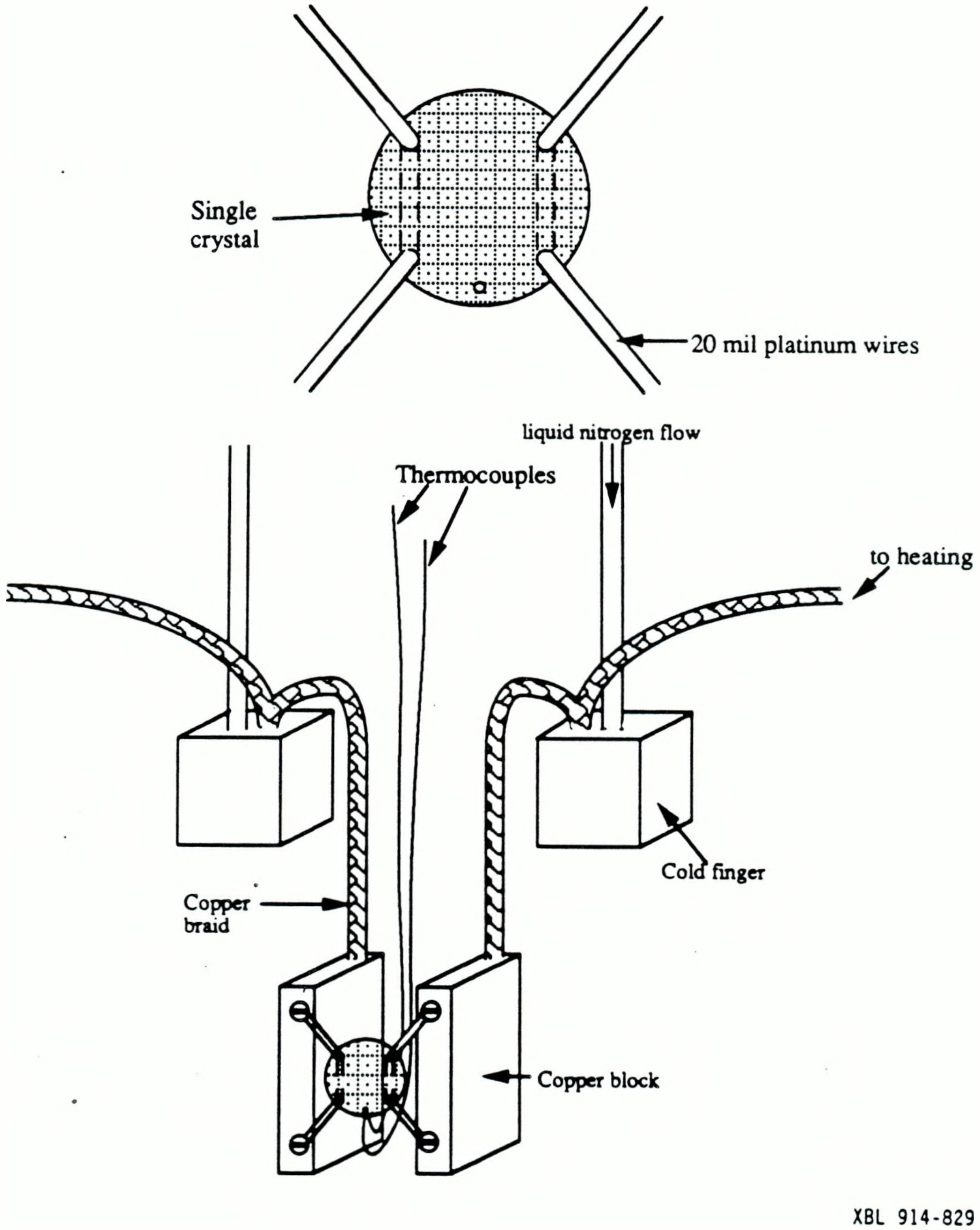

Figure 2.9: Sample mounting and manipulator.

Table 2.2: Reagents

Reagents	Source	Purity	Contaminants
zinc	Aldrich	99.999%	—
CO_2	Matheson	99.99%	—
CO	Matheson	99.5%	—
O_2	Matheson	99.99%	—
D_2	Matheson	99.5%	—
$C^{18}O_2$	Cambridge Isotopes	99% ^{18}O enriched	$C^{16}O_2$
$^{18}O_2$	Cambridge Isotopes	50% ^{18}O enriched	$^{16}O_2$
CH_3OH	Aldrich	99.9%	—

stainless steel gas manifold.

All reagents were used as received except for methanol. The methanol was stored in a glass vial fitted with a teflon stopcock, and was taken through several freeze-pump-thaw cycles before use to remove gases trapped within the vial.

Gas Dosing

The manifold was pumped with sorption pumps to less than 10^{-3} Torr, and flushed several times with the gas to be used to avoid contaminants. Gases were admitted to the chamber through four variable leak valves, and gas purity was checked by mass spectroscopy before and after each set of experiments.

All gas exposures are reported in Langmuirs (L), 1.0 L being an exposure of 1×10^{-6} Torr gas for one second. The reported exposures are not corrected for different ion gauge sensitivities of the gases. However, the ion gauge sensitivity was taken into account when the relative sensitivity of the mass spectrometer to CO and CO_2 was determined.

General Experimental Procedure

A typical experimental procedure was as follows: Once the copper crystal was cleaned and sample cleanness is checked by AES and its structure by LEED, various overlayers were deposited and characterized by AES and LEED. The sample was then cooled to 150 K (or 130 K for Cu(111)), positioned 2 mm in front of the mass spectrometer, dosed with a known amount of gas, and then the sample temperature was ramped linearly at 30 K/sec (or 10 K/sec for the Cu(311) crystals) with the mass spectrometer tuned to a particular mass. AES spectra were obtained between TPD experiments to correlate surface composition to the CO and CO_2 TPD spectra. For the methanol decomposition studies, methanol TPD experiments began after characterizing each surface by AES, LEED, CO and CO_2 TPD, with further characterization between methanol TPD experiments. After examining each Cu-Zn-O sample by various surface analysis techniques, the crystal temperature was ramped to ~1100 K while monitoring zinc, oxygen, copper, or carbon dioxide to further characterize these surfaces.

For TPD of CO, CO_2, H_2, D_2, $^{18}O_2$, $H_2^{18}O$, CH_2O, and H_2O, the respective parent $\frac{m}{e}$ fragment was followed. For O_2, the parent fragment of $\frac{m}{e}$=32 was used except in the presence of zinc, as the signal from Zn^{2+} interferes with the O_2 parent signal. Thus, when zinc was also present, $\frac{m}{e}$=16 was used to monitor O_2 signal. The $\frac{m}{e}$ ratio of 63 (Cu^+) was used to follow copper, and the $\frac{m}{e}$ ratio of 64 (Zn^+) was used to follow zinc. For CH_3OH, $\frac{m}{e}$=31 (CH_3O^-) was followed as it is 50% greater in signal than $\frac{m}{e}$=32.

Chemisorption studies on pure Zn were performed by depositing multilayers of the pure metal onto Cu(110). The term multilayers used throughout this thesis means that enough material was deposited so that the substrate AES peaks could not be detected. Chemisorption studies on submonolayers to multilayers of ZnO_y deposited on gold foils were performed to discern the relative rôle of copper compared to that of a more inert metal.

To determine the chemisorption properties of oxidized copper, a Cu_xO surface was prepared by oxidizing a copper foil in 190 mTorr of O_2 at 470 K for 30 minutes. This Cu_xO surface appears to be mainly Cu_2O as shown by the lack of satellite peaks in the copper 2p XPS spectrum (analysis done by air transfer to a PHI 5300 system).

The contribution from background desorption (from the Pt supports, etc.) of CO, Zn, and CO_2 was examined using a gold foil. For CO TPD using 2.0 L CO exposure, no contribution from background desorption was found. For Zn TPD, up to 2.0 ML zinc produced no contribution from the background. For CO_2 TPD using 4.0 L CO_2 exposure, the background contributed ~1% of the CO_2 TPD signal obtained from a freshly prepared 1.0 ML ZnO_x overlayer on Cu(110).

References

1. C.L. Briant and R.P. Messmer (eds.), Auger Electron Spectroscopy; Treatise on Materials Science and Technology, Academic Press, Inc., New York (1988).

2. P.A. Redhead, Vacuum 12 (1962) 203.

3. D.A. King, Surf. Sci. 47 (1975) 384.

4. E. Shustorovich, Accounts of Chem. Research, 21 (1988) 183.

5. C.-M. Chan, R. Aris, and W.H. Weinberg, Applications of Surface Science, 1 (1978) 360.

6. M.A. Van Hove, W.H. Weinberg, and C.-M. Chan, Low Energy Electron Diffraction, Springer, Berlin (1986).

7. L.J. Clarke, Surface Crystallography, John Wiley and Sons Ltd., Chichester (1985).

8. G. Ertl and J. Küppers, Low Energy Electrons and Surface Chemistry, Verlag Chemie, Weinheim (1974).

9. P.B. Needham, T.J. Driscoll, and N.G. Rao, Appl. Phys. Lett. 21 (1972) 502.

10. L.E. Davis, N.C. MacDonald, P.W. Palmberg, G.E. Riach, and R.E. Weber, Handbook of Auger Electron Spectroscopy, Perkin-Elmer (1972).

11. G. Ertl, Surf. Sci. 6 (1967) 208.

12. K. Horn, M. Hussain, and J. Pritchard, Surf. Sci. 63 (1977) 244.

13. L. deBroglie, Phil. Mag. 47, 446 (1924).

Chapter 3

Interactions of O_2, CO, CO_2, and D_2 with the Stepped Cu(311) Crystal Face: Comparison to Cu(110)

3.1 Introduction

Cu-Zn-O catalysts are important methanol synthesis catalysts which produce over thirteen million tons of methanol each year from CO, CO_2, and H_2. Hence, it is not surprising that understanding the rôles the surface plays in catalyzing this reaction is of great interest [1,2]. In spite of the large number of works published on both the working Cu-Zn-O catalysts and model methanol synthesis catalysts, little work has been done on the structure sensitivity of methanol synthesis catalysts [3,4], or on the importance of copper surface structure in methanol synthesis.

A number of studies on Cu/metal oxide catalysts have suggested a direct correlation between methanol production and copper surface area [5-7]. However, other studies have shown that there is no correlation between activity and copper surface area [8,9]. This, along with the fact that Cu/metal oxides prepared differently do not give the same methanol activity per copper surface area (compare reference [7] to reference [9]), suggests methanol synthesis may be structure sensitive. In this chapter, we compare two copper surfaces – Cu(311) and Cu(110) – by examining their interaction with the reactant gases of methanol synthesis (CO, CO_2 and H_2

(D_2)), and the effect pre-adsorbed oxygen has on their interactions. We concentrate on the pure copper component for we have seen that zinc oxide islands on Cu(110) and Cu(311) do not alter the binding of CO or CO_2 to the copper component [10,11]. We will show that Cu(311) is much more reactive to CO_2 and D_2 dissociative adsorption, and to the formation of CO_2 by the reaction

$$CO + O_{(surface)} \leftrightarrow CO_2,$$

which is important under methanol synthesis reaction conditions. These chemisorption studies suggest that methanol synthesis over copper may be a structure sensitive reaction.

3.2 Results

Interaction of Oxygen with Cu(311) and Cu(110)

Oxygen dissociative chemisorption on Cu(311) produced streaks in the $[\bar{2}33]$ direction from 0.1 ML to 0.2 ML oxygen. At 0.3 ML oxygen, half-order spots begin to appear in this direction for the LEED pattern, corresponding to a $p(2\times1)$ surface structure by 0.4-0.5 ML oxygen. This $p(2\times1)$ pattern is accompanied by a diffuse background at $\geq$0.4 ML oxygen. A coverage of >0.6 ML oxygen was achieved by dosing the Cu(311) surface with 6,000 L O_2. This high coverage produced no visible diffraction pattern.

Half-order spots also form on Cu(110) with oxygen chemisorption, but the diffraction pattern is much sharper than on Cu(311). Patches of a $p(2\times1)$ surface structure begin at 0.2 ML oxygen and becomes a well-ordered, sharp pattern by 0.5 ML oxygen. At oxygen coverages greater than 0.5 ML, extra spots in addition to the half order spots appear, forming a LEED pattern corresponding to a real-space $p(2\times1)$+c(6X2) pattern [12].

Adsorption of oxygen onto Cu(311) appears to produce two types of oxygen, one which remains on the surface up to 1000 K, and one which desorbs as molecular oxygen in a broad peak, beginning at 180 K, as shown in figure 3.1A. We have used oxygen gas which is 50% enriched in ^{18}O in order to obtain clear results on

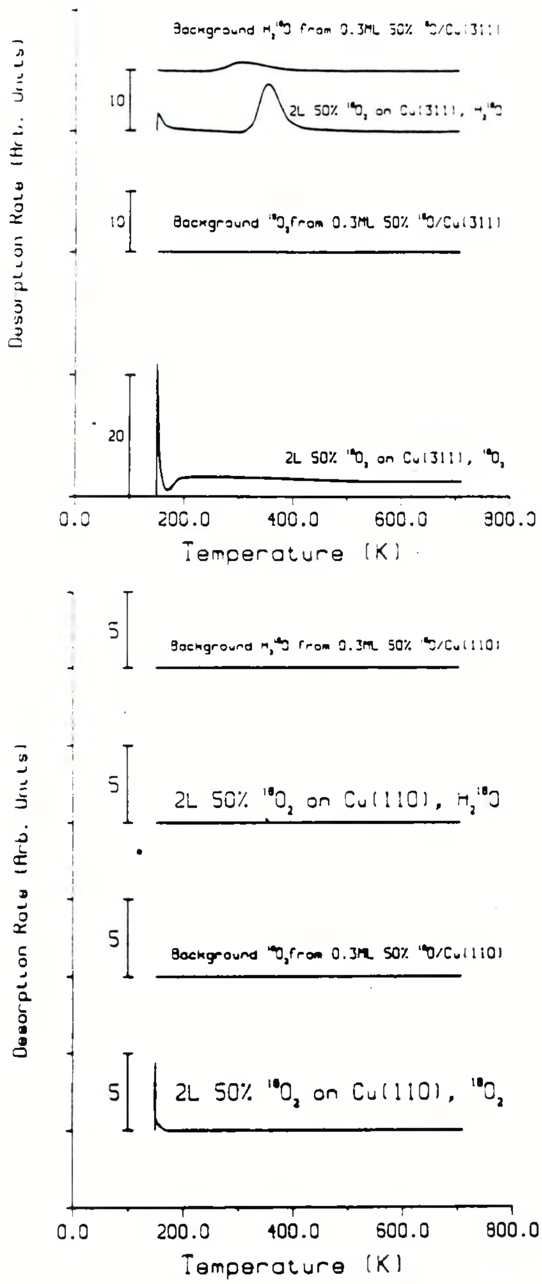

Figure 3.1: (A) Oxygen on Cu(311). A small amount of oxygen initially desorbs from Cu(311) after exposure to 2.0 L or greater of $^{18}O_2$. The oxygen remaining on the surface after the initial desorption does not desorb as $^{18}O_2$ until >1000 K. Some of the surface oxygen reacts with background hydrogen to form $H_2^{18}O$ ($\frac{m}{e}$=20). The amounts of oxygen lost from the surface due to water formation in the time scale of TPD experiments is not detectable by AES. (B) Oxygen on Cu(110). Unlike oxygen on Cu(311), oxygen on Cu(110) is very unreactive. Oxygen does not desorb from Cu(110) until >1000 K. Scale for these spectra are 100× the sensitivity of the reference scale (CO TPD spectra).

the origin of the oxygen for several reactions. There is no additional desorption of molecular oxygen after the initial desorption. However, there is a slight loss of surface oxygen due to reaction with background H_2 as shown in figure 3.1A. The loss of atomic oxygen from the surface due to water formation is extremely small and a background check showed no change in the AES oxygen signal during the time span of each set of TPD experiments. Notice that the $H_2^{18}O$ desorption occurs at different temperatures depending on the type of oxygen on the surface.

Although the sticking coefficient of oxygen on Cu(311) and Cu(110) are roughly the same at 150 K, $^{18}O_2$ adsorption on Cu(110) does not produce any $^{18}O_2$ desorption until >1000 K. Additionally, no ^{18}O is lost by water formation with background H_2 as shown in figure 3.1B. Thus, oxygen on Cu(110) is less reactive than oxygen on Cu(311). We will see further evidence of this in the following sections.

Interaction of CO with Clean and Oxygen Covered Cu(311) and Cu(110)

Carbon monoxide TPD near and at saturation coverage on Cu(311) is shown in figure 3.2A. The low temperature adsorption site has a T_p (temperature at peak desorption) of 203 K at saturation coverage. But in addition to the low temperature adsorption site, is a high temperature adsorption site at ~430 K. We will see that this high temperature adsorption site is responsible for the formation of CO_2 from surface CO and chemisorbed oxygen on Cu(311).

The change in CO adsorption with 0.5 ML O/Cu(311) is also shown in figure 3.2A. There are two adsorption sites in the low temperature region and oxygen blocks only one of these adsorption sites. The high temperature peak at ~430 K is not seen because at these saturation doses of 20 L CO, there is a high rising background due to desorption from the manipulator parts that hides the high temperature CO peak. At lower CO doses, we see that the high temperature CO peak at ~430 K remains unchanged with pre-adsorbed oxygen.

Saturation coverage of CO produces a similar CO TPD spectrum on Cu(110) as on Cu(311) (with T_p=218 K instead of T_p=203 K), but an order in magnitude

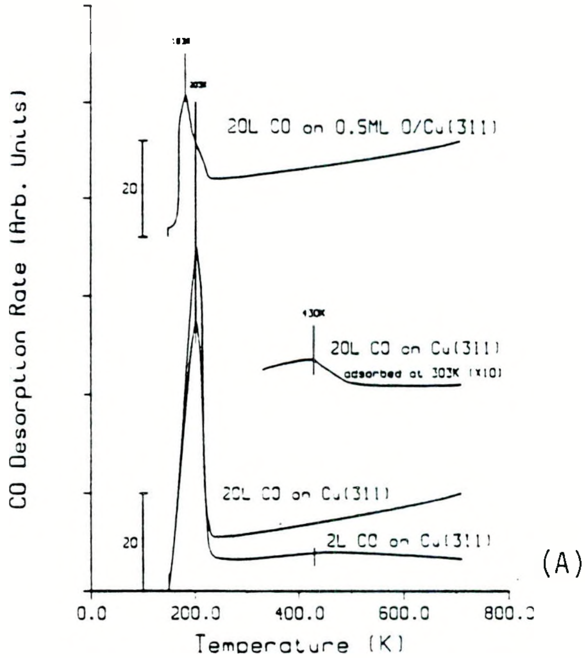

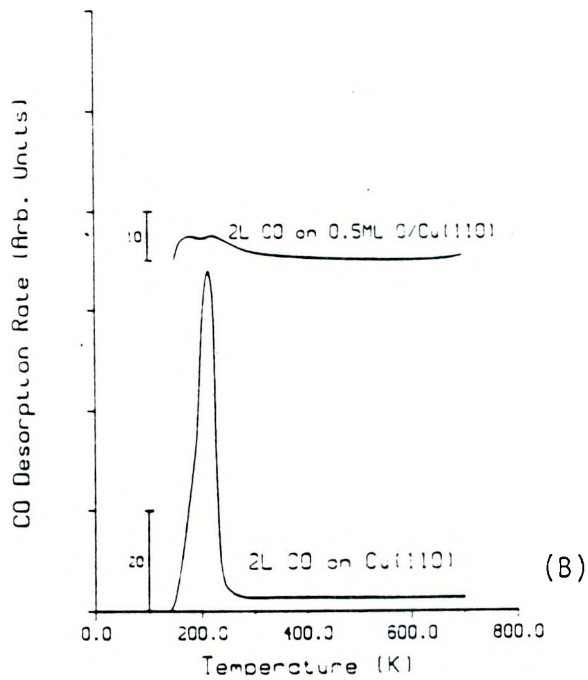

Figure 3.2: (A) The main CO peak from Cu(311) has T_p=203 K at saturation coverage. Adsorption at 303 K shows that the broad high temperature peak at ~430 K remains at this adsorption temperature. The monotonic rise in CO signal from TPD experiments at 150 K and 20 L CO is due to desorption from the manipulator parts which hides the small CO peak from Cu(311) centered at ~430 K. Saturation coverages of CO at 150 K on 0.5 ML O/Cu(311) shows that oxygen decreases the saturation coverage of CO by blocking one type of site. (B) CO TPD from Cu(110). Saturation dose (2.0 L) produces a desorption peak with T_p=218 K. Oxygen blocks CO adsorption more effectively on Cu(110) than on Cu(311).

less CO exposure is needed to reach saturation coverage on Cu(110) at 150 K. This is shown in figure 3.2B. Half monolayer of pre-adsorbed oxygen blocks more CO adsorption on Cu(110) than on Cu(311).

In addition to observing changes in CO adsorption as a function of temperature and oxygen coverage, we monitored for reaction products between CO and oxygen with the use of O_2 gas 50% enriched in ^{18}O. Figure 3.3 shows the results of dosing 20 L CO onto Cu(311) pre-adsorbed with various amounts of 50% ^{18}O and monitoring for $CO^{18}O$. A few points are to be noted from this figure:

1. The same amount of $CO^{18}O$ (2×10^{12} $CO^{18}O$ molecules/cm^2 of Cu(311), which means twice as much carbon dioxide was produced as only half of the oxygen are ^{18}O) is produced with oxygen coverages ranging from 0.15 ML to 0.4 ML at 150 K.

2. No change for $CO^{18}O$ production is observed when the dosing temperature is changed from 150 K to 300 K.

3. CO dosed at 370 K produced less $CO^{18}O$ than at 300 K.

4. Cu(311) covered with 0.3 ML of 50% ^{18}O in a background less than 2×10^{-10} Torr CO for 12 hours (less than 10 L CO) produced almost four times as much $CO^{18}O$ as a a dose of 1×10^{-7} Torr CO for 200 seconds (20 L).

On the same figure, we show that ^{18}O/Cu(110) does not react with CO to form $CO^{18}O$. We checked background formation of $CO^{18}O$ by dosing a clean Cu(311) surface with 20 L CO, and found no $CO^{18}O$ formation.

The overnight dose of background CO was done with all filaments in the vacuum chamber off. The reason for this is the observation that $CO^{18}O$ formation can be accelerated by an electron beam. The electron beam used for LEED has no detectable effect on the time scale of <5 minutes exposure, but the 2.0 KeV electron beam used for AES does produce $CO^{18}O$ from background CO plus surface ^{18}O. Hence, the crystal was flashed to 700 K after each exposure to the Auger electron beam. This brings us to the possibility that the whole $CO^{18}O$ formation is stimulated by

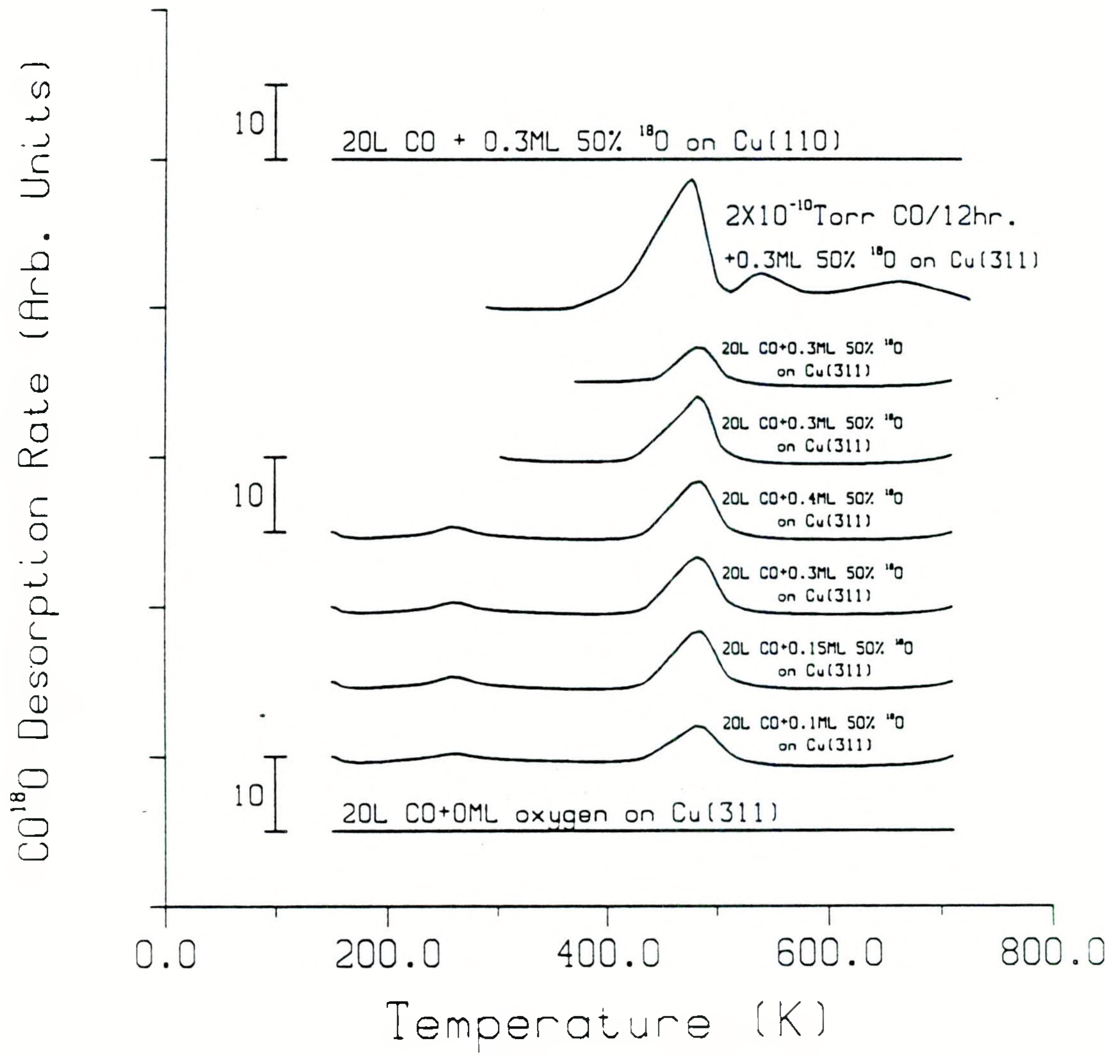

Figure 3.3: Reaction of CO with surface ^{18}O to form $CO^{18}O$. CO was dosed at 1×10^{-7} Torr for 200 seconds for the 20 L dose. The same amount of $CO^{18}O$ was produced between oxygen coverages of 0.15 ML and 0.4 ML with a 20 L dose of CO. Adsorption of CO at 300 K instead of 150 K did not change the amount of $CO^{18}O$ produced, but changing the CO adsorption temperature to 370 K did decrease the amount of $CO^{18}O$ produced. Exposing a 0.3 ML O/Cu(311) surface with background CO for 12 hours (<10 L CO), with all filaments off, produced almost four times the quantity of $CO^{18}O$ than with a 20 L dose of CO given over 200 seconds. In comparison, Cu(110) does not form carbon dioxide from CO and surface oxygen under these low pressures and temperatures. Y-axis scale is $10\times$ the reference scale.

the one filament it is necessary to turn on – the mass spectrometer filament. Two checks were make concerning this possibility: 1) The O/Cu(311) sample was held at a -90 eV bias during the TPD experiment and this was shown to have no effect on the amount of $CO^{18}O$ produced. 2) A Cu(311) covered with 0.3 ML 50% ^{18}O was left in the chamber with about 2×10^{-10} Torr CO and all filaments turned off in the chamber for 28 hours (20 L). This process produced greater than an order in magnitude amount of $CO^{18}O$ (4×10^{13} molecules/cm^2 of Cu(311)) as dosing a 0.3 ML 50% ^{18}O on Cu(311) with 20 L of CO in a 200-second period. These experiments show that although the formation of carbon dioxide can be accelerated by an electron beam, the process does occur in the absence of an electron beam.

The fact that dosing 20 L of CO in a 200-second period produces an order in magnitude less CO_2 from the same surface than dosing the 20 L over a 28 hour time period, suggests that the reaction of CO plus surface oxygen is activated. The fact that less CO_2 is produced when Cu(311) is exposed to CO at 370 K instead of 300 K suggests a surface reaction rather than an Eley-Rideal reaction.

The consumption of surface oxygen can be observed by AES and LEED. Continually dosing the surface with 20 L of CO followed by desorption of $CO^{18}O$ shows a slow decline in the oxygen AES signal and loss of the half-order spots in the LEED pattern. But the most dramatic change is seen when the sample is left overnight: a diffuse p(2×1) pattern is observed from O/Cu(311) the night before with a specific oxygen AES signal, and the next morning, the AES spectrum looks the same but the half-order spots in the LEED pattern are gone. Desorption indicates $CO^{18}O$ formation, and AES after desorption shows a large loss in oxygen signal.

If a 0.3 ML O/Cu(311) surface is left in the UHV chamber with the ion guage filament on for 20 hours, the sample produces both H_2O and CO_2, leaving the Cu(311) surface oxygen free after desorption of these molecules. We have a calibration for CO_2, but not for H_2O. Assuming H_2O has about the same mass spectrometer sensitivity as CO_2, we determined that 1.0×10^{14} molecules of CO_2 and 1.0×10^{14} molecules H_2O desorbed from the surface. As we assume that the CO_2 we detect is from background CO plus surface oxygen and the H_2O is from background hydrogen plus surface oxygen, we conclude that 2.0×10^{14} atoms of oxygen existed on the surface prior to reaction. We had started out with 0.3 ML oxygen (AES calibration) on a 0.8 cm^2 Cu(311) - 2.2×10^{14} oxygen atoms. Hence, the calibrations for quantitative analysis by Auger and mass spectrometry appear to be consistent.

Interaction of CO_2 with Clean and Oxygen Covered Cu(311) and Cu(110)

Carbon dioxide TPD spectra from clean Cu(311) and Cu(110) are shown in figure 3.4. Cu(110) surfaces do not adsorb CO_2, while Cu(311) surfaces do adsorb CO_2 at 150 K and $<10^{-7}$ Torr pressure. The CO_2 desorption from Cu(311) consists of a low temperature peak, and a very broad high temperature peak. The low temperature peak, centered at ~200 K, appears first at low coverages of CO_2, followed by the broad high temperature peak. The low temperature state appears to be a precursor for the high temperature states as no CO_2 adsorption could be detected at an adsorption temperature of 300 K.

In addition to CO_2 adsorption on Cu(311) and Cu(110), we investigated CO_2 adsorption on oxygen covered Cu(311) and Cu(110). This is shown in figure 3.5. Pre-adsorbed oxygen does not change CO_2 interaction with Cu(110); there is no CO_2 desorption with oxygen modified Cu(110). Pre-adosrbed oxygen on Cu(311) increases the CO_2 population on the higher energy adsorption sites.

We had seen, in the previous section, that CO reacts with surface oxygen to produce CO_2. We investigated the reverse reaction of CO_2 dissociation by use of $C^{18}O_2$ and found that a small amount (approximately 6×10^{12} molecules/cm^2) of carbon dioxide does dissociate to form carbon monoxide for a 4.0 L dose of $C^{18}O_2$. (We stayed at low $C^{18}O_2$ exposures to avoid ion pump dissociation of $C^{18}O_2$.) This is shown in figure 3.6. The amount of oxygen from this dissociation process cannot be detected by AES until $>3\times10^{13}$molecules CO_2/cm^2 has dissociated on clean Cu(311). No $^{18}O_2$ was detected, but approximately $\leq1\times10^{11}$ $H_2^{18}O$ molecules/cm^2 could be detected during each TPD experiment. This is due to the reaction $C^{18}O_2+H_{2(background)} \rightarrow C^{18}O+H_2^{18}O$, the water-gas shift reaction. In con-

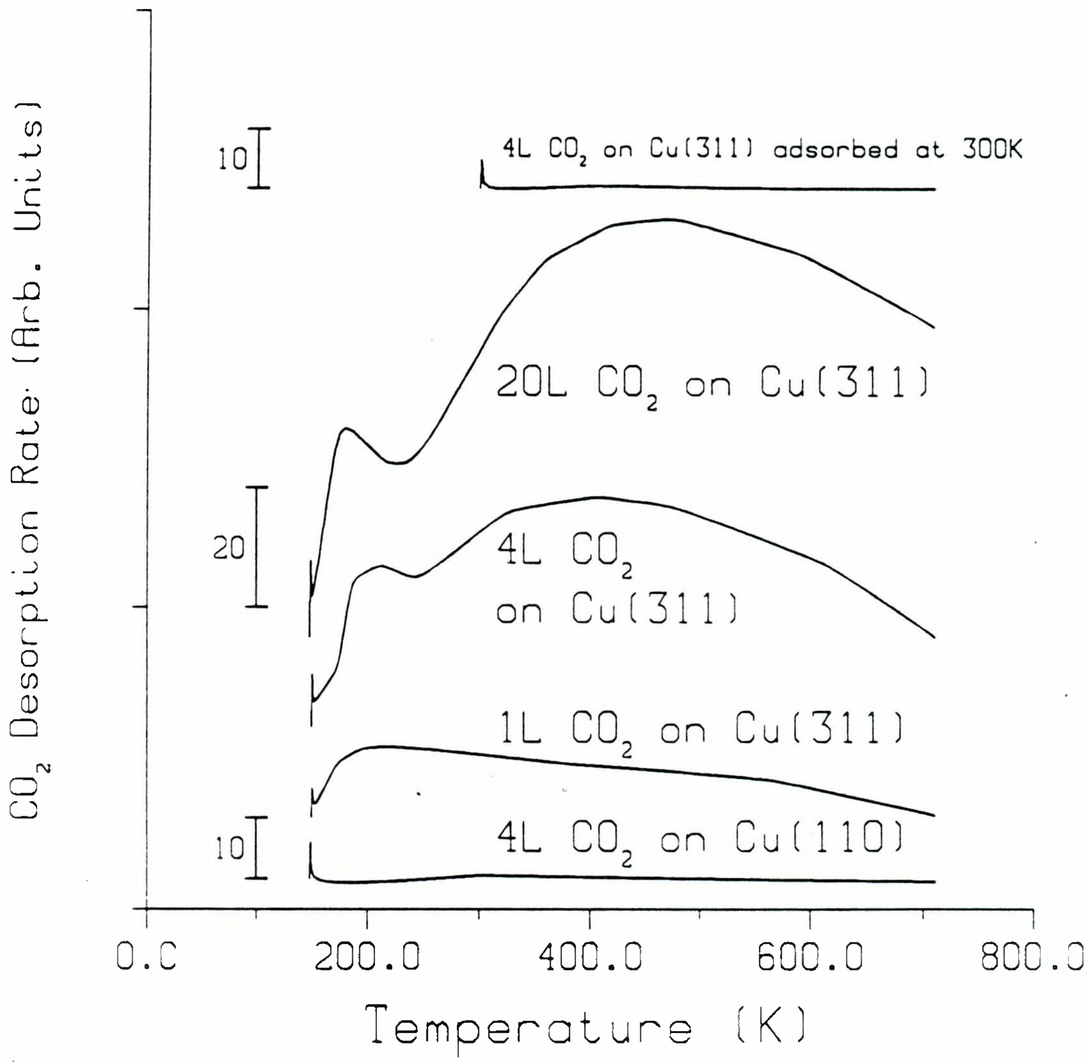

Figure 3.4: CO_2 desorption from Cu(311) and Cu(110). Cu(110) does not adsorb CO_2 at these low temperatures and pressures. On the other hand, Cu(311) does adsorb CO_2. The low energy CO_2 site fills first, and then the high energy sites. The low energy state appears to be a precursor for the high energy states as no CO_2 adsorption was detected at an adsorption temperature of 300 K. Notice that the peak due to $CO^{18}O$ formation from CO and $^{18}O_{(surface)}$ lies within the broad high temperature CO_2 peak. Y-axis scale is 10× the reference scale.

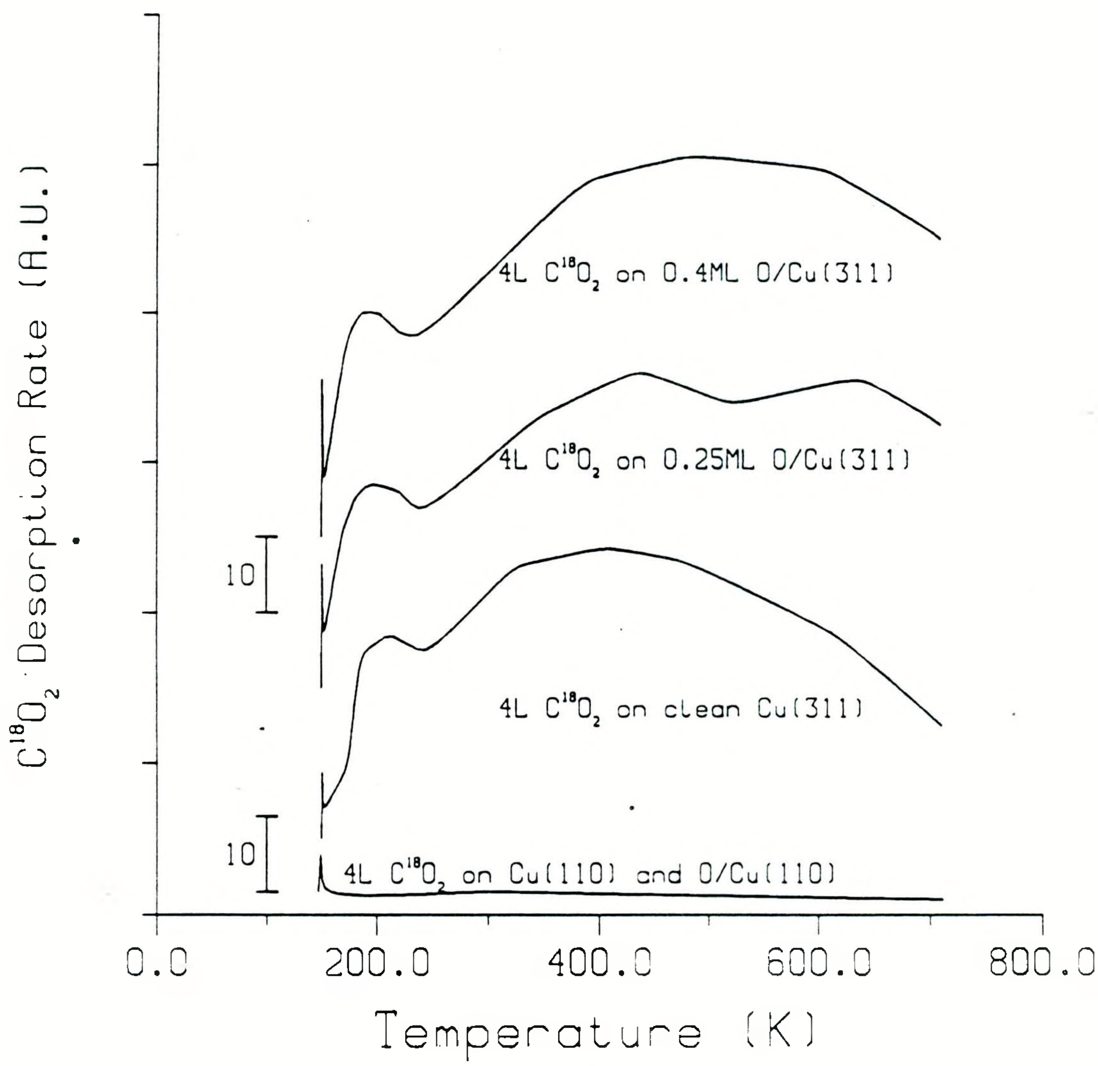

Figure 3.5: Effect of oxygen on $C^{18}O_2$ desorption from Cu(311) and Cu(110). Pre-adsorbed oxygen does not change CO_2 interaction with Cu(110). Pre-adsorbed oxygen on Cu(311) increases the CO_2 population of the higher energy binding states. Y-axis scale is $10\times$ the reference scale.

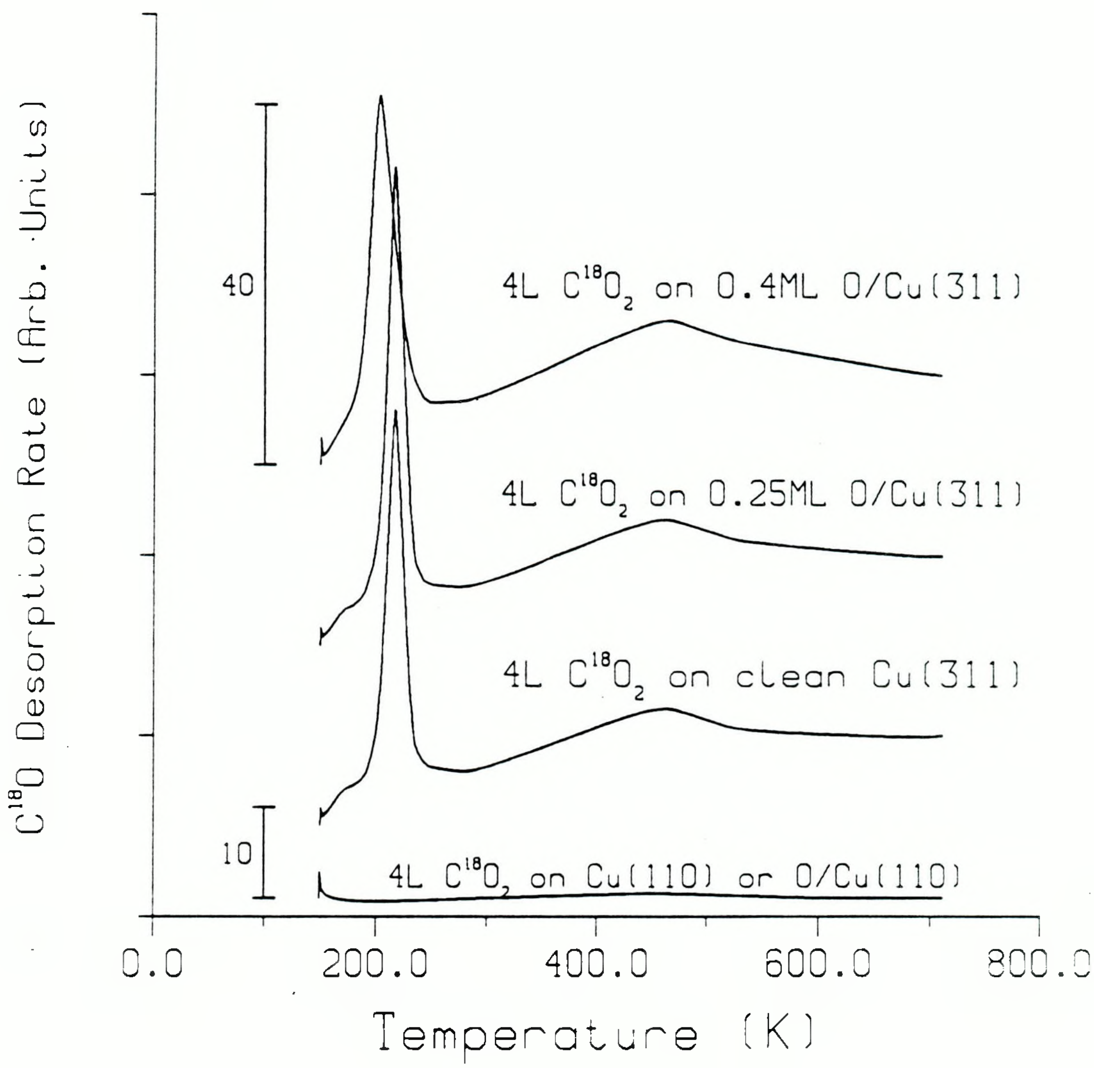

Figure 3.6: Decomposition of $C^{18}O_2$ on Cu(311) and Cu(110). On Cu(311), $C^{18}O_2$ decomposes to form $C^{18}O$ and surface oxygen. The oxygen produced from this reaction is not detectable by AES until >20 L $C^{18}O_2$ exposure. Up to 0.4 ML oxygen does not alter the dissociative probability of $C^{18}O_2$ on Cu(311). The ability to dissociate carbon dioxide at these low pressures and temperatures have not been seen on Cu(110) or oxygen modified Cu(110). Y-axis scale is 10× the reference scale.

trast to Cu(311), on Cu(110) and oxygen modified Cu(110), carbon dioxide does not dissociate to carbon monoxide and oxygen.

One may argue that the $C^{18}O$ detected is due to impurities in the $C^{18}O_2$ gas. This was checked as follows: 1×10^{-8} Torr $C^{18}O_2$ and a 2.0 KeV electron beam were simultaneously exposed to ^{16}O covered Cu(311) surfaces for 10 minutes. Then the crystal was ramped and $C^{16}O^{18}O$ ($\frac{m}{e}$=46) monitored. No signal was detected. If there was $\geq$1% $C^{18}O$ impurities in the $C^{18}O_2$, we would have detected a signal for $C^{16}O^{18}O$ formation under those conditions. Hence, we are confident that the decomposition of carbon dioxide occurs as well as the formation of carbon dioxide on oxygen covered Cu(311) surfaces.

Interaction of D_2 with Clean and Oxygen Covered Cu(311) and Cu(110)

Figure 3.7 shows that D_2 does adsorb on Cu(311) at low pressures and 150 K. Pre-adsorbed oxygen enhances the ability of Cu(311) to adsorb D_2. In contrast, we see that D_2 does not interact with Cu(110) or oxygen modified Cu(110) at $<10^{-7}$ Torr and 150 K. This is in agreement with studies which have shown that H_2 dissociation on low Miller index copper surfaces and O/Cu(110) is an activated process [13-15], while H_2 dissociation on Cu(311) is spontaneous [16].

Some Co-Adsorption Studies

Some co-adsorption studies of CO and D_2, and CO_2 and D_2 were performed on Cu(311). All co-adsorption studies were performed at a total pressure of 1×10^{-7} Torr, with 50% of each gas, uncorrected for different ion guage sensitivities. On clean Cu(311), CO blocks D_2 adsorption almost to 100%, and to a lesser extent on 0.4 ML O/Cu(311).

The co-adsorption of $C^{18}O_2$ and D_2 on Cu(311) produced adsorption similar to the absence of each other. Hence, the adsorption sites for $C^{18}O_2$ and D_2 on Cu(311) appear to be independent of each other.

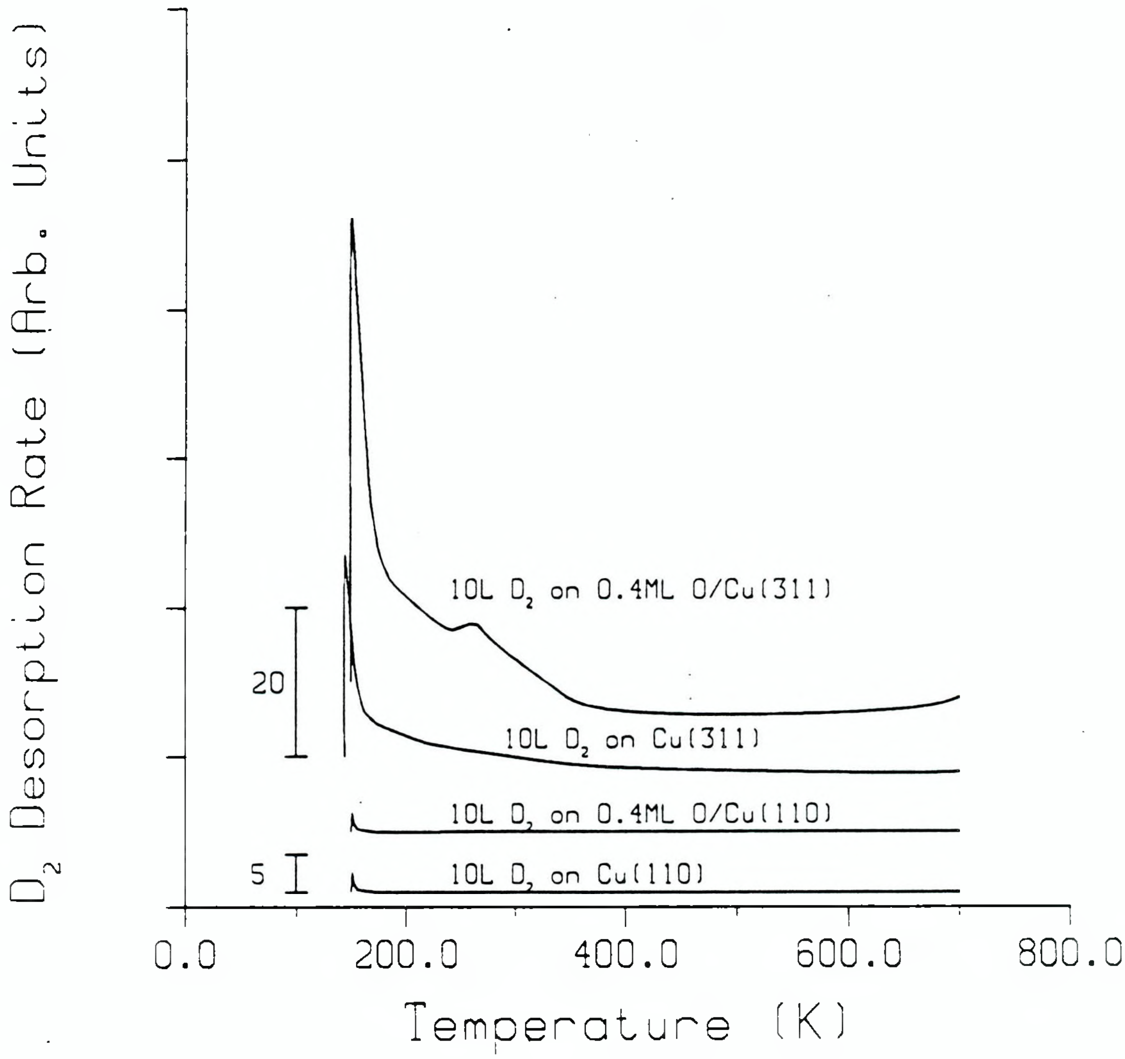

Figure 3.7: D_2 does adsorb on Cu(311), and the amount of adsorption increases with 0.4 ML O/Cu(311). In contrast, D_2 does not adsorb on either Cu(110) or oxygen modified Cu(110). Y-axis scale is 10× the reference scale.

3.3 Discussion

We have shown that Cu(311) is much more reactive toward CO-CO_2 exchange than Cu(110), and Cu(311) faces adsorb CO_2 and D_2 at low pressures (<10^{-6} Torr) while Cu(110) does not interact with either CO_2 or D_2 under low pressures and temperatures of <10^{-6} Torr and 150 K. We choose Cu(311) because our earlier work on copper foil [17] led us to believe that atomic steps may play an important rôle by interacting with CO_2, and Cu(311) has one of the highest step densities available, and is an open surface.

The greater reactivity of O/Cu(311), compared to oxygen chemisorbed on low Miller index copper faces, to H_2 and CO have been shown by Arlow and Woodruff [18] at higher pressures. They examined a cylindrical single crystal which contained the three low Miller index faces, the (311) face, and vicinal faces, all pre-adsorbed with 0.5 ML oxygen. This O/Cu cylindrical single crystal was then rotated in 10^{-6}-10^{-4} Torr of CO or H_2. The rate of oxygen consumption was monitored by AES. They showed that oxygen disappeared two to five times faster from the (311) and (311)/(100) (orientation between (311) and (100)) and (311)/(111) faces than from the low Miller index faces. Hence, this structure sensitivity for CO-CO_2 exchange at higher pressures of 10^{-6}-10^{-4} Torr is consistent with our UHV studies.

In addition to showing that CO_2 forms from CO and surface oxygen on Cu(311) at low pressures and temperatures, we showed that the reverse reaction of CO_2 dissociation also occurs on Cu(311). This is important because CO-CO_2 exchange is believed to be part of the mechanism for methanol synthesis over Cu-Zn-O catalysts [19,20] and the ability for this exchange may be important in determining the activity and selectivity of methanol synthesis.

The importance of copper structure in methanol synthesis under industrial conditions could explain the discrepancy in the catalytic literature between various copper/metal oxide catalysts, as has been suggested by Burch and Chappell [9]. It would be interesting to determine the effect of stepped copper sites on the activity of methanol synthesis by comparing the methanol synthesis activity of Cu(110) crystals to those of Cu(311) crystals.

Dissociation of CO_2 and H_2 are important steps in methanol synthesis. The ability for CO-CO_2 exchange can also be a significant step as the competing reaction of the water-gas shift reaction ($CO + H_2O \leftrightarrow CO_2 + H_2$) occurs under industrial conditions. As we have shown that Cu(311) is much more reactive for these processes than Cu(110), methanol synthesis from CO, CO_2, and H_2 is likely a structure sensitive reaction.

3.4 Conclusion

We have compared the reactivity of Cu(110) and Cu(311) to the reactant gases of methanol synthesis (CO, CO_2, and D_2 (H_2)) in UHV. It is shown that important differences exist between the two surfaces: (1) CO_2 and D_2 chemisorb on Cu(311) and oxygen modified Cu(311), but not on Cu(110) or O/Cu(110). (2) The forward and reverse reaction of $CO+O_{(surface)} \leftrightarrow CO_2$ can be seen on Cu(311), but not on Cu(110).

References

1. G.C. Chinchen, P.J. Denny, J.R. Jennings, M.S. Spencer, and K.C. Waugh, Applied Catal. 36 (1988) 1.
2. K. Klier, Adv. Catal. 31 (1982) 243.
3. M. Bowker, H. Houghton, and K.C. Waugh, J. Catal. 84 (1983) 252.
4. W.H. Cheng, S. Akhter, and H.H. Kung, J. Catal. 82 (1983) 341.
5. W.X. Pan, R. Cao, D.L. Roberts, and G.L. Griffin, J. Catal. 114 (1988) 440.
6. A.J. Bridgewater, M.S. Wainwright, and D.J. Young, Applied Catal. 28 (1986) 241.
7. G.C. Chinchen, K.C. Waugh, and D.A. Whan, Applied Catal. 25 (1986) 101.
8. G.J.J. Bartley and R. Burch, Applied Catal. 43 (1988) 141.
9. R. Burch and R.J. Chappell, Applied Catal. 45 (1988) 131.
10. S.S. Fu and G.A. Somorjai, Surface Sci. 237 (1990) 87.
11. S.S. Fu and G.A. Somorjai, to be published.
12. G.W. Simmons, D.F. Mitchell, and K.R. Lawless, Surf. Sci. 8 (1967) 130.
13. M. Nakashima, Y. Zhou, and J.M. White, Surf. Sci. 206 (1988) 395.
14. F. Greuter and E.W. Plummer, Solid State Communications, 48(1) (1983) 37.
15. M. Balooch, M.J. Cardillo, D.R. Miller, and R.E. Stickney, Surf. Sci. 46 (1974) 358.
16. J. Pritchard, R. Catterick, and R.K. Gupta, Surf. Sci. 53 (1975) 1.
17. S.S. Fu and G.A. Somorjai, unpublished work.
18. J.S. Arlow and D.P. Woodruff, Surf. Sci. 180 (1987) 89.

19. Z.X. Ren, J. Wang, L.J. Jia, and D.S. Lu, Applied Catal. 49 (1989) 83.

20. M. Bowker, H. Houghton, and K.C. Waugh, J. Chem. Soc., Faraday Trans. 77 (1981) 3023.

Chapter 4

Surface Studies of Zinc Oxide Growth on Cu(110)

4.1 Introduction

In the previous chapter, we examined, in vacuum, the different reactivities of Cu(311) and Cu(110) to the reactant gases of methanol synthesis - CO, CO_2, and H_2 (D_2). We now examine Cu-Zn-O interaction on the Cu(110) face.

Since Cu-Zn-O species are important as methanol synthesis catalysts, it is not surprising that several studies on the interaction of copper, zinc, and oxygen have been published [1-6], although none on the growth and characterization of submonolayers to multilayers of zinc and oxygen on copper single crystals. Campbell and co-workers [3] deposited copper on ZnO(000$\bar{1}$) and characterized its growth by XPS, ISS, and LEED. These same researchers formed ZnO_x on Cu(111) by depositing in air, a droplet of ZnO-saturated water solution and then analyzed the resulting surface by XPS before catalytic studies. Chan and Griffin [5] examined the decomposition of methanol over copper deposited on oriented ZnO thin films, and found the properties of Cu/ZnO to be primarily a superposition of the separate copper and zinc oxide components. Didziulis and co-workers [6] performed a detailed surface science study of copper overlayers on ZnO(0001), (000$\bar{1}$), and (10$\bar{1}$0). Heating in UHV resulted in loss of copper XPS intensity which they interpreted as being due to three-dimensional clustering of the copper. They also found that copper deposited on Zn^{2+} terminated ZnO(0001) surfaces are most easily oxidized.

In this chapter we present the results of our studies on the growth and chemical properties of the system formed when zinc vapor and oxygen are deposited onto copper single crystal surfaces of (110) orientation. The probes we used are AES, LEED, chemisorption of CO and CO_2, and Zn TPD. Carbon monoxide has been known to adsorb mainly on the copper part of reduced Cu-Zn-O catalysts [7], and this was confirmed by our studies of CO adsorption on Cu(110), half a monolayer of oxygen on Cu(110) (henceforth denoted 0.5 ML O/Cu(110)), Zn, and ZnO_y. Carbon dioxide, on the other hand, adsorbs only on ZnO [8] and not on clean Cu(110) [9], or O/Cu(110), or Zn at 150 K. By using selective CO and CO_2 adsorption to determine surface composition in Cu-Zn-O systems, we found rapid clustering of the initial two-dimensional ZnO_x islands above 300 K.

4.2 Experimental

In addition to the experimental chapter, a few experimental notes for this particular chapter are given below.

A typical experimental procedure is as follows: The copper single crystal is cleaned by cycles of sputtering with 5×10^{-5} Torr argon at 300 K and 910 K, and then annealed at 950 K for fifteen minutes. Sample cleanness is then checked by AES and its structure by LEED. Once the sample is cleaned, the desired amount of zinc and oxygen are deposited. Unless otherwise noted, all zinc depositions reported in this chapter are done in an ambient of 1×10^{-7} Torr O_2. Only zinc, oxygen, and copper could be detected by AES after zinc and oxygen depositions onto the copper. After producing the desired amount of ZnO_x, TPD experiments begin. The sample is cooled to 150 K, an AES spectrum is taken, the sample is positioned 2 mm in front of the mass spectrometer, dosed with a known amount of gas, and then the sample temperature is ramped linearly at 30 K/s with the mass spectrometer tuned to a particular mass. AES spectra were obtained after each TPD experiment to correlate composition to CO and CO_2 TPD spectra. After characterizing each surface by AES, LEED, CO and CO_2 TPD, the sample temperature was ramped to ~1100 K while monitoring zinc, oxygen, or copper to further characterize these surfaces.

All CO and CO_2 TPD data presented in this chapter were obtained from saturation coverages after dosing 2.0 L of CO and 3.0 L of CO_2 (without correction for ion gauge sensitivity). All TPD data in this chapter were collected using a 30 K/s linear ramp, and by monitoring $\frac{m}{e}$=44 for CO_2 and $\frac{m}{e}$=28 for CO.

For zinc TPD, $\frac{m}{e}$=64, corresponding to the most abundant zinc isotope, was used. Mass 63 was monitored to determine copper desorption. There is no natural isotope of zinc at this mass. For oxygen desorption, $\frac{m}{e}$=16 was used since there is contribution from zinc to $\frac{m}{e}$=32 signal but not to $\frac{m}{e}$=16 signal as determined by TPD of pure zinc from Cu(110).

4.3 Results

There are several difficulties in forming and studying zinc oxide overlayers on copper. We can see some of these difficulties when we examine and compare the interactions of the various two-component systems. For example, oxygen is readily dissociated onto Cu(110) at room temperature [10] and can dissolve into the bulk of copper [11]. In our laboratory, we have observed both the dissolution and segregation of oxygen on Cu(110). Not only does oxygen readily dissolve into copper, but so does zinc. Hence, we have the possibility of both zinc and oxygen dissolved in copper. Zinc can be oxidized in the presence of O_2, but the dissociation of oxygen on zinc is a slow process relative to the dissociation of oxygen on Cu(110). In addition, the oxidation of zinc occurs via three-dimensional zinc oxide island formation surrounded by elemental zinc [12,13]. Figure 4.1 shows schematically the different possibilities for zinc oxide growth on Cu(110).

Although figure 4.1 creates a very complicated picture of the Cu-Zn-O system, we will see that by combining several surface sensitive probes, we can understand what occurs upon deposition of zinc and oxygen onto Cu(110) and the effects that heat and further oxygen treatment has on these surfaces. In order to comprehend the three-component system of copper, zinc, and oxygen, an understanding of simpler one and two-component systems must be known. The first two subsections are

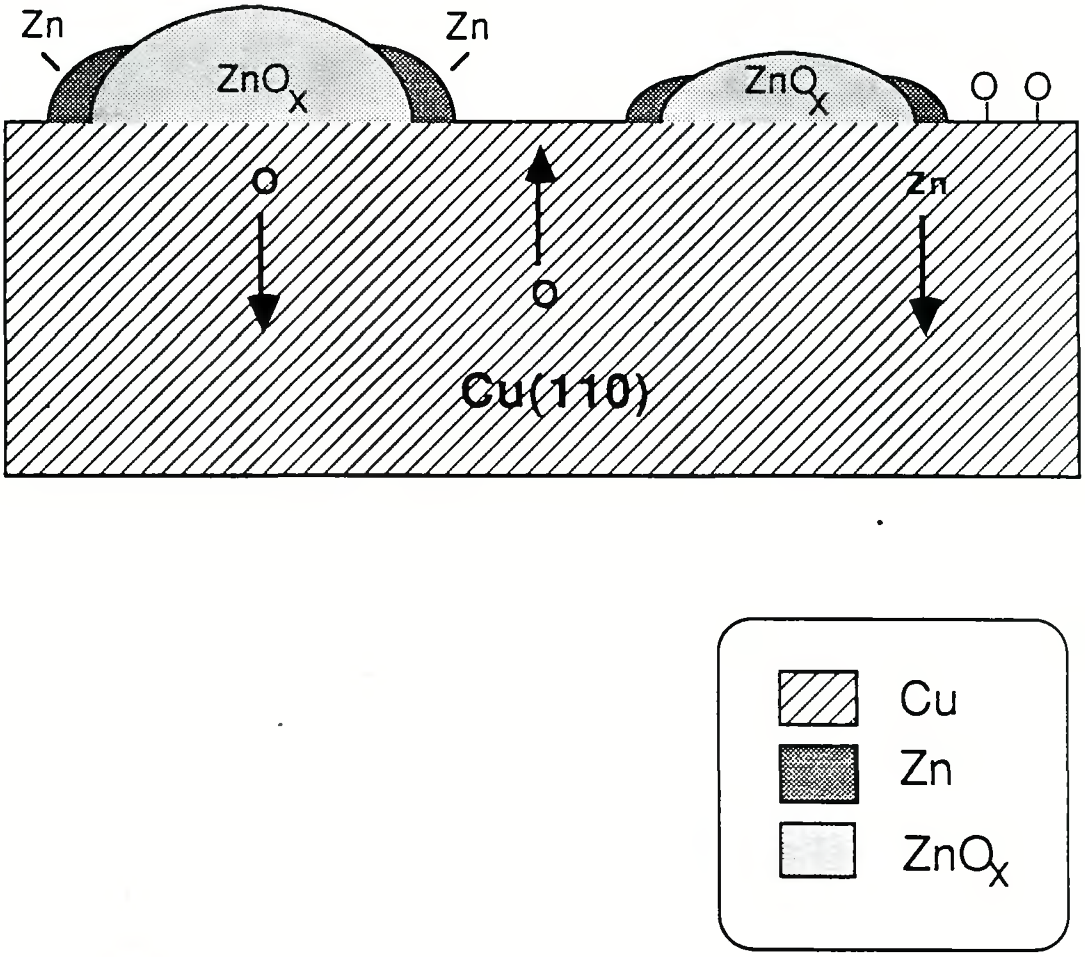

Figure 4.1: Schematic drawing of some of the species possible in Cu-Zn-O interaction on Cu(110).

Table 4.1

CO and CO_2 Desorption from Various Surfaces (Adsorption at 150K)

Surfaces	CO T_p	CO $\theta_{sat.}$	CO_2 T_p	CO_2 $\theta_{sat.}$
Cu(110)	218K	0.5ML	no ads.	—
0.5ML O/Cu(110)	222K & 180K	<0.05ML	no ads.	—
Cu_xO	222K & 180K	<0.03ML	no ads.	—
Zn	no ads.	—	no ads.	—
ZnO_y	203K	<0.05ML	340K & 175K	0.2ML

a. Each surface prepared as described in the experimental section.
b. T_p=temperature at peak desorption and $\theta_{sat.}$=saturation coverage where $\theta=1$ is defined as 1.1×10^{15} molecules/cm^2 corresponding to the number of copper atoms on the Cu(110) surface.

devoted to present the results of several one and two component systems.

CO and CO_2 Chemisorption Properties on Cu, O/Cu, Cu_xO, Zn, and ZnO

Table 4.1 summarizes the chemisorption properties of CO and CO_2 on Cu(110), 0.5 ML O/Cu(110) (0.5 ML O/Cu is defined by a sharp LEED pattern corresponding to a well-ordered p(2×1) surface structure [10]), oxidized copper, zinc, and zinc oxide. On Cu(110), CO adsorbs readily at 150 K giving a narrow desorption peak at T_p=218 K, with a saturation coverage of 0.5 ML CO. Carbon dioxide, on the other hand, does not adsorb on Cu(110) at 150 K [9]. Exposing Cu(110) to oxygen decreases its CO adsorption capacity [14]. Molecular oxygen does not desorb below 1000 K. With 0.5 ML O/Cu(110), the saturated CO adsorption has decreased to <10% of that on clean Cu(110). Carbon dioxide does not adsorb onto the oxygen covered Cu(110) surface.

In addition to O/Cu(110), we examined CO and CO_2 chemisorption on a Cu_xO surface, prepared by bulk oxidation of a copper foil. This surface behaves similarly to that of 0.5 ML O/Cu(110); it adsorbs <0.05 ML CO and does not adsorb detectable amounts of CO_2 at 150 K.

We examined CO and CO_2 adsorption on multilayers of zinc deposited onto both gold foil and Cu(110). In both cases, we observed no detectable adsorption of CO or CO_2 on zinc.

Finally, we examined the CO and CO_2 TPD spectra of ZnO_y on gold substrates. Saturated CO adsorption by multilayers of ZnO_y is less than 0.05 ML with a desorption peak centered at ~200 K. In contrast, CO_2 adsorption is readily observed and reaches saturation at about 2.5×10^{14} molecules/cm^2 (see experimental section for determination). This corresponds to a CO_2 coverage of $\theta \approx 0.23$ (θ=1 is defined as 1.1×10^{15} molecules/cm^2). The CO_2 desorption peak from submonolayers to multilayers of ZnO_y on gold is always centered at 340 K and 175 K, even after annealing to 1170 K. This indicates that ZnO_y overlayers on gold substrates are stable even after exposure to such elevated temperatures.

LEED patterns

Oxygen on Cu(110) forms a sharp LEED pattern corresponding to a well-ordered p(2×1) surface structure at 0.5 ML oxygen [10]. But various domains of a p(2×1) pattern can be seen above a coverage of 0.2 ML oxygen. No new LEED pattern could be seen upon the deposition of ZnO_x onto Cu(110). By comparing I-V curves of (1×1) and p(2×1) surface structures, with and without ZnO_x on the surface, we can show that all LEED patterns are due to long range order of either Cu(110) or O/Cu(110), and are not due to the ZnO_x overlayer.

Preparation and Thermal Stability of Oxidized Zinc Layers on Cu(110)

The oxidation state of zinc layers on copper depends upon the oxygen content of the surface. AES shows a peak at 988 eV (Zn LVV) for all surfaces independent of the oxygen treatment condition (temperature and exposure) except for zinc on clean copper, in which case the LVV transition occurs at 992 eV. (note: Although we cannot resolve the 988 eV and 992 eV peaks, we can detect the 4 eV shift.) The shift in the LVV zinc transition is indicative of the oxidation of zinc, but is not a good indicator of the stoichiometry of the oxide. From the oxygen AES peak alone, we cannot distinguish between the oxygen associated with copper and that associated with zinc.

The stability of the zinc layers as a function of oxidation extent was studied by TPD and the results are shown in figure 4.2. Zinc was adsorbed at 300 K under four different conditions; 1) on clean Cu(110), 2) on 0.5 ML oxygen preadsorbed on Cu(110), 3) in an ambient of 1×10^{-7} Torr O_2, and 4) same as (3) with additional oxidation in 5×10^{-7} Torr O_2 for 20 minutes at 300 K. Zinc desorbs from the surface in the range of 700-1100 K, depending on oxidation treatments. It is interesting to note that the two highest zinc desorption peaks from ZnO_x/Cu(110) occur at about the same temperature as two of the zinc desorption peaks from ZnO(0001)

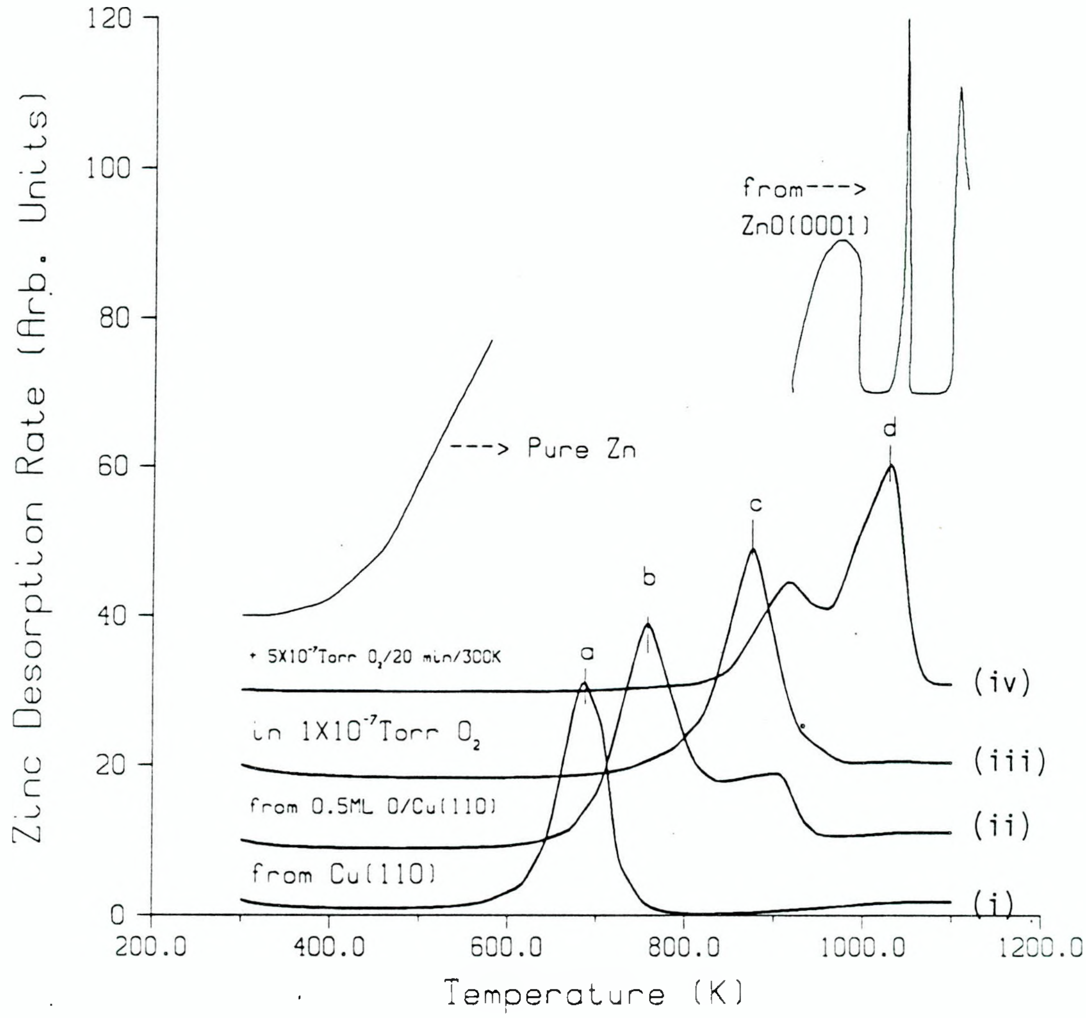

Figure 4.2: Desorption of 0.1 ML zinc adsorbed on Cu(110) under various oxidation conditions. All zinc and oxygen depositions were done at 300 K. Similar results are obtained for zinc and oxygen depositions at 150 K. AES shows a peak at 988 eV for all these surfaces except for zinc on clean copper (i), which has its LVV transition at 992 eV. No zinc could be detected by AES after each TPD ending at 1100 K. As reference, zinc desorption from multilayers of pure zinc and zinc desorption from ZnO(0001) [15] are shown. The zinc desorption from ZnO(0001) [15] is not on the same scale as the rest of the data. TPD spectra are 100× the reference scale.

surfaces [15]. No zinc could be detected by AES after each of our zinc TPD experiment. Only oxygen was left on the copper surface as detected by AES, except where pure zinc was deposited on clean Cu(110) (figure 4.2(i)).

Although the vast majority of zinc has desorbed by 1000 K, oxygen and copper desorption from these Cu-Zn-O surfaces are not detected below 1000 K. Both the copper and oxygen signal continues to rise from 1000 K to 1100 K, where the TPD experiments end. Only when the temperature of the crystal approaches the melting point of copper does oxygen desorb. This indicates that the species on these Cu-Zn-O surfaces decompose by desorption of $Zn_{(g)}$ atoms, leaving oxygen adsorbed on the copper surface and also absorbed into the bulk of copper. The absorption of oxygen into copper is clearly observed when >2 ML ZnO_x is heated to 1000 K. No O_2 desorption is detected by the mass spectrometer (and virtually no H_2O) and yet the AES oxygen signal decreases considerably (always down to ~0.6 ML oxygen) after heating the surface to 1000 K.

In addition to examining the thermal stability of ZnO_x overlayers on Cu(110), we calculated the desorption energy for ZnO_x, as represented by peak d of figure 4.2. The T_p of peak d of figure 4.2 increases with increasing ZnO_x surface coverage. This is indicative of zero and half order desorption processes. Hence, zinc desorption from ZnO_x, as represented by peak d of figure 4.2, was analyzed using a zero order and half order analysis, as described in chapter 2. From that discussion, the equations for zero and half order desorptions are:

$$\ln\left(\frac{d\sigma_p}{dT_p}\right) = \ln\left(\frac{\nu\sigma_o}{\beta}\right) - \frac{E}{RT_p} \qquad \text{(zero order)}$$

and

$$\ln\left(\frac{E}{RT_p}\right) = \ln\left(\frac{c\nu}{2\beta}\right)\sigma_o^{1/2} + \ln\left(\frac{T_p}{\sigma_p^{1/2}}\right) - \frac{E}{RT_p} \qquad \text{(half order).}$$

where

T_p=the temperature at peak rate of desorption,

σ_p is the coverage at the temperature of peak desorption,

σ_o is the initial coverage,

ν=the rate constant for the particular desorption process,

c is a constant,

and E is the desorption energy.

A plot of $\ln(\frac{d\sigma_p}{dT_p})$ vs $\frac{1}{T_p}$ and $\ln(\frac{T_p}{\sigma_p^{1/2}})$ vs. $\frac{1}{T_p}$ shows that the desorption of zinc from ZnO_x overlayers on Cu(110) is best described as a half order process. This is shown in figure 4.3. The slope of the plot of $\ln(\frac{T_p}{\sigma_p^{1/2}})$ vs. $\frac{1}{T_p}$ is equal to $\frac{E}{R}$, giving a value of 150 kJ/mole for the desorption energy of zinc from ZnO_x on Cu(110).

Initial two-dimensional growth of ZnO_x and the effect of heat

Oxygen produces a sharp p(2×1) structure on Cu(110) after an exposure of ≥10 L O_2 corresponding to a coverage of half monolayer. For exposures between 10 L and >300 L O_2 at 150-300 K, the AES spectrum and LEED pattern do not change. In contrast, even a 3000 L O_2 exposure at 300 K is not sufficient to form a uniform ZnO surface from Zn(0001) surfaces [12]. Since oxygen is much more readily dissociated on Cu(110) than on zinc, we began all our preparations of ZnO_x overlayers with 0.5 ML O/Cu(110).

In figure 4.4(i), we plot AES signal intensities of copper, zinc, and oxygen versus zinc deposition time. Zinc was dosed in an ambient of 1×10^{-7} Torr O_2 onto a 0.5 ML O/Cu(110) (p(2×1)) surface at 150 K (the need for low temperatures will become clear later). The p(2×1) surface structure disappears after 10 minutes deposition time. From the plot of AES intensities versus deposition time, it is hard to determine the monolayer completion point. A better determination is by CO_2 adsorption on each freshly prepared ZnO_x surface. This is shown in figure 4.4(ii). A plot of the amount of CO_2 at saturation adsorption versus deposition time indicates the ZnO_x monolayer is completed after 20 minutes deposition time. The attenuation of the copper signal from its clean value is 25%, which is approximately the expected reduction for 918 eV electrons going through one monolayer.

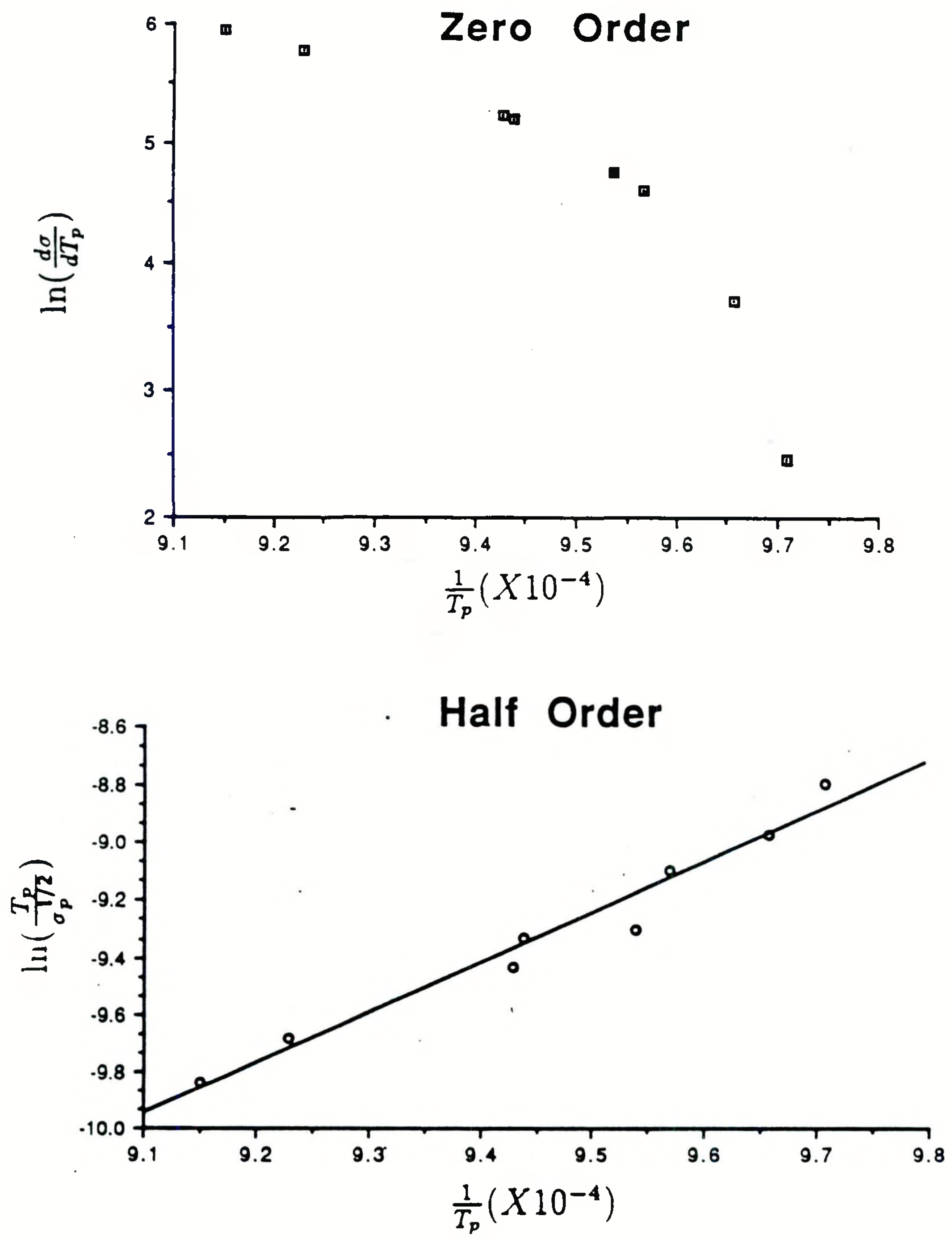

Figure 4.3: Zero and half order desorption analyses of zinc desorption, as represented by peak d of figure 4.2, from ZnO_x on Cu(110). Half order analysis shows the best fit. The slope of the plot of $\ln(\frac{T_p}{\sigma_p^{1/2}})$ versus $\frac{1}{T}$ is equal to $\frac{E}{R}$, giving a value of E=150 kJ/mole for the desorption energy of zinc from ZnO_x overlayers on Cu(110).

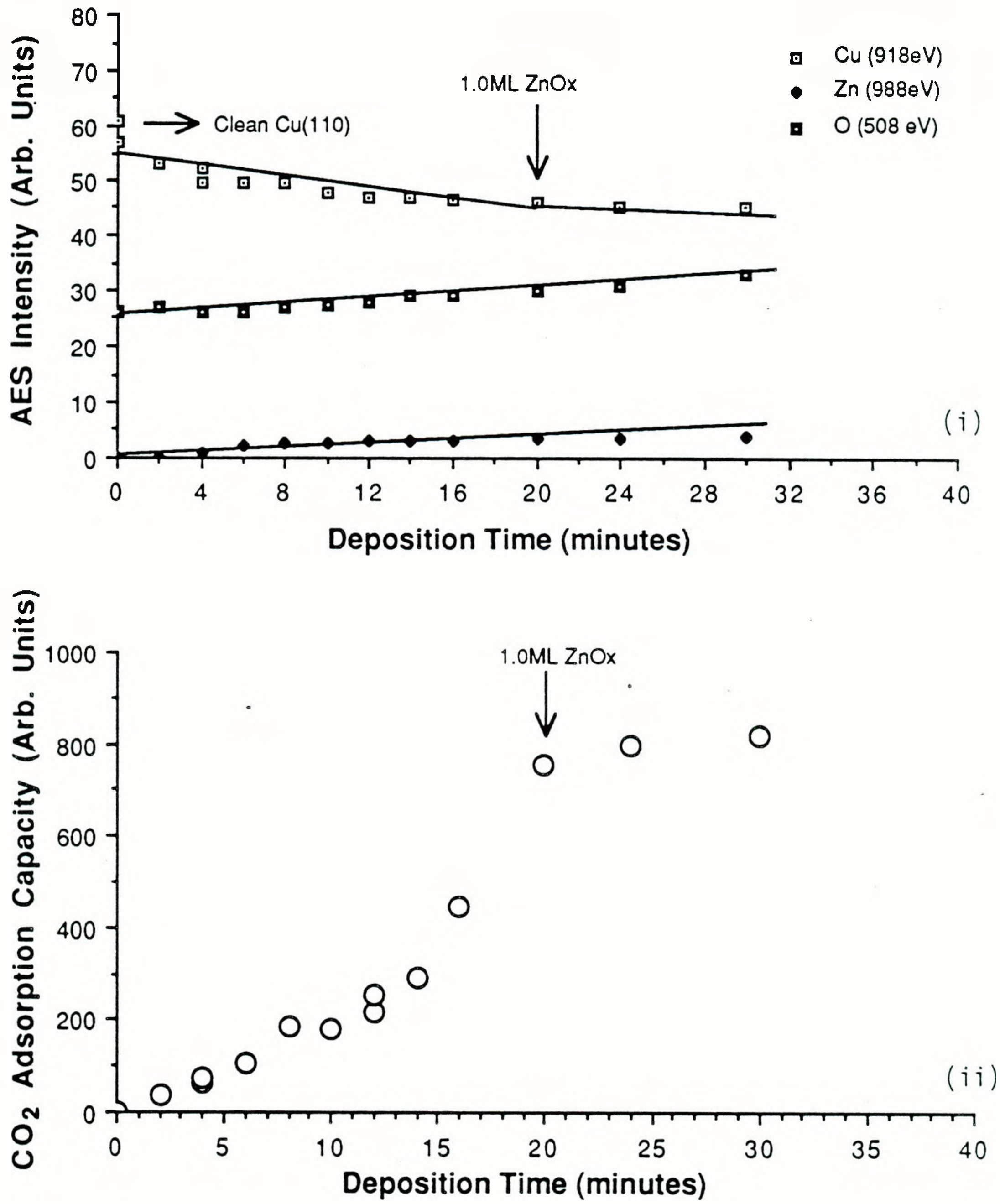

Figure 4.4: (i) AES intensities of Cu, Zn, and O peaks vs. zinc deposition time. Zinc was dosed in 1×10^{-7} Torr O_2 at 150 K. Arrow points to copper AES intensity from clean Cu(110). By depositing 0.5 ML oxygen onto Cu(110), the copper 918 eV AES signal attenuates by 10%. (ii) Accompanying saturation CO_2 adsorption for each coverage in (i). From the CO_2 adsorption versus zinc and oxygen deposition time, monolayer completion occurs after 20 minutes deposition time. Each surface is prepared fresh from 0.5 ML O/Cu(110).

Carbon monoxide and carbon dioxide TPD spectra from freshly prepared 1.0 ML ZnO_x surfaces are shown in figure 4.5(i). These surfaces adsorb less than 10% of the amount of CO that can adsorb on clean Cu(110) surfaces (and has CO desorption peak at T_p=190 K rather than T_p=218 K), and adsorbs 6.3×10^{13} CO_2 molecules/cm^2. This indicates that at saturation θ ~0.06 for CO_2 adsorption. A value of θ ~0.1 was found for the saturation coverage of CO_2 adsorption on ZnO(000$\bar{1}$) surfaces [16]. The most strongly bound CO_2 molecules on these two-dimensional ZnO_x islands desorb at T_p=510 K, 170 K higher than CO_2 from ZnO_y overlayers on gold.

This initial ZnO_x overlayer on Cu(110) undergoes very drastic changes after heating to 700 K. The new surface obtained after cooling to 150 K does not adsorb CO_2, and CO adsorption is restored to 100% of clean Cu(110) capacity with the same temperature at peak desorption (T_p=218 K) as CO from Cu(110). This is shown in figure 4.5(ii). At this point, LEED shows a diffuse (1×1) pattern. AES shows only a 20% loss in zinc and oxygen intensities after the heat treatment.

The effect of heat upon 1.0 ML ZnO_x overlayers can be seen by performing the following experiment; dose 2.0 L CO onto a freshly prepared 1.0 ML ZnO_x/Cu(110) surface, observe the CO desorption from the surface to >250 K, cool the surface back down, and titrate with CO all over again, each time increasing the temperature at which the TPD experiment ends. This is shown in figure 4.6. The ability of the surface to adsorb CO increases as the surface is exposed to higher temperatures.

For a more detailed study of the effect of temperature upon the two-dimensional ZnO_x overlayers on Cu(110), the following experiments were performed: We deposited zinc and oxygen at 150 K, and increased the temperature of the crystal to a particular value. We then examined first the CO and CO_2 adsorption capacity of the surface, and finally, we examined the zinc desorption spectrum. Each experiment required the preparation of a fresh surface, since above 300 K, the initial ZnO_x overlayer changes. A plot of the area of CO and CO_2 desorption peaks versus the annealing temperature is shown in figure 4.7. The ability of ZnO_x overlayers to adsorb CO_2 decreases by 350 K, and the ability to adsorb CO begins to increase,

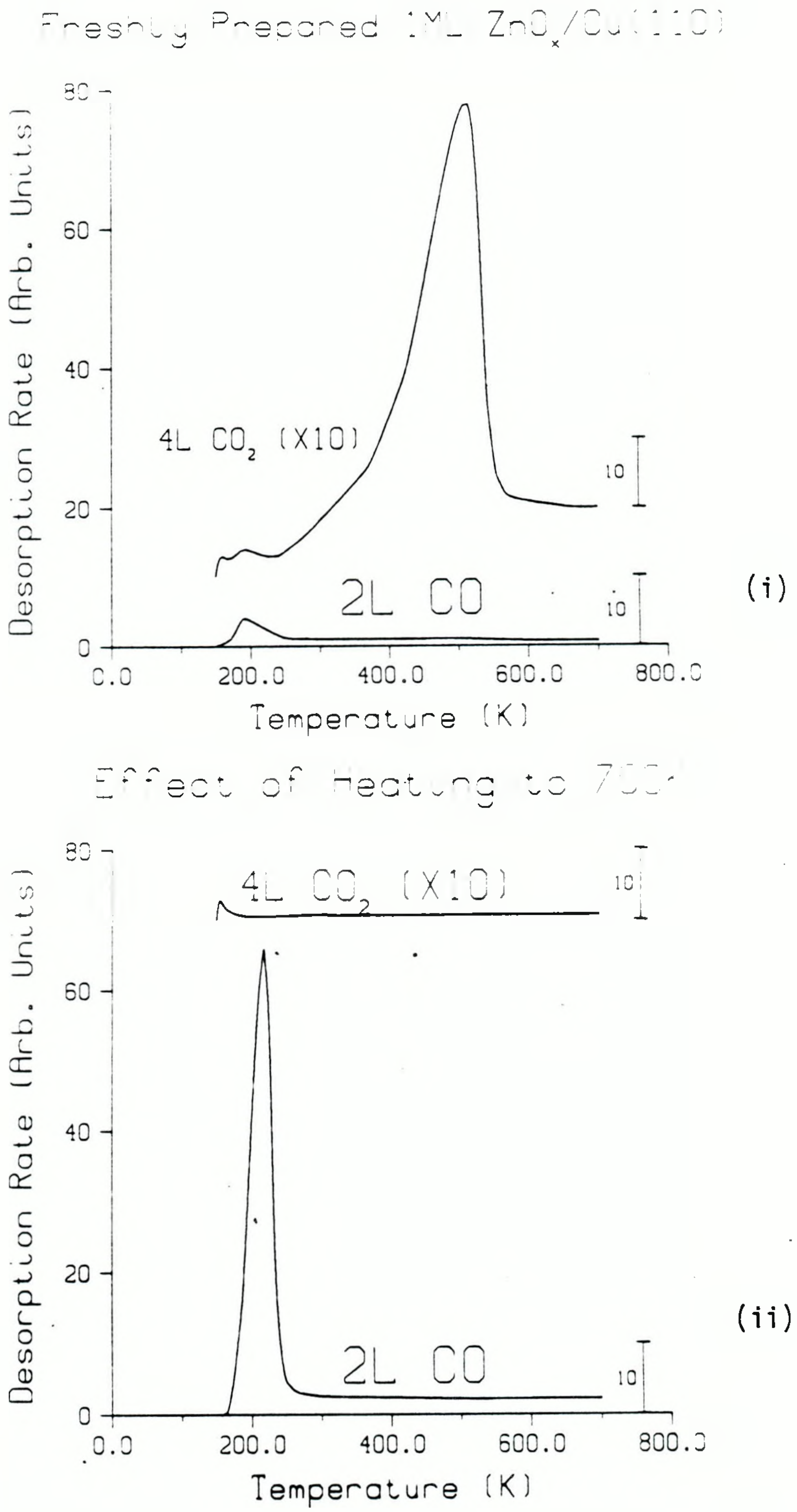

Figure 4.5: (i) CO and CO_2 TPD from a freshly prepared surface of 1.0 ML ZnO_x on Cu(110). (ii) After the first TPD; saturation CO adsorption is now 100% of that from clean Cu(110), and the surface no longer adsorbs CO_2. The third, the fourth, the fifth, etc. TPD spectrum are all exactly like (ii). The CO_2 spectra are offset from the CO spectra for clearer viewing. There is no visible order by LEED for the freshly prepared surfaces. After the first TPD, LEED shows a diffuse (1×1) pattern.

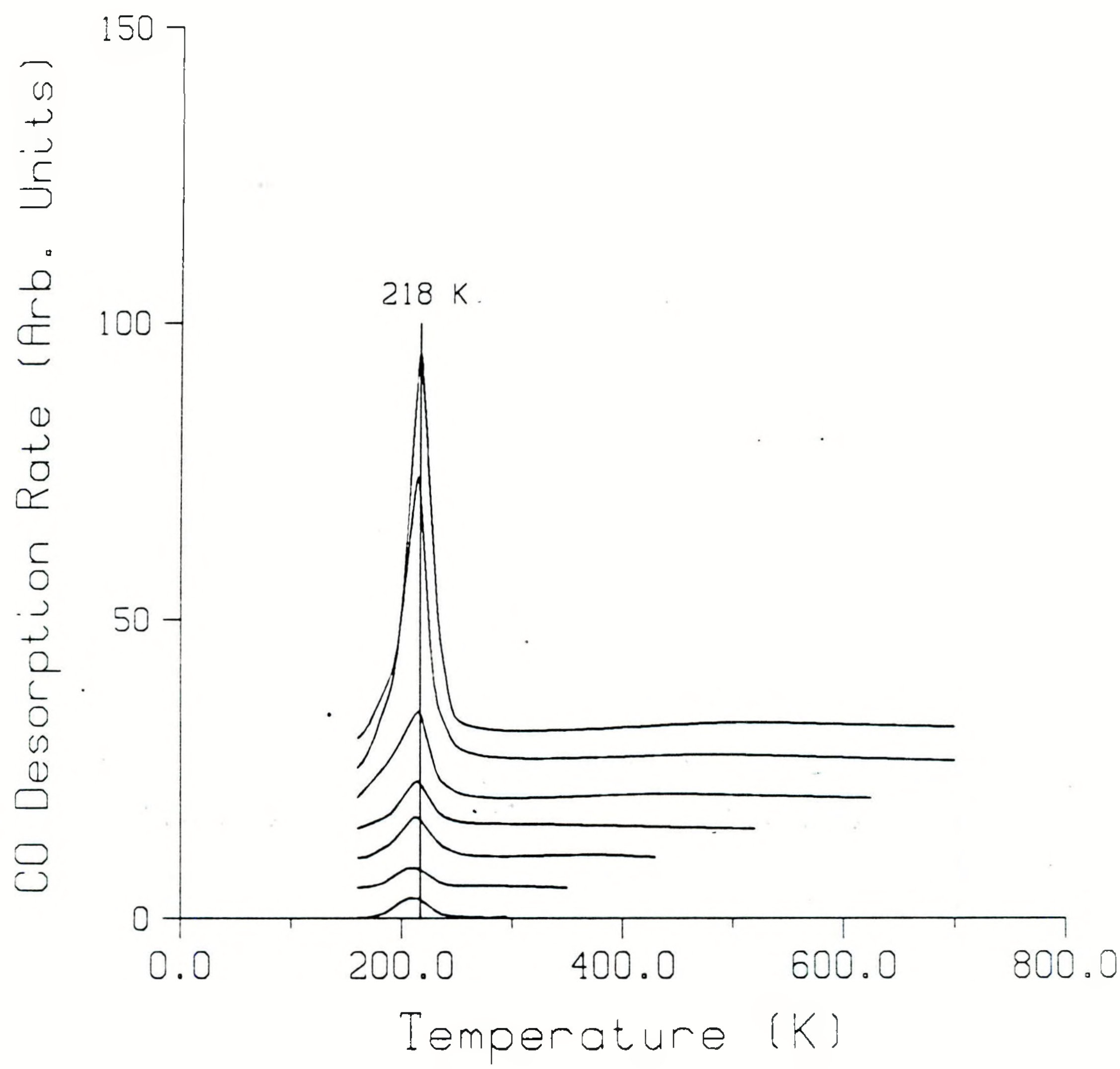

Figure 4.6: The effect of heat on the amount of CO adsorbed on 1.0 ML $ZnO_x/Cu(110)$. The sample was prepared at 150 K. Each TPD experiment consisted of a 2.0 L dose of CO at 150 K, with each consecutive CO TPD experiment ending at a higher temperature.

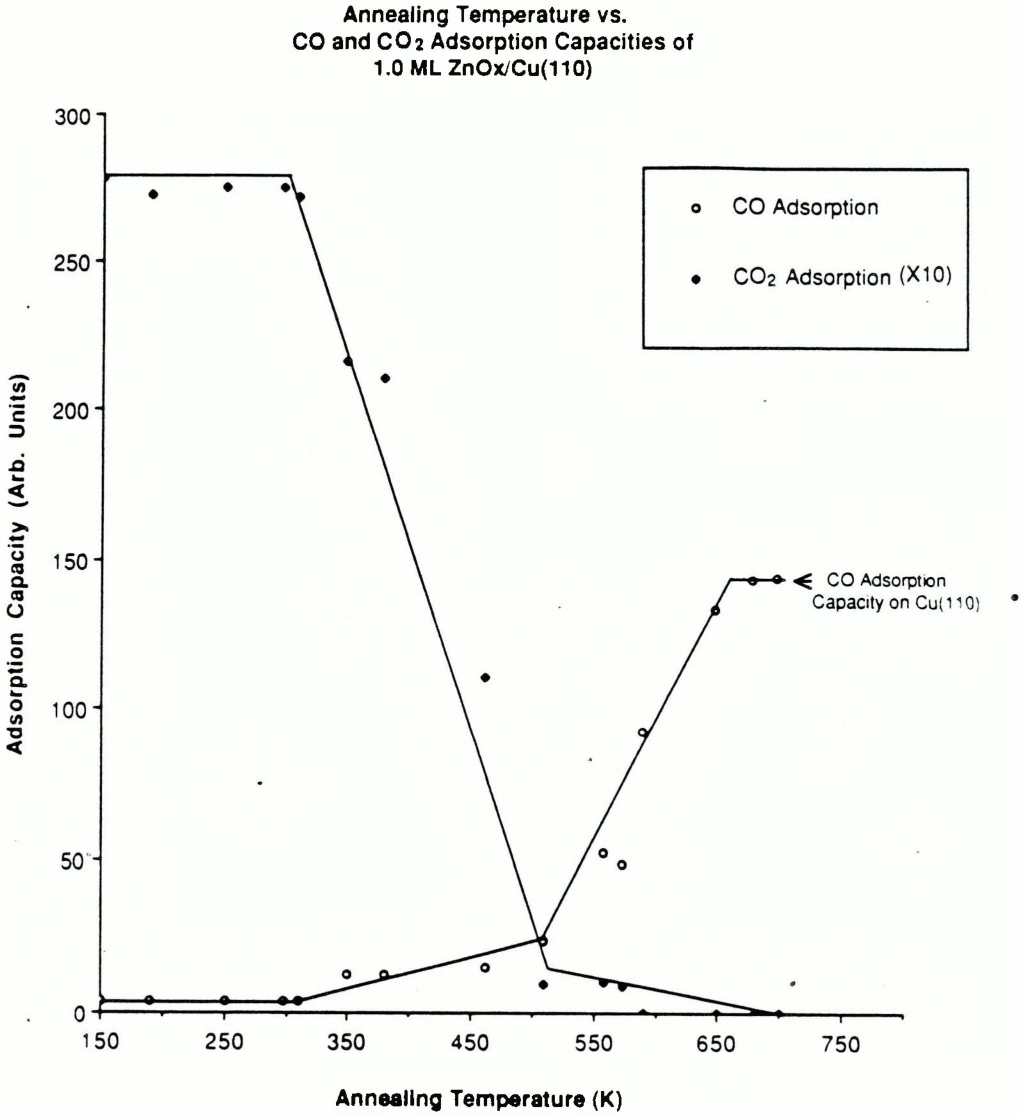

Figure 4.7: CO and CO_2 adsorption capacity vs. annealing temperature of the ZnO_x overlayer on Cu(110). Each experiment requires the preparation of a fresh surface, since above 300 K, the ZnO_x/Cu(110) surface changes.

slowly first at 350 K, and then rapidly above 500 K. Both these changes, along with no detectable desorption of zinc from the surface for temperatures $\leq$700 K point to either clustering of the ZnO_x overlayer into three-dimensional islands or diffusion of ZnO_x into the copper single crystal.

If ZnO_x dissolved into the subsurface region of copper, further annealing at 670 K would dissolve more of the ZnO_x into the bulk of copper, and hence, less zinc would be detected during zinc TPD. Figure 4.8 shows the resulting zinc TPD from a) 0.8 ML ZnO_x, and b)-c) same as (a) but with the addition of annealing at 670 K for 5 minutes (b) and 10 minutes (c). In all three cases, the amount of zinc desorbed remains the same within a 10% experimental error. This could only be true if the ZnO_x overlayer formed three-dimensional islands since increased ZnO_x dissolution into copper would result in smaller amounts of zinc desorption after annealing treatments. AES indicates that there may be further clustering of the ZnO_x islands as there is a 30-40% loss in zinc AES intensity after 5 minutes of annealing at 670 K. There is no difference by AES between the 5 minutes and 10 minutes annealing treatments.

We have seen from zinc TPD and CO chemisorption that upon heating to 700 K, the initial two-dimensional ZnO_x overlayer clusters to form three-dimensional ZnO_x islands. We believe that these ZnO_x islands are oxygen deficient due to the inability of these islands to adsorb CO_2. The detection limit of CO_2 by our mass spectrometer is about 2×10^{11} molecules which is about $(\frac{1}{300})^{th}$ of the CO_2 adsorption capacity on the initial two-dimensional ZnO_x overlayer. Within this detection limit, we do not observe any CO_2 adsorption after annealing the initial surface (prepared at 150 K) to $\geq$600 K for a fraction of a second. This inability of ZnO_x islands to adsorb CO_2 may be due to a slight loss of oxygen during the clustering process. Cheng and Kung [17] have noted that reduced ZnO single crystals of $(10\bar{1}0)$ orientation do not adsorb CO_2. If it is true that these ZnO_x islands are unable to adsorb CO_2 because they are oxygen deficient, then adding oxygen should restore their CO_2 adsorption capability. We will see in the next section that this is indeed so.

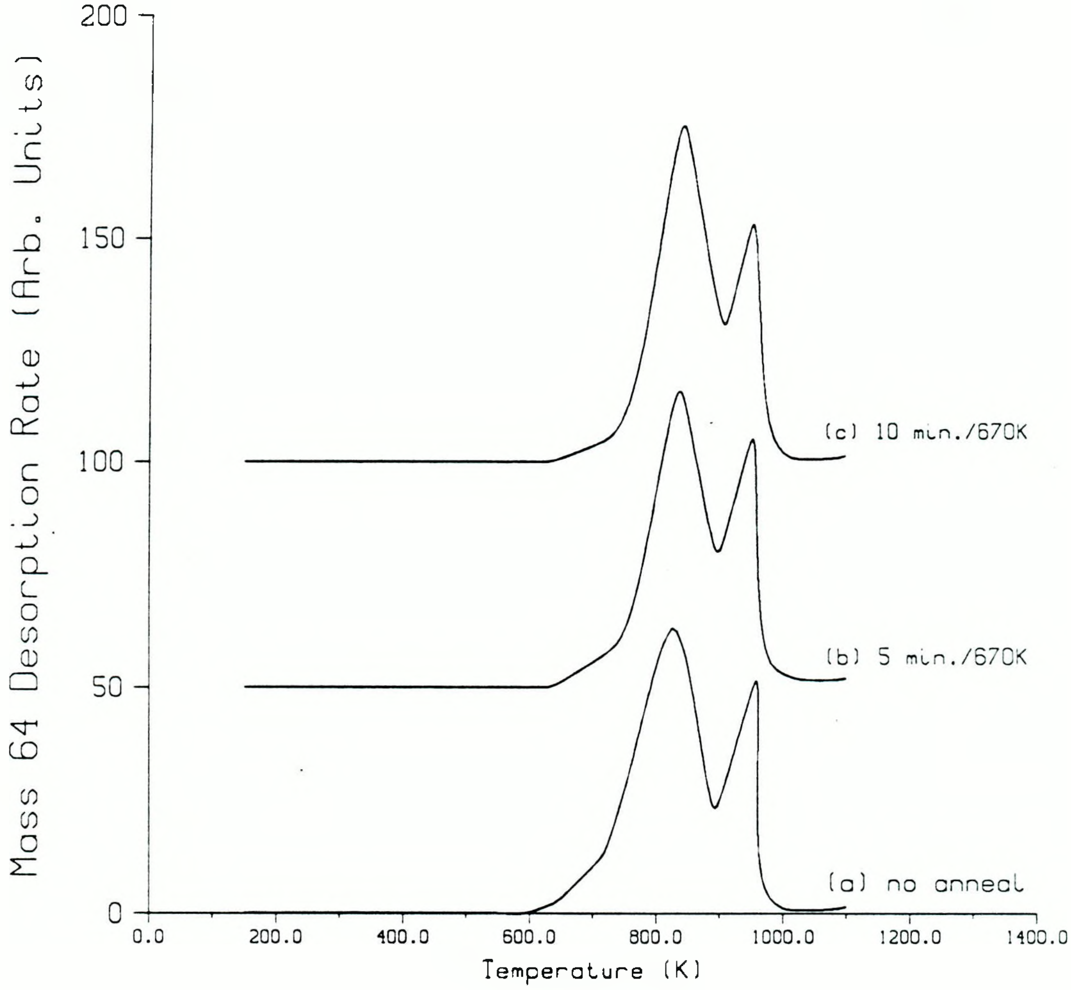

Figure 4.8: Effect of annealing on Zn TPD: a) 0.8 ML ZnO_x, b) same as (a) but annealed at 670 K for 5 minutes before Zn TPD, and c) same as (b) but annealed for 10 minutes at 670 K. TPD spectra are 100× the reference scale.

Effect of further oxygen and heat treatments on three-dimensional ZnO_x islands on Cu(110)

We show in figure 4.9(i) the effect of treating oxygen deficient three-dimensional ZnO_x islands on Cu(110) with more oxygen. We took the surface described in figure 4.5(ii) (a surface seen by AES to contain zinc, oxygen, and copper, but shown by CO and CO_2 TPD to be predominantly Cu(110)) and exposed it to 5×10^{-7} Torr O_2 for 10 minutes at 300 K followed by annealing at 700 K for 2 seconds. This treatment restores the ability of the ZnO_x islands to adsorb CO_2 (note that the highest T_p is now at 550 K) and decrease the CO adsorption capacity by ~40%. This may be interpreted as the spreading of ZnO_x islands onto Cu(110) or oxygen incorporation into deficient ZnO_x islands and adsorption of some oxygen on Cu(110). We believe the latter case to be true as patches of diffuse p(2×1) domains appear on the surface after the oxygen and annealing treatments described above, indicating oxygen adsorption on Cu(110).

Another indication that the oxygen and annealing treatments restore oxygen to deficient ZnO_x islands is that of CO and CO_2 adsorption capacity with the annealing treatment as compared to no annealing treatment. If CO is dosed onto the surface after O_2 treatment, the CO adsorption capacity decreases by 95%. But with each TPD experiment, CO adsorption capacity increases (up to that shown in figure 4.9(ia)) as each TPD experiment effectively anneals the surface for a fraction of a second at 700 K. In addition, these non-annealed oxygen treated surfaces exhibit increasing CO_2 adsorption capacity with each TPD (up to that shown in figure 4.9(ib)). All this indicates diffusion of oxygen from Cu(110) to the oxygen-deficient ZnO_x islands when the surface is heated to 700 K, hence increasing both the CO and CO_2 adsorption capacity of the surface.

We can continue oxygen treatment by an additional 5×10^{-7} Torr O_2 exposure for 10 minutes at 300 K. Carbon dioxide TPD indicates that the ZnO_x islands have remained unchanged, while the CO TPD indicates further oxygen adsorption on Cu(110). This is shown in figure 4.9(ii). Annealing this surface at 700 K for a few seconds does not change the CO and CO_2 chemisorption properties. It is because

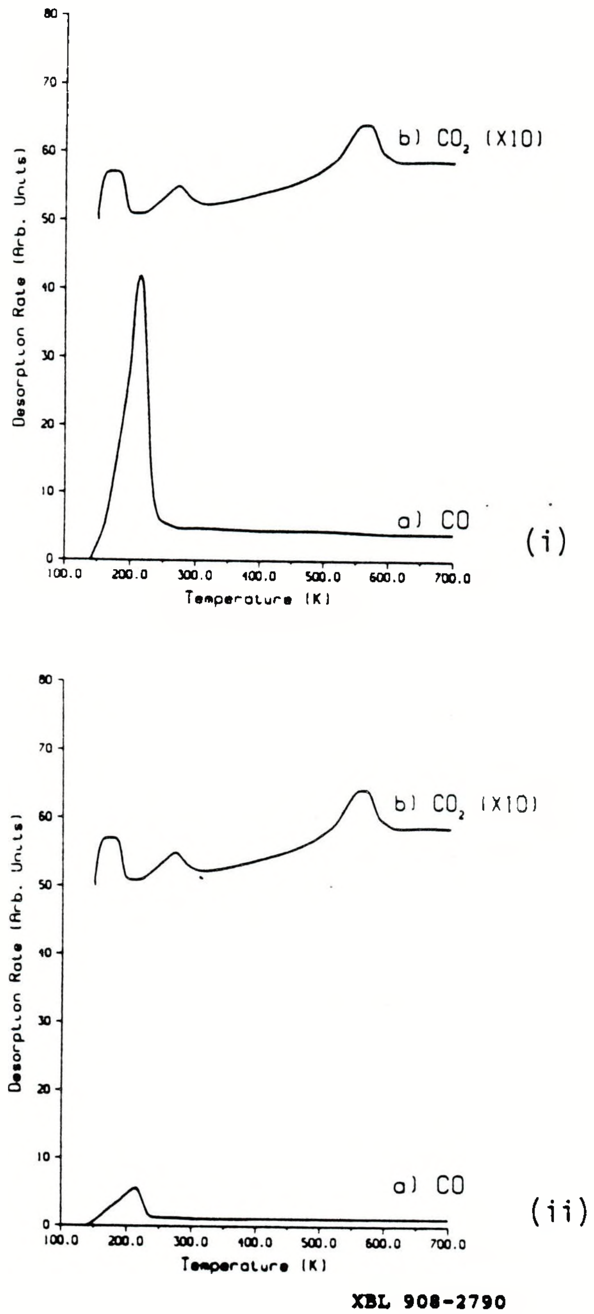

Figure 4.9: (i) Chemisorption of surface produced after surface represented in figure 4.5(ii) was exposed to 5×10^{-7} Torr O_2 for 10 minutes at 300 K and annealed at 700 K for 2 seconds. (ii) CO and CO_2 desorption spectra after an additional exposure of 5×10^{-7} Torr O_2 for 10 minutes at 300 K. All TPD data were obtained from saturation coverages of CO or CO_2. Surfaces which give CO_2 desorption spectra similar to figure 4.9 contain the highest zinc desorption peak (peak d of figure 4.2) in their zinc TPD spectra. LEED shows diffuse p(2×1) patterns throughout these oxygen treatments.

Table 4.2
Effect of Co-Adsorption on CO & CO_2 Adsorption Capacity

Treatment	Amount of CO desorbed molecules/cm^2	Amount of CO_2 desorbed molecules/cm^2
3L CO_2 then 2L CO	4.1×10^{14}	9.0×10^{13}
2L CO alone	$4.0\pm0.1\times10^{14}$	———
2L CO then 3L CO_2	3.9×10^{14}	8.8×10^{13}
3L CO_2 alone	———	$8.7\pm0.3\times10^{13}$

the ZnO_x islands no longer need oxygen that annealing at 700 K for 2 seconds does not result in loss of oxygen from the copper to the ZnO_x islands.

Zinc TPD from these stable three-dimensional ZnO_x islands always contain the highest zinc desorption peak at T_p ~1000 K (the desorption is half order so it is hard to define one T_p). This is the main difference between the zinc TPD spectra from the oxygen deficient ZnO_x islands and these "stoichiometric" ZnO_x islands.

The hypothesis that the CO and CO_2 TPD spectra shown in figure 4.9(i) are due to ZnO_x islands on Cu(110) may be further tested by co-adsorption of CO and CO_2. If there are ZnO_x clusters on Cu(110), co-adsorption of saturation coverages of CO and CO_2 should have little or no effect on CO and CO_2 adsorption capacities. Table 4.2 shows the amount of CO and CO_2 adsorbed on a "3.0 ML ZnO_x" overlayer on Cu(110). From CO titrations, this surface has ~70% of the copper surface area of clean Cu(110). No change in either CO_2 or CO adsorption capacity could be detected by co-adsorption of the two molecules, further indicating the model of three-dimensional ZnO_x islands on bare Cu(110).

We can obtain reproducible CO_2 and CO TPD spectra ending at 700 K from these three-dimensional ZnO_x islands on Cu(110). But as TPD experiments are performed with a heating rate of 30 K/s, each TPD only anneals the surface for a fraction of a second at 700 K. If we anneal these Cu-Zn-O surfaces for longer periods of time, we see changes by AES, LEED, and CO and CO_2 TPD. The changes in CO_2 TPD spectra for a 3.0 ML ZnO_x/Cu(110) surface are shown in figure 4.10 and all the changes observed are summarized in table 4.3. Carbon dioxide TPD spectra show changes in the ZnO_x overlayer from the heat treatments at 700 K. A new peak at 340 K appears and increases with annealing treatment. This indicates new adsorption sites for CO_2. But the total CO_2 adsorption capacity does not increase; on the contrary, it decreases slightly due to a decrease in the other types of adsorption sites. Auger indicates a loss in both zinc and oxygen intensity after annealing at 700 K for 2.0 minutes. This is most likely due to additional clumping of ZnO_x islands. There are no changes in either CO adsorption or in the LEED

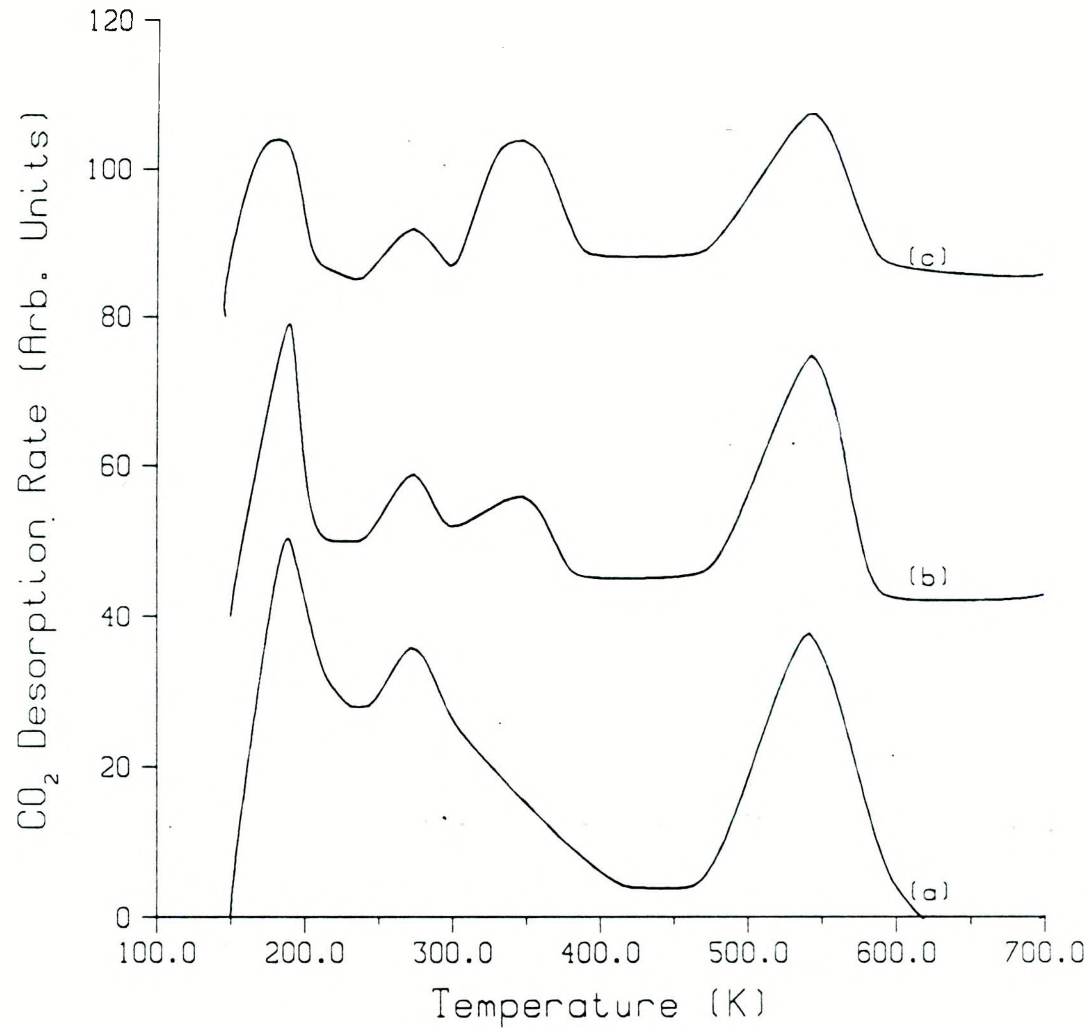

Figure 4.10: Effect of annealing at 700 K on CO_2 chemisorption properties: a) 3.0 ML ZnO_x/Cu(110), b) after annealing (a) to 700 K for 2.0 minutes, and c) after an additional 10 minutes anneal at 700 K. TPD spectra are 10× the reference scale.

Table 4.3

Summary of AES, LEED, and CO & CO_2 TPD data for 3.0ML ZnO_x/Cu(110) annealed at 700K

Surface	AES Intensities (Arb. Units) Cu Zn O	LEED Pattern	CO Adsorption Capacity (molecules/cm^2)	CO_2 Adsorption Capacity from T_p=340K (molecules/cm^2)	Amount of CO_2 from all other desorption peaks (molecules/cm^2)	Total CO_2 Adsorption Capacity (molecules/cm^2)
(a) "3.0ML ZnO_x"*	39 10 40	(1×1)	4.0×10^{14}	$<3\times10^{11}$	9.0×10^{13}	9.0×10^{13}
(b) After 700K/2.0 min.	39 6.7 32	(1×1)	4.1×10^{14}	1.4×10^{13}	6.1×10^{13}	7.5×10^{13}
(c) After an additional 700K/10.0 min.	39 6.0 32	diffuse p(2×1)	1.2×10^{14}	2.9×10^{13}	4.4×10^{13}	7.3×10^{13}

*Coverage determined by AES

pattern after the 2.0 minutes annealing treatment. However, after an additional 10.0 minutes of annealing at 700 K, CO adsorption capacity does decrease by 70%. This decrease in CO adsorption capacity is accompanied by a diffuse LEED pattern corresponding to a poorly ordered p(2×1) surface structure, indicating that the decrease in CO adsorption capacity is due to oxygen adsorption on Cu(110). The oxygen is believed to surface from the bulk of copper as the annealing is done in vacuum. Similar results were obtained for a wide range of ZnO_x coverages from 0.5 ML to 3.0 ML ZnO_x.

The heat treatments were performed in an attempt to spread the three-dimensional ZnO_x islands onto Cu(110). Since heating in vacuum failed to spread these islands, heating in oxygen was attempted; up to 5×10^{-8} Torr O_2 was used. There was no additional effect of the oxygen ambient other than to create an oxygen covered Cu(110) surface more rapidly.

We can continue to deposit zinc and oxygen and obtain approximately the same CO_2 and CO adsorption capacity (9×10^{13} molecules/cm^2 and 4×10^{14} molecules/cm^2 respectively) from about 3.0 ML to 7 ML ZnO_x (coverage determined by AES). A diffuse (1×1) LEED pattern due to the copper substrate can still be observed at ~7 ML ZnO_x. At coverages above 7 ML, the ZnO_x islands begin to collapse as evidenced by an increase in CO_2 adsorption capacity. The diffuse (1×1) LEED pattern does not completely disappear until >8 ML ZnO_x, and evidence of bare Cu(110) as detected by CO adsorption remains until >15 ML ZnO_x.

4.4 Discussion

We have seen evidence of some of the complexities anticipated in attempting to grow ZnO_x overlayers on copper single crystals; oxygen adsorption onto copper as well as zinc oxide formation, diffusion of oxygen into and out of bulk copper, and so on. We have also seen an additional complication of rapid clustering of ZnO_x into three-dimensional islands at temperatures above 300 K. Hence, to avoid three-dimensional islands, we evaporated zinc in an oxygen ambient at 150 K.

Ideally, we would like an ordered ZnO overlayer on copper. Examining the unit cells of various zinc oxide and copper single crystals, the best fit is between ZnO($10\bar{1}0$) and Cu(110): For Cu(110), a=3.61 $\AA$, b=2.55 $\AA$, and for ZnO($10\bar{1}0$), a=3.2495 $\AA$, b=5.2069 $\AA$. There is a 10% mismatch between the Cu(110) and ZnO($10\bar{1}0$) faces for one side of their unit cell, and taking twice the distance of b=2.55 $\AA$ for Cu(110) (so the overlayer is a p(2×1)), there is a 2% mismatch between the other side of the two faces. Hence, by requirement of similar unit cell dimensions, ordered ZnO layers on Cu(110) seemed plausible. However, we have seen that even with an ordered Cu(110) p(2×1)O surface prior to zinc deposition, the resulting ZnO_x overlayer displayed no long range order.

We have seen that by depositing zinc vapor and oxygen onto Cu(110), a surface species forms which adsorbs CO_2. This indicates the formation of zinc oxide. The temperature at maximum rate of desorption of CO_2 from this ZnO_x surface is 510 K, 170 K higher than from submonolayers to multilayers of ZnO_y on gold foils. This shift in binding energy may be due to interactions between copper and zinc oxide or it may be due to the structure of the ZnO_x overlayer on Cu(110). Reports in the literature have shown CO_2 desorption to occur between T_p=350 K and 400 K for ZnO single crystal orientation of ($10\bar{1}0$), ($40\bar{4}1$), and ($50\bar{5}1$) [8,17]. In contrast, the polar ZnO single crystal of (0001) orientation interacts with CO_2 more strongly, as indicated by the maximum rate of desorption of 670 K [17]. Hence, the difference in binding energy of CO_2 on the three-dimensional ZnO_x islands/Cu(110) and on ZnO_y/Au may be due to differences in the overlayer structure (i.e. dipole moment and defect density).

We have noted that the temperature of peak desorption changes for CO_2 from the two-dimensional ZnO_x islands to the three-dimensional islands. For example, the highest T_p for the two-dimensional ZnO_x overlayer is at 510 K, while for the three-dimensional ZnO_x islands, the highest T_p is at 550 K. This is most likely due to different faces of ZnO exposed in the two different cases. With additional annealing, we obtained more and more CO_2 adsorption indicative of non-polar faces of ZnO (T_p=340 K).

While we have observed various CO_2 desorption peaks depending on preparation of the surface, CO desorption is always a narrow peak centered at T_p=218 K except when the copper is covered with ≥0.4 ML oxygen. It may be surprising that ZnO_x islands have no influence on the binding energy of CO to Cu(110), but this insensitivity of CO adsorption on copper has been previously seen for CO adsorption on cobalt modified Cu(100) [18].

It would be interesting to observe the interaction of copper, zinc, and oxygen by scanning tunneling microscopy (STM) in the barrier height mode; the initial two-dimensional structures, the three-dimensional island formation upon heating above 300 K, and changes in structure and composition upon further oxygen and heat treatments.

4.5 Conclusion

It is possible to grow two-dimensional ZnO_x islands on Cu(110), but these islands cluster into three-dimensional islands above 300 K. These three-dimensional ZnO_x islands do not adsorb detectable amounts of CO_2 because of oxygen deficiency. Once these oxygen deficient ZnO_x islands are oxidized, CO_2 adsorption capacity increases to detectable levels. Carbon dioxide chemisorption properties on three-dimensional islands vary depending upon heat treatments. At first, strong adsorption associated with polar faces and/or defect sites are observed. With increasing heat treatments at 700 K, adsorption indicative of non-polar faces of ZnO increases.

Carbon monoxide adsorption on Cu(110) is unaffected by the presence of ZnO_x. Hence, CO titration can be used to determine the amount of exposed Cu(110). From a combination of CO and CO_2 titrations, it appears that zinc oxide prefers to grow as three-dimensional islands on Cu(110). These ZnO_x islands do not collapse until AES indicates >7 ML ZnO_x. Heating in vacuum and in oxygen failed to spread these islands onto the copper substrate.

References

1. R.G. Herman, K. Klier, G.W. Simmons, B.P. Finn, and J.B. Bulko, J. Catal. 56 (1979) 407.

2. J.A. Rodriguez and C.T. Campbell, J. Phys. Chem. 91 (1987) 6648.

3. C.T. Campbell, R.A. Daube, and J.M. White, Surface Sci. 182 (1987) 458.

4. K.L. Siefering and G.L. Griffin, Surface Sci. 207 (1989) 525.

5. L. Chan and G.L. Griffin, Surface Sci. 173 (1986) 160.

6. S.V. Didziulis, K.D. Butcher, S.L. Cohen, and E.I. Solomon, J. Am. Chem. Soc. 111 (1989) 7110.

7. E. Giamello, B. Fubini, and V. Bolis, Applied Catal. 36 (1988) 287.

8. W. Hotan, W. Göpel, and R. Haul, Surface Sci. 83 (1979) 162.

9. J. Nakamura, J.A. Rodriguez, and C.T. Campbell, J. Phys. Condensed Matter. 1SB (1989) 149.

10. G. Ertl, Surface Sci. 6 (1967) 208.

11. G.W. Simmons, D.F. Mitchell, and K.R. Lawless, Surface Sci. 8 (1967) 130.

12. L. Chan and G.L. Griffin, J. Vac. Sci. Technol. A3(3) (1985) 1613.

13. C.R. Brundle and R.I. Bickley, J. Chem. Soc. Faraday Trans. II 75 (1979) 1030.

14. I. Wach and R. Madix, J. Catal. 53 (1978) 208.

15. D. Kohl, M. Henzler, and G. Heiland, Surface Sci. 41 (1974) 403.

16. C.T. Au, W. Hirsch, and W. Hirschwald, Surface Sci. 197 (1988) 391.

17. W.H. Cheng and H.H. Kung, Surface Sci. 122 (1982) 21.

18. F. Falo, I. Cano, and M. Salmeron, Surface Sci. 143 (1984) 303.

Chapter 5

A Comparative Study of ZnO_x Overlayers on Cu(311), Cu(110), and high defect concentration Cu(111)

5.1 Introduction

We began our work on ZnO_x overlayers on copper with Cu(110) as the substrate (chapter 4 and reference [1]). The (110) face of copper was used as it has a small mismatch to a ZnO face; a 2% mismatch on one side of the unit cell and a 10% mismatch on the other side to a $ZnO(10\bar{1}0)$ face. Unfortunately, we found no ordered ZnO_x overlayer on Cu(110). Instead, we found ZnO_x to be most stable as three-dimensional islands at temperatures greater than 300 K in vacuum. As Cu(110) is an open, flat surface, we decided to investigate ZnO_x formation on two surfaces which represent two other distinct types of surfaces; a close-packed surface, Cu(111), and a stepped surface, Cu(311), and compare them to ZnO_x formation on Cu(110).

In this chapter, we show that upon heating above 300 K, ZnO_x clusters on all three surfaces. The clustering appears to be most extensive on the (110) and (111) faces of copper. Our use of a high defect density Cu(111) shows ZnO_x prefers to cluster to the defect sites. In addition, we show that the temperature of ZnO_x decomposition is dependent on the structure of the copper substrate.

5.2 Results

CO and CO_2 Desorption from copper (311), (110), and (111), and oxygen covered copper (311), (110), and (111)

Figure 5.1 shows CO desorption after saturation exposures on Cu(110), a high defect concentration Cu(111), and Cu(311), along with CO desorption from their 0.5 ML oxygen covered counterparts. CO desorption from Cu(110) occurs with T_p=218 K. This is in agreement with previous work which shows CO desorption with T_p=223 K [2]. CO desorption from Cu(111) produces two peaks – one centered at 165 K and the other one centered at 225 K. The peak centered at 165 K is in agreement with previous work which shows CO desorption at 168 K [3]. We believe that the peak centered at 225 K is due to defects on the Cu(111) surface. We shall see later that this defect site appears to be favored by ZnO_x islands. No previous work other than ours has been reported on CO TPD from Cu(311) (chapter 3 and reference [4]).

The common feature observed from CO TPD is that when oxygen is pre-adsorbed on the three copper surfaces, it blocks CO adsorption. From figure 5.1, we see that of the three surfaces, oxygen blocks CO adsorption most effectively on the Cu(110) surface.

Though CO desorption from the three different copper surfaces is very similar, CO_2 desorption is not. In chapter 3, we found CO_2 to adsorb on Cu(311), whilst no adsorption is observed on Cu(110) [4]. Although it has been reported that CO_2 does not interact with Cu(111) [5], we have observed some CO_2 adsorption on our Cu(111), as shown in figure 5.2. We believe this is due to adsorption by the defects on our Cu(111). Note that for the high defect density Cu(111), pre-adsorbed oxygen decreases subsequent CO_2 adsorption and blocks the defect site represented by CO desorption at T_p=225 K.

CO and CO_2 Titration of 1.0 ML ZnO_x/Cu before and after heating to 700 K

We have shown in chapter 4 (and reference [1]) that CO and CO_2 are good

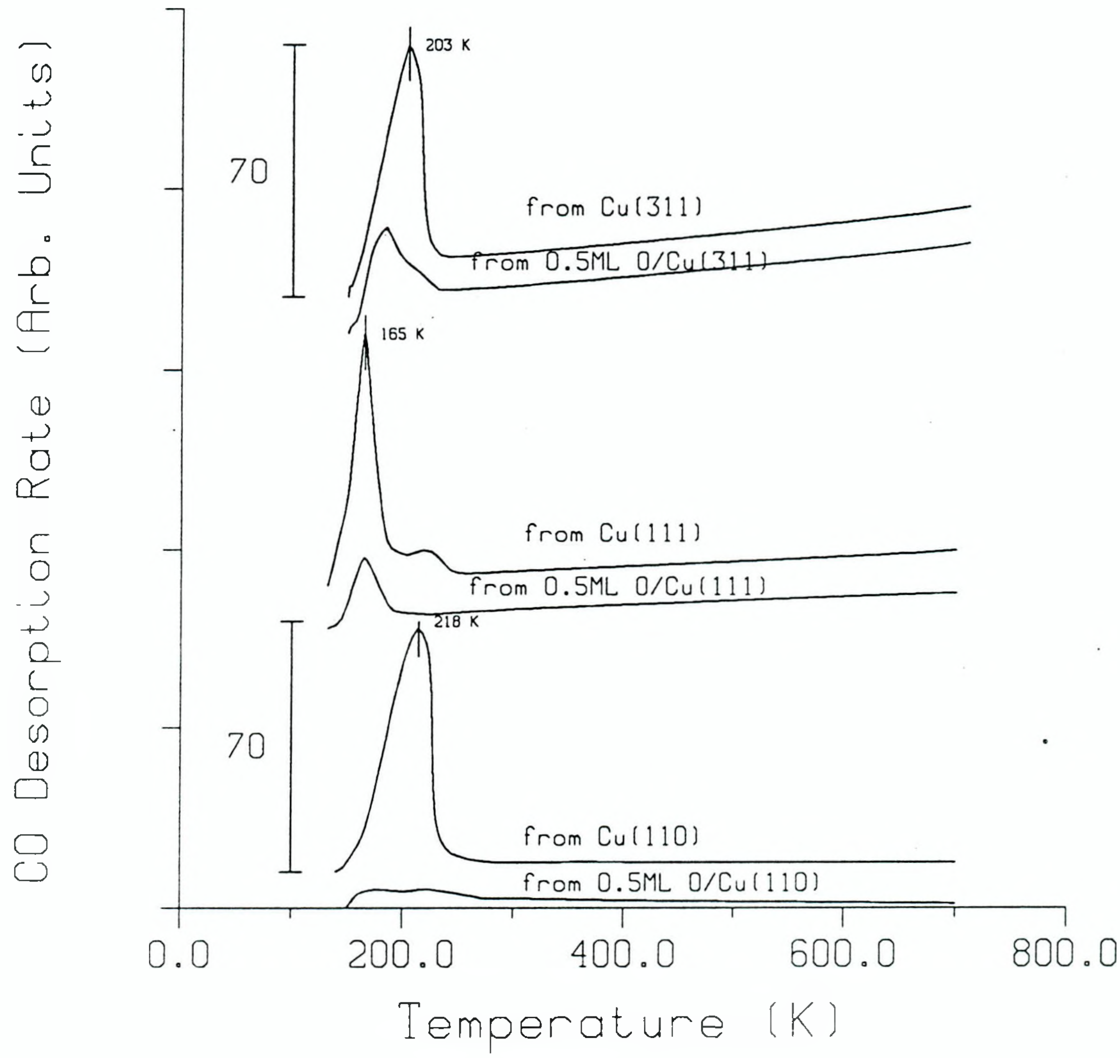

Figure 5.1: CO desorption from Cu(110), a defective Cu(111), and Cu(311), and the effect of pre-adsorbed oxygen upon CO adsorption. Enough CO was exposed to each surface to produce saturation coverages – 2.0 L CO for Cu(110), 10 L CO for Cu(111), and 20 L CO for Cu(311).

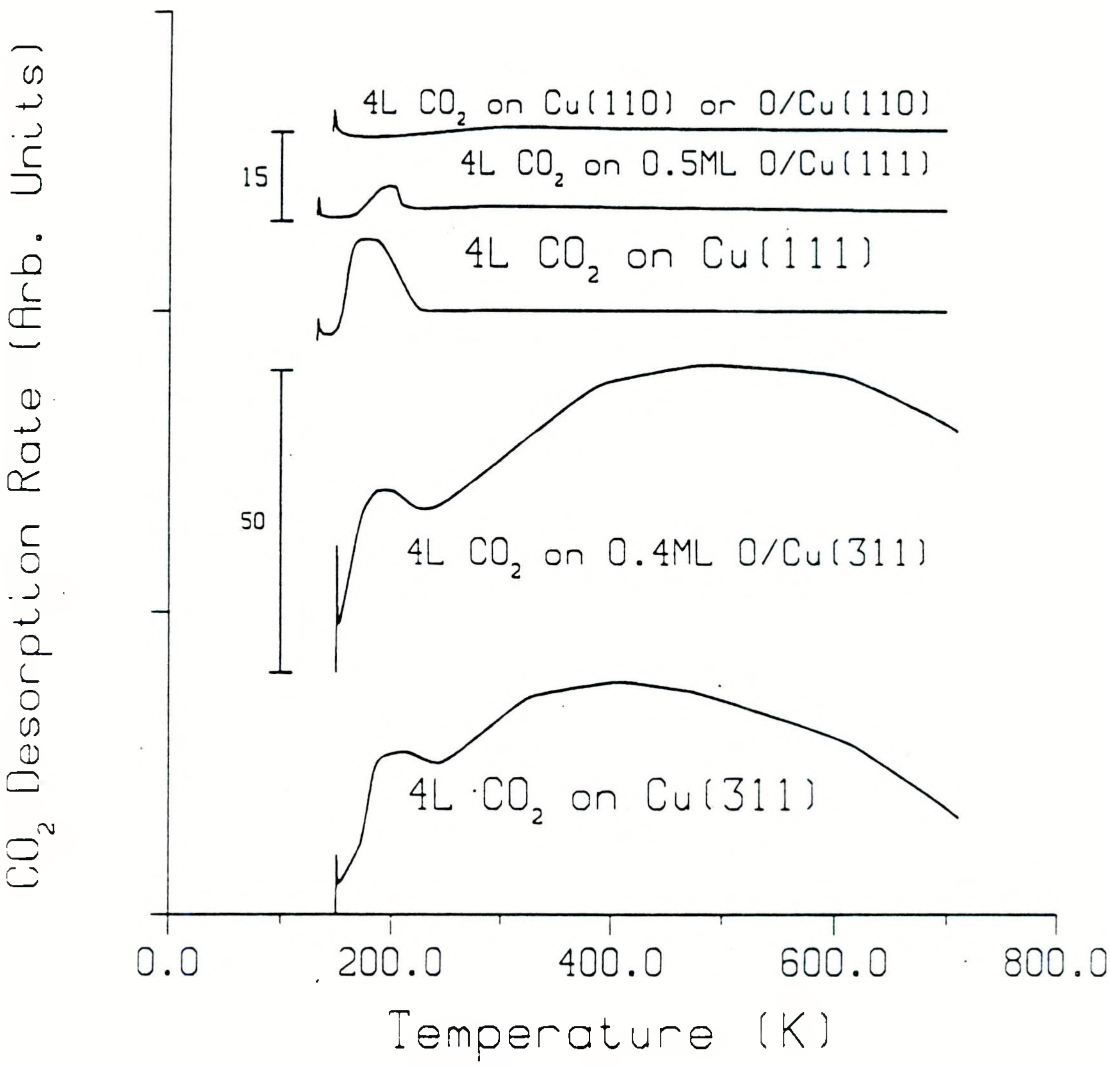

Figure 5.2: CO_2 desorption from Cu(110), a defective Cu(111), and Cu(311), and the effect of pre-adsorbed oxygen upon CO_2 adsorption. TPD spectra are 10× the reference scale of CO TPD spectra.

titration probes for Cu(110) and zinc oxide surfaces, respectively. We will use similar techniques to probe changes of the ZnO_x overlayers on the Cu(111) and Cu(311) surfaces.

Figure 5.3 shows CO and CO_2 desorption from a freshly prepared 1.0 ML ZnO_x/Cu(110) surface, and the effect heating to 700 K has on that surface. The freshly prepared ZnO_x overlayer adsorbs CO_2, but very little CO, and shows no visible LEED pattern. This surface changes dramatically after heating to 700 K. The surface then adsorbs as much CO as clean Cu(110) and with the same temperature at peak desorption. There is only a 20-30% decrease in zinc and oxygen AES signal upon heating to 700 K.

Similar changes in CO adsorption capacity occur after heating 1.0 ML ZnO_x/Cu(311) and 1.0 ML ZnO_x/Cu(111) to 700 K, as shown in figures 5.4 and 5.5. Additionally, upon heating to 700 K, we found that the amount of CO_2 desorbed between 400-500 K decreases on all three surfaces. Remember that, in the absence of ZnO_x, CO_2 adsorbs on both the Cu(311) and defective Cu(111). Hence, the interpretation of CO_2 TPD spectra for the ZnO_x overlayers on Cu(311) and Cu(111) surfaces is not as clear-cut as it was for the Cu(110) substrate. However, it is apparent that the copper surface area increases upon heating the ZnO_x overlayer on all three copper surfaces. As with 1.0 ML ZnO_x/Cu(110), no visible LEED pattern could be seen on a freshly prepared 1.0 ML ZnO_x/Cu(311) and 1.0 ML ZnO_x/Cu(111). After annealing to 700 K, all three surfaces displayed a poorly ordered (1×1) surface structure together with a reduction of the zinc and oxygen Auger signal by approximately 30%.

The change in the CO TPD spectrum of 1.0 ML ZnO_x/Cu(111) upon heating is of particular interest. Comparing figure 5.5B to figure 5.1, one can see that CO desorption from a 1.0 ML ZnO_x/Cu(111) surface heated to 700 K is very similar to that of CO desorption from Cu(111) except for the peak centered at 225 K. This high temperature peak is not visible on the ZnO_x/Cu(111) surface, indicating that ZnO_x has clustered onto the defect sites of Cu(111).

We have seen that drastic changes in chemisorption properties of 1.0 ML ZnO_x

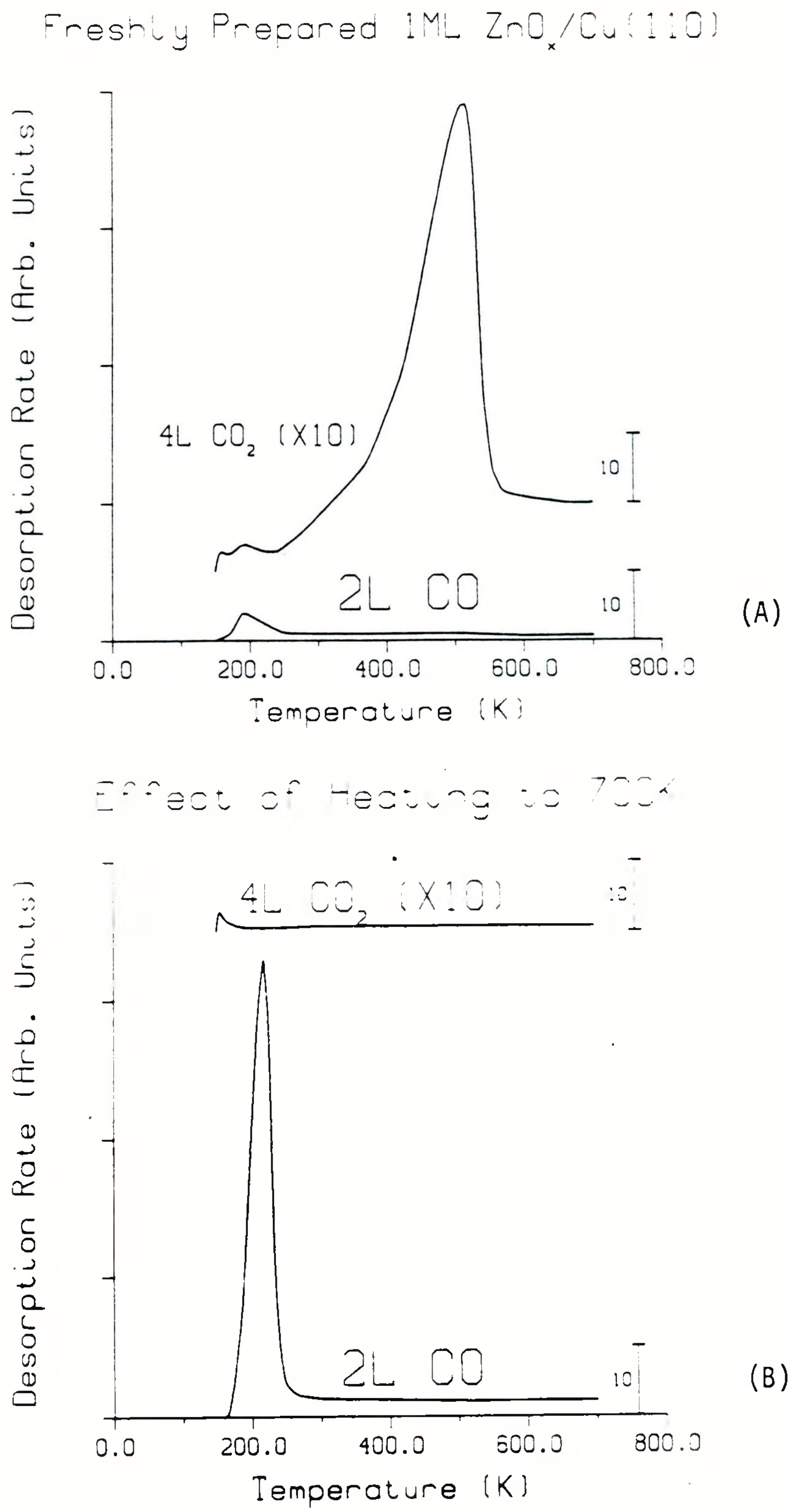

Figure 5.3: (A) CO and CO_2 TPD from freshly prepared 1.0 ML ZnO_x/Cu(110) surfaces. (B) The effect of annealing a 1.0 ML ZnO_x/Cu(110) surface to 700 K as seen by CO and CO_2 titration. AES zinc and oxygen signals decrease by 20-30% and a visible (1×1) LEED pattern appears after annealing to 700 K.

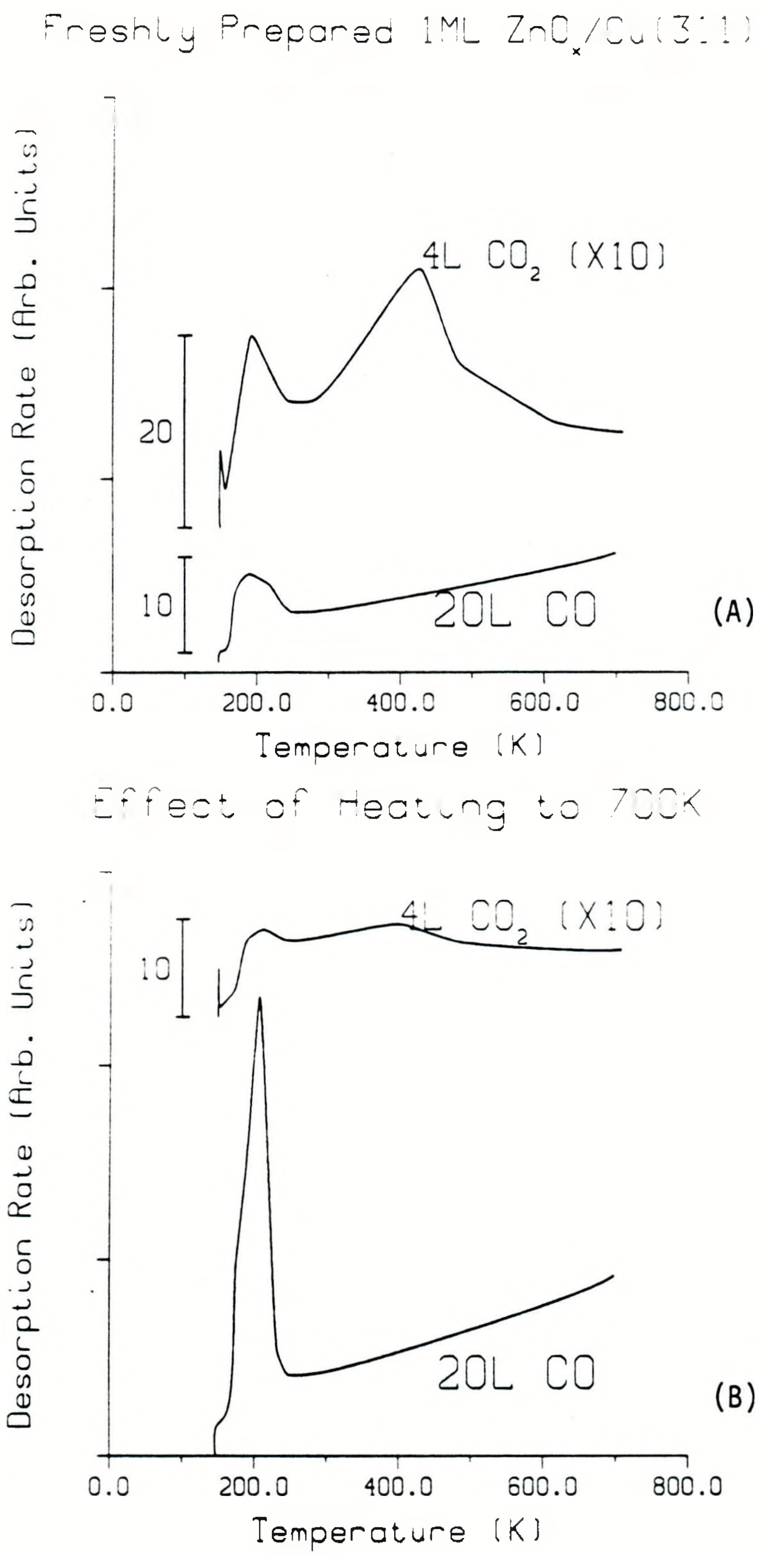

Figure 5.4: (A) CO and CO_2 TPD from freshly prepared 1.0 ML ZnO_x/Cu(311) surfaces. (B) The effect of annealing a 1.0 ML ZnO_x/Cu(311) surface to 700 K as seen by CO and CO_2 titration. AES zinc and oxygen signals decrease by ~30% and a visible (1×1) LEED pattern appears after annealing to 700 K.

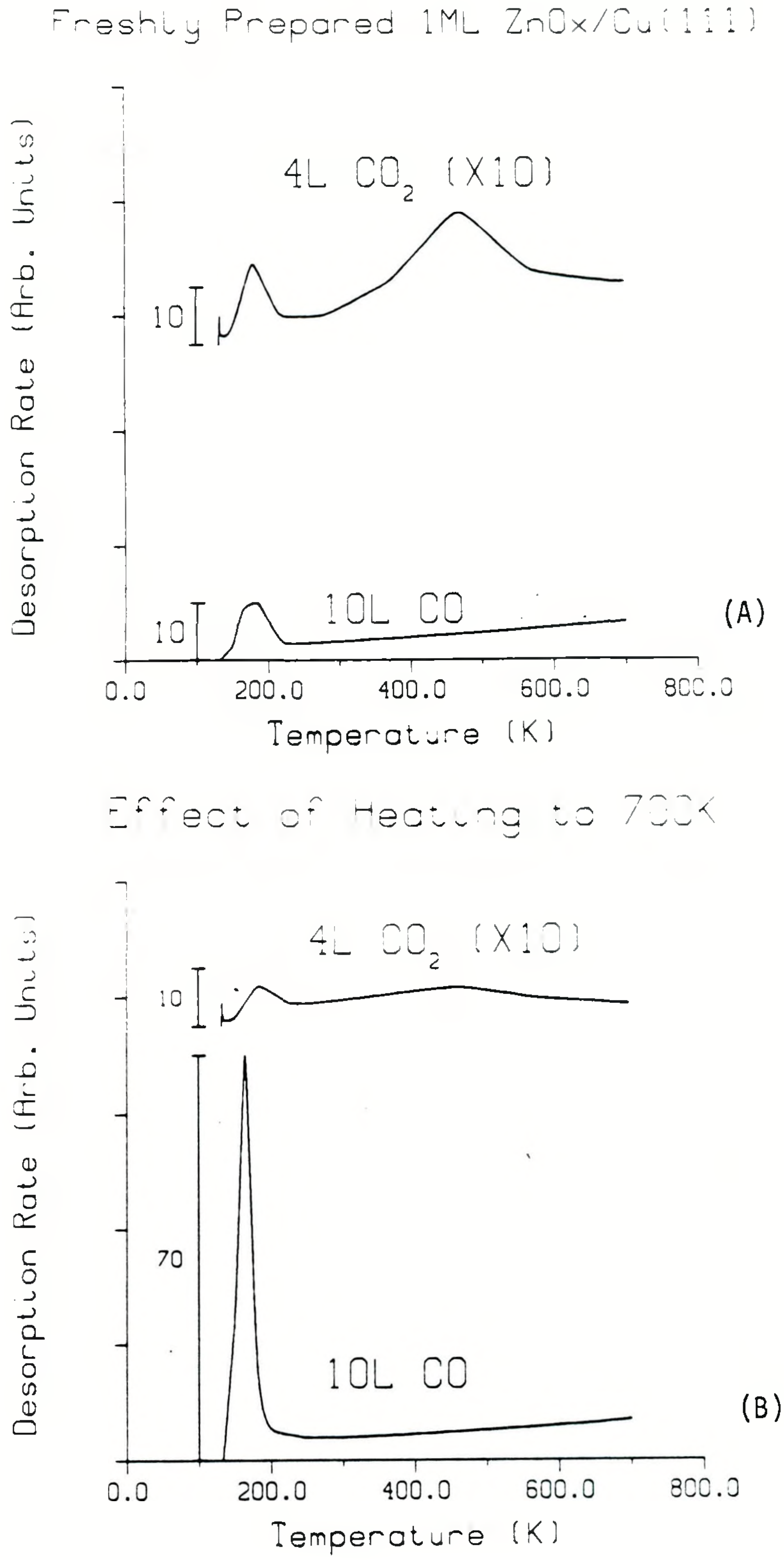

Figure 5.5: (A) CO and CO_2 TPD from freshly prepared 1.0 ML ZnO_x/Cu(111) surfaces. (B) The effect of annealing a 1.0 ML ZnO_x/Cu(111) surface to 700 K as seen by CO and CO_2 titration. AES zinc and oxygen signals decrease by ~30% and a visible (1×1) LEED pattern appears after annealing to 700 K.

overlayers on three different copper surfaces occur upon heating to 700 K. Next, we examined the effect of heat upon CO and CO_2 adsorption capacities of 1.0 ML ZnO_x overlayer on Cu(110), Cu(311), and Cu(111) substrates. This is shown in figure 5.6. Each sample was heated to the annealing temperature indicated for a fraction of a second, cooled back down to 150 K (or 130 K for Cu(111)), and then CO or CO_2 TPD experiments performed. Each sample had to be freshly prepared as the surface changes after heating above 300 K. For 1.0 ML ZnO_x/Cu(110), CO adsorption capacity increases and CO_2 adsorption capacity decreases with increasing annealing temperature. For 1.0 ML ZnO_x/Cu(311) and 1.0 ML ZnO_x/Cu(111), the CO adsorption capacity also increases as the annealing temperature is raised.

We have shown that for 1.0 ML ZnO_x on Cu(110), this change in adsorption capacity is due to clustering of ZnO_x (chapter 4 and reference [1]). The extent of ZnO_x clustering is large enough for 1.0 ML ZnO_x/Cu(110) to obtain 90-100% of the CO adsorption capacity of clean Cu(110) after annealing to >650 K. For 1.0 ML ZnO_x/Cu(111), the extent of clustering is again large enough to obtain 90-100% of the CO adsorption capacity of clean Cu(111). These two cases contrast with that of 1.0 ML ZnO_x/Cu(311) annealed to 700 K, which achieves only 60-70% of the adsorption capacity of clean Cu(311). This may be due to a larger ZnO_x island perimeter in the case of 1.0 ML ZnO_x/Cu(311), but it is difficult to conclude anything without knowledge of CO and ZnO_x adsorption sites on Cu(311).

One may argue that it is excess oxygen on the Cu(311), and not ZnO_x islands, which is blocking CO adsorption. Excess oxygen may also be responsible for the blocking of the CO adsorption site with T_p=225 K on the Cu(111). To investigate this, we performed the following experiment: half a monolayer of oxygen was deposited on each copper surface, and then, in an ambient pressure of 10^{-10} Torr, zinc was evaporated onto each copper single crystal, annealed at 700 K for a second, and the resulting surface titrated with CO. By evaporating zinc onto the oxygen covered copper surface, and annealing to 700 K, the zinc combines with oxygen adsorbed on the copper surfaces to form ZnO_x islands. Thus, the resulting surface has more free copper surface area than the 0.5 ML O/Cu we began the experiments with. This

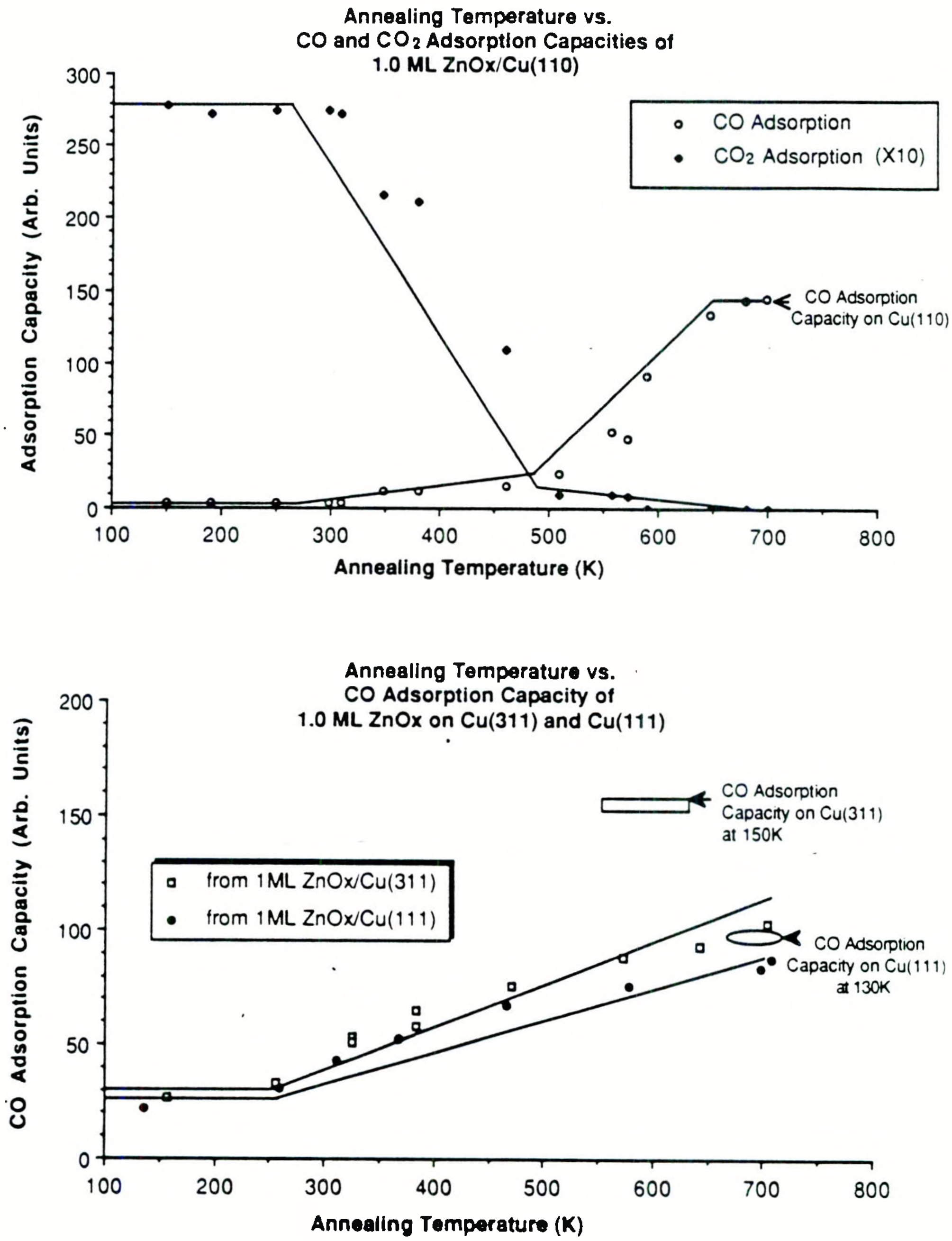

Figure 5.6: (A) CO and CO_2 adsorption capacities as a function of annealing temperature for 1.0 ML ZnO_x/Cu(110). Each surface was prepared at 150 K, and heated to the indicated annealing temperature for a fraction of a second, and then the CO or CO_2 adsorption capacity measured. (B) CO adsorption capacity as a function of annealing temperature for 1.0 ML ZnO_x overlayers on Cu(311) and Cu(111). The ZnO_x/Cu(111) surfaces were prepared at 130 K and the ZnO_x/Cu(311) surfaces were prepared at 150 K. Each experiment requires the preparation of a fresh surface since above 300 K, the ZnO_x/Cu surfaces change.

change in copper surface area is monitored by CO titration. For all three copper substrates, a plateau in the CO adsorption capacity was reached after 0.4-0.5 ML zinc had been deposited onto 0.5 ML O/Cu and annealed to 700 K. The maximum CO adsorption capacity on ZnO_x/Cu(111) and ZnO_x/Cu(110) is, again, 90-100% of the adsorption capacity of the corresponding clean surface, as shown in figure 5.7. The CO adsorption from a 0.5 ML O/Cu(111) that has reacted with 0.5-0.7 ML zinc is just like figure 5.5B – the CO peak with T_p=225 K is missing. For 0.5 ML O/Cu(311) reacted with 0.5-0.7 ML zinc, the CO adsorption capacity reached upon annealing to 700 K is only 60-70% of the CO adsorption capacity of clean Cu(311). This is also shown in figure 5.7. These studies suggest that it is ZnO_x islands, and not surface oxygen chemisorbed on copper, that is blocking the CO adsorption sites.

Zn Desorption from ZnO_x/Cu(311), ZnO_x/Cu(110), and ZnO_x/Cu(111)

Zinc desorption from Cu(110), Cu(311), and Cu(111) under various oxidation conditions is shown in figure 5.8. The temperature at peak desorption of zinc from the various surfaces is dependent on:

1) The crystal face of the substrate.

2) The extent of oxidation, which is dependent on crystal face as well as oxidation conditions.

Oxygen dissociation is a prerequisite for ZnO_x formation from zinc and O_2. Molecular oxygen can be dissociated on zinc or on the copper substrate. We have found that the formation of a 0.5 ML coverage of oxygen requires an order of magnitude greater O_2 exposure for Cu(111) than for either Cu(110) or Cu(311) between 150-300 K. This indicates that dissociation of molecular oxygen occurs at a rate which is an order of magnitude slower on Cu(111) than on Cu(311) and Cu(110). Similar results have been found for oxygen interaction with Cu(111) and Cu(110) by other investigators [7,8]. In addition, we have observed that zinc is at

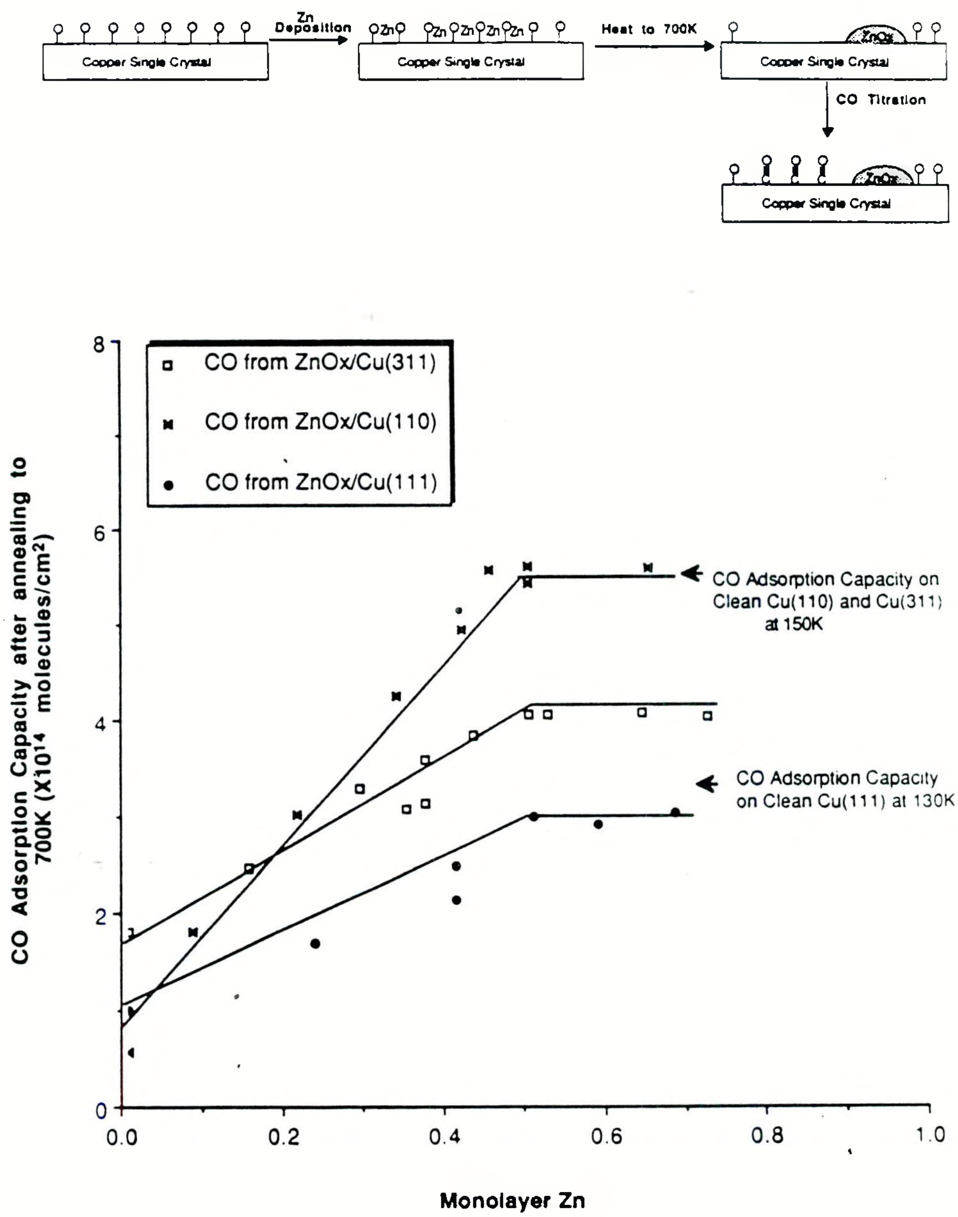

Figure 5.7: Removal of oxygen on copper single crystals with elemental zinc. Zinc takes away the chemisorbed oxygen on copper to form ZnO_x islands. The extent of the clustering is titrated by saturation coverages of CO.

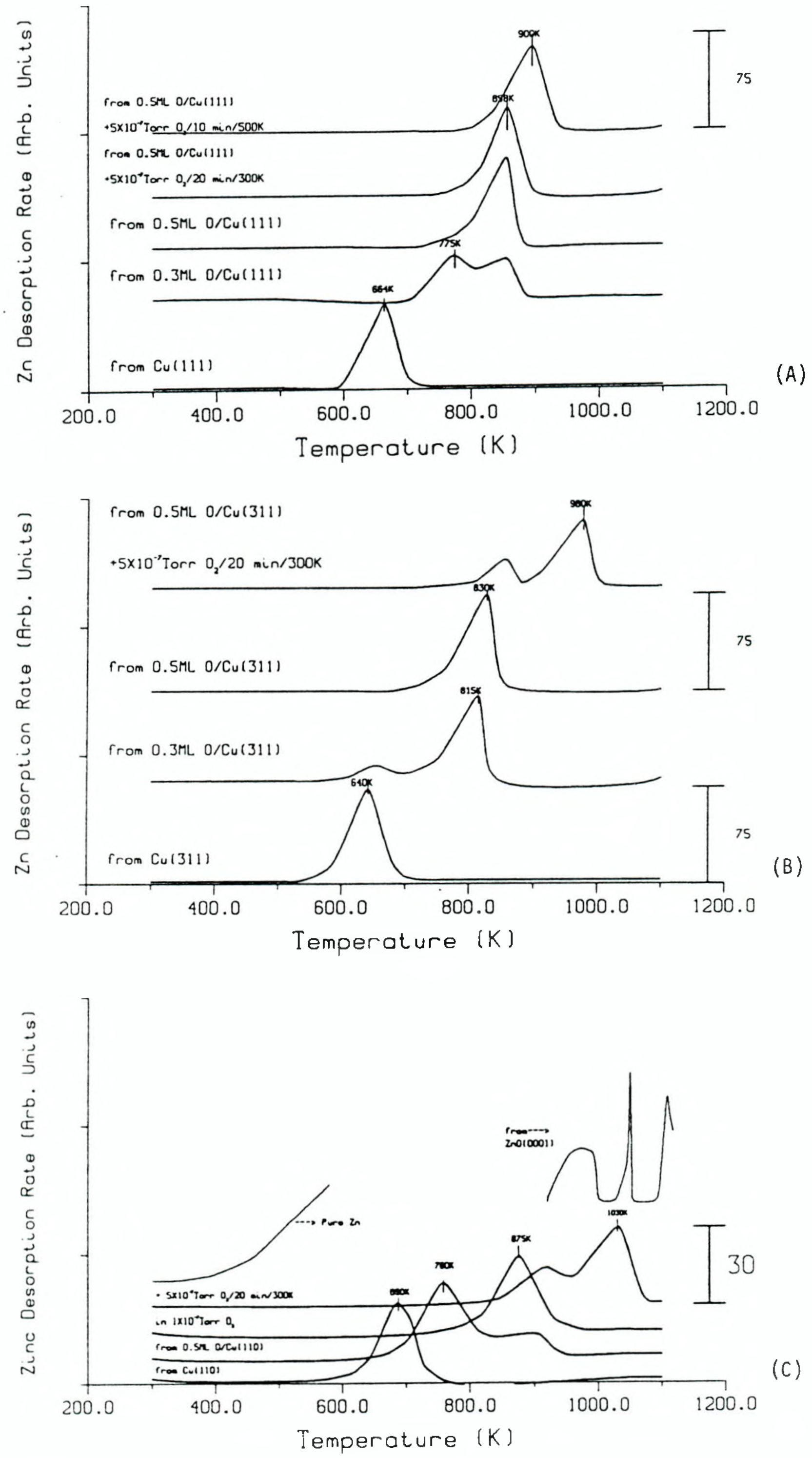

Figure 5.8: The desorption of zinc after various oxidation treatments for three different copper substrates. (A) 0.3 ML of zinc from Cu(111). (B) 0.3 ML of zinc from Cu(311). (C) 0.1 ML of zinc from Cu(110). AES shows that no zinc is left on any of these Cu-Zn-O surfaces after heating to 1100 K. As reference, zinc from multilayers of zinc on Cu(110) and zinc from a ZnO(0001) single crystal are shown. The desorption of zinc from ZnO(0001) is reproduced with permission from the authors of reference [6] and is not on the same scale as the rest of the TPD curves. All Zn TPD spectra are 100× the reference scale.

least an order in magnitude slower at dissociation of molecular oxygen than Cu(110). Hence, it is not surprising that highly oxidized zinc (represented by zinc desorption at T_p ~1000 K) requires more severe oxidation conditions to form on Cu(111) than on Cu(311) or Cu(110). This is shown in figure 5.8.

We believe that the temperature of peak desorption of zinc is dependent on crystal face as well as oxidation conditions. This can be seen by comparing zinc desorption from Cu(110) and Cu(311). The difference between the T_p for zinc desorption from Cu(110) and for zinc desorption from 0.5 ML O/Cu(110) is 70 K, whilst the difference is 175 K for the case of Cu(311). This difference in temperature is much greater than our ± 5 K error bar. AES shows that no zinc is left on any of these Cu-Zn-O surfaces after heating to 1100 K.

We did not find simultaneous copper and oxygen desorption with the zinc from any of the model Cu-Zn-O surfaces. Oxygen from ZnO_x decomposed to form surface oxygen on the copper substrate, and does not begin to desorb until greater than 1000 K, along with the copper.

5.3 Discussion

We have compared the formation of ZnO_x overlayers on three different copper surfaces. By CO titration, AES, and LEED, we see that zinc oxide clusters above 300 K on all three surfaces, and appears to cluster more extensively on the Cu(111) and Cu(110) surfaces than on the Cu(311) surface. We cannot be certain that the differences seen by CO titration are due to differences in ZnO_x cluster size on each substrate since we do not know the binding sites of CO nor of ZnO_x islands on Cu(311). It would be interesting to see the difference in ZnO_x island perimeter size on Cu(311) and Cu(110) substrates by scanning tunneling microscopy (STM). Even more interesting would be to observe the image, on an atomic scale, of CO interaction to these Cu-Zn-O surfaces; the adsorption sites of CO on Cu(311) and the changes in CO adsorption on Cu(311) in the presence of ZnO_x islands.

Zinc desorption resulting from the decomposition of ZnO_x on the three different copper surfaces appears to depend on the structure of the copper substrate as well as the extent of oxidation. Although ZnO_x decomposes at different temperatures on the three substrates studied, in all cases, ZnO_x decomposition produces surface oxygen and zinc vapor. It would be interesting to observe, by a combination of STM and TPD, the adsorption sites corresponding to the various binding energies observed by TPD. In addition, the decomposition process of

$$ZnO_x \rightarrow O_{(surface)} + Zn_{(g)}$$

should be investigated on the atomic scale in order to understand the reaction pathway.

5.4 Conclusions

We have seen that ZnO_x clusters above 300 K on all three copper substrates, and that the ZnO_x clusters on Cu(311) block more CO adsorption sites on Cu(311) than on the Cu(110) and Cu(111) substrates. By comparing the CO TPD of a high defect density Cu(111) and the CO TPD of 1.0 ML ZnO_x/Cu(111) that has been annealed to 700 K, we see that ZnO_x clusters at the defect sites. The decomposition of submonolayers of ZnO_x on copper substrates produces zinc vapor and surface oxygen. The temperature at which ZnO_x decomposes on copper is dependent on the structure of the copper substrate.

References

1. Sabrina S. Fu and G.A. Somorjai, Surf. Sci. 237 (1990) 87.

2. I.E. Wachs and R.J. Madix, J. Catal. 53 (1978) 208.

3. W. Kirstein, B. Krüger, and F. Thieme, Surf. Sci. 176 (1986) 505.

4. Sabrina S. Fu and G.A. Somorjai, submitted to Surf. Sci.

5. F.H.P.M. Habraken, E. Kieffer, and G.A. Bootsma, Surf. Sci. 83 (1979) 45.

6. D. Kohl, M. Henzler and G. Heiland, Surf. Sci. 41 (1974) 403.

7. H. Niehus, Surf. Sci. 130 (1983) 41.

8. A.R. Balkenende, Ph.D. Thesis, (1990) 62.

Chapter 6

The Rôles of Chemisorbed Oxygen and Zinc Oxide Islands on Cu(110) surfaces for Methanol Decomposition

6.1 Introduction

We have seen, in chapters 4 and 5, that ZnO_x clusters to three-dimensional islands upon heating above 300 K on Cu(110), Cu(311), and Cu(111). In this chapter, we use the most well-characterized of these surfaces – ZnO_x on Cu(110) – and add chemisorbed oxygen onto the copper part of the surface. We then examine methanol interaction with these model Cu-Zn-O surfaces.

Several investigators [1,2] have found that after reaction in $CO/CO_2/H_2$ gases, the more active Cu-Zn-O catalysts have 30-60% of their copper surface area covered with oxygen. Ren and co-workers [3] have shown that CO_2 has an inhibiting effect on methanol synthesis catalysts that do not contain copper but has a promotional effect on catalysts containing copper. This, along with studies which have shown that CO_2 produces chemisorbed oxygen on the copper component of the catalysts [4], suggests that chemisorbed oxygen on the copper component has a promotional effect on methanol synthesis over Cu-Zn-O surfaces. It has been proposed by Chinchen, Spencer, Waugh, and Whan [4] that the rôle of chemisorbed oxygen on supported copper catalysts is to promote CO_2 adsorption on the copper component of the catalysts. In this chapter, we will show that chemisorbed oxygen on the copper component also plays a rôle in promoting the total amount of formate formation.

In addition to studies of Cu-Zn-O catalysts, various investigations concerning methanol interaction with zinc oxide and oxygen modified Cu(110) have been reported. Wachs and Madix [5] monitored methoxy and formate formation upon chemisorption of methanol on oxygen modified Cu(110) (henceforth denoted O/Cu(110)) surfaces by observing their decomposition into CH_2O and CO_2, respectively. They found that both the amount of $[CH_2O]_{methoxy}/CH_3OH$ (to emphasize the relationship between the various species, we have used the notation $[X]_Y/Z$, where X is the decomposed product from intermediate Y, produced by adsorption of Z) and $[CO_2]_{formate}/CH_3OH$ production increased, and then decreased with increasing oxygen coverage, forming a characteristic volcano plot. Investigations of the interaction of methanol with ZnO powders, oriented thin films, and single crystals [6-12] have shown that methanol decomposes sequentially into methoxy and formate species. Chan and Griffin [11] have observed methanol decomposition over copper overlayers on zinc oxide oriented thin films. They observed a new CO_2 desorption peak (from methanol decomposition) which they interpreted as evidence for dispersed copper cation sites.

In this chapter, we take a new approach to the modelling of Cu-Zn-O catalysts: We use ZnO_x islands on Cu(110) that is covered with various amounts of oxygen as a model for studying the interaction of methanol with Cu-Zn-O surfaces.

Electron microscopy studies of Cu-Zn-O methanol synthesis catalysts [13] have shown copper and zinc oxide components in separate phases; hence, the appropriativeness of using ZnO_x islands on copper as our model. Our previous studies have shown that ZnO_x overlayers on Cu(110) can be characterized by a combination of CO_2 and CO TPD (along with AES and LEED), since CO preferentially chemisorbs on copper while CO_2 chemisorbs on ZnO_x [14, chapter 4]. We use the same characterization techniques to follow changes in our model Cu-Zn-O surfaces after methanol decomposition. We show that the rôle of chemisorbed oxygen on Cu(110) is two-fold. There is transfer of oxygen from the copper to the zinc oxide which keeps the zinc oxidized under the reducing conditions of formate production from methanol. Furthermore, oxygen on copper promotes the total amount of surface formate produced by methanol decomposition. The rôle of ZnO_x islands is to increase the surface formate:methoxy ratio, from 1:9 in the absence of ZnO_x, to 1:3 in the presence of ZnO_x.

6.2 Experimental

General experimental comments are the same as chapter 2. In addition to chapter 2, there are some additional experimental notes needed to understand this chapter. They are discussed below.

All of the ZnO_x overlayers described in this chapter were prepared in the same manner so as to obtain approximately "2.0 ML" (AES calibration) of ZnO_x. The procedure used was as follows: Zinc vapor was deposited onto Cu(110) which had been pre-dosed with 0.5 ML oxygen (henceforth denoted 0.5 ML O/Cu(110)) at 150 K in an oxygen ambient of 1×10^{-7} Torr O_2. After zinc deposition, the surface was further oxidized with 300 L O_2 at 250 K. This last step determines the difference between oxygen deficient zinc oxide, which cannot adsorb CO_2 under our conditions, and zinc oxide, which can adsorb CO_2. Finally, the surface was annealed at 710 K for 2 seconds to produce three-dimensional ZnO_x islands on essentially oxygen-free Cu(110). (The presence of oxygen adsorbed on Cu(110) can be detected by CO_2 production from CH_3OH decomposition.)

A typical experimental procedure is as follows: The copper single crystal is cleaned by cycles of sputtering with 5×10^{-5} Torr argon at 300 K and 910 K, and then annealed at 910 K for fifteen minutes. Sample cleanness is then checked by AES and surface order by LEED. Once the sample is cleaned, ZnO_x and/or oxygen overlayers are produced and characterized as described above, and then TPD experiments begin. The sample is cooled to 150 K, positioned 2 mm in front of the mass spectrometer, dosed with a known amount of gas, and then the sample temperature is ramped linearly at 30 K/sec with the mass spectrometer tuned to a particular mass. After characterizing each surface by AES, LEED, CO and CO_2

TPD [14], the interaction of methanol with the model Cu-Zn-O surface was determined. Each methanol TPD experiment ended at 710 K because that is the temperature where oxidized zinc begin to desorb. AES spectra and LEED patterns were obtained after TPD experiments, to correlate composition and structure of the surface to methanol decomposition. By the end of each day of methanol TPD studies, the surface had accumulated ~5% of a monolayer of carbon. This does not alter the data as shown by performing the same set of experiments over again on this 5% carbon contaminated surface.

As methanol reduces zinc oxide and takes away oxygen from Cu(110) (see results), each ZnO_x/O/Cu(110) (or O/Cu(110)) surface changes after each methanol TPD. The same procedure was used for each methanol TPD reported in this chapter: We dose the surface with 1×10^{-8} Torr methanol at 150 K for 200 seconds (2.0 L CH_3OH), wait 200 seconds to pump out the methanol, and then ramp the temperature of the crystal at 30 K/second while monitoring a particular mass. It takes 300-400 seconds (variation in cooling rates from day to day) to cool back down to 150 K after each TPD ending at 710 K.

During TPD experiments, only one $\frac{m}{e}$ unit at a time was followed in order to obtain the best signal to noise ratio possible. Hence, many surfaces had to be prepared to check reproducibility. As an extra check on reproducibility, in some of the experiments, two masses which produced signals in different temperature ranges were followed. For example, after methanol adsorption, $\frac{m}{e}$=31 (methanol) would be followed up to 450K, after which the $\frac{m}{e}$ center was switched to $\frac{m}{e}$=44 (CO_2) in order to obtain the products from 450 K to 710 K. All these experiments indicated that these model Cu-Zn-O surfaces are very reproducible.

The products observed were identified by comparing their observed cracking pattern in the mass spectrometer with those in the literature. Once the products were identified, the parent $\frac{m}{e}$ fragment was followed except for CH_3OH, in which case $\frac{m}{e}$=31 methoxy signal was followed as it is 50% greater in signal than $\frac{m}{e}$=32.

Table 6.1a: Products from methanol adsorption on 0.5 ML O/Cu(110)

CH_3OH	CH_2O	H_2	CO_2	H_2O
183 K 220 K 275 K 420 K	410 K	200 K 410 K	490 K	230 K 490 K

Table 6.1b: Products from methanol adsorption on ZnO_x/0.5 ML O/Cu(110)

CH_3OH	CH_2O	H_2	CO	CO_2	H_2O	Zn
183 K 220 K 270 K 310 K 440 K	410 K (490 K) 560 K	260 K 410 K 560 K	660 K	490 K 660 K	220 K 300 K 490 K 660 K	starts desorbing at 600 K

6.3 Results

Methanol Decomposition on Cu(110)

The products from methanol TPD on Cu(110) are shown in figure 6.1. On clean Cu(110), the decomposition of methanol produces simultaneous formaldehyde and hydrogen desorption at T_p=370 K. Wachs and Madix also obtained simultaneous desorption of formaldehyde and hydrogen at T_p=365 K and have assigned this result to the decomposition of methoxy surface species [5]. Our results agree well with those of Wachs and Madix except for the desorption of undissociated methanol. This discrepancy is due to a difference in adsorption temperature between our studies and theirs: our adsorption temperature is 150 K while their adsorption temperature is 180 K.

Methanol Decomposition from O/Cu(110)

In addition to methanol decomposition on clean Cu(110), we investigated how oxygen on Cu(110) influences methanol decomposition. The products from methanol TPD from 0.5 ML oxygen on Cu(110) surfaces are shown in figure 6.2. This was the highest coverage of oxygen investigated. Several differences can be seen between this spectra and that obtained for methanol decomposition over clean Cu(110) (figure 6.1):

1) CO_2 and H_2O are now products of methanol decomposition, with both CO_2 and H_2O desorbing at T_p=490 K. This indicates the presence of chemisorbed formate parent species [5].

2) CH_3OH desorption peaks change, with the appearance of a peak at T_p=420 K, disappearance of the peak at T_p=380 K, and a decrease in the amount of undissociated methanol.

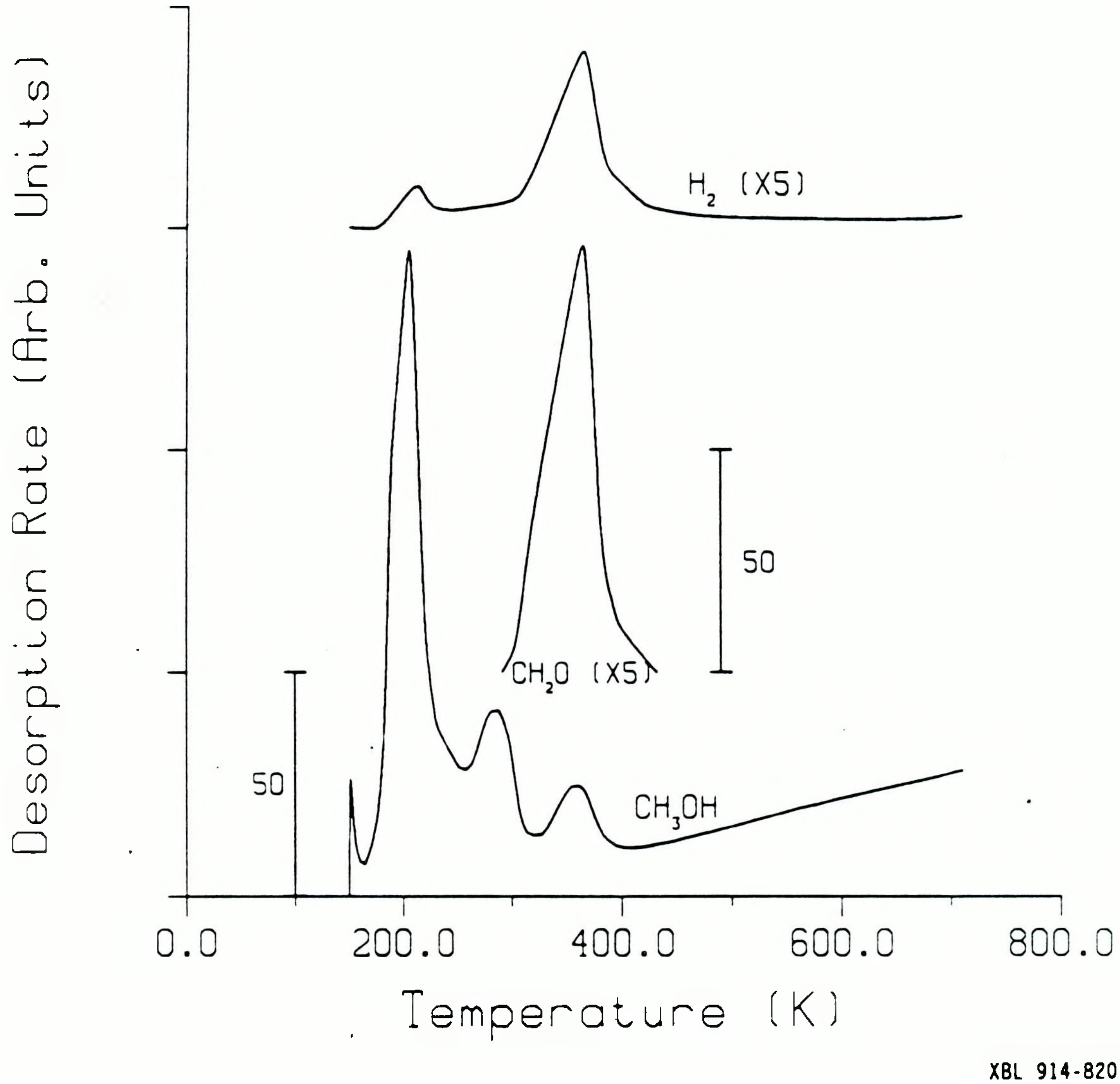

Figure 6.1: Products from 2.0 L methanol adsorption on Cu(110) at 150 K. Methanol decomposes to methoxy which then decomposes to formaldehyde and hydrogen at 370 K. All the products which could be detected from methanol decomposition are shown above.

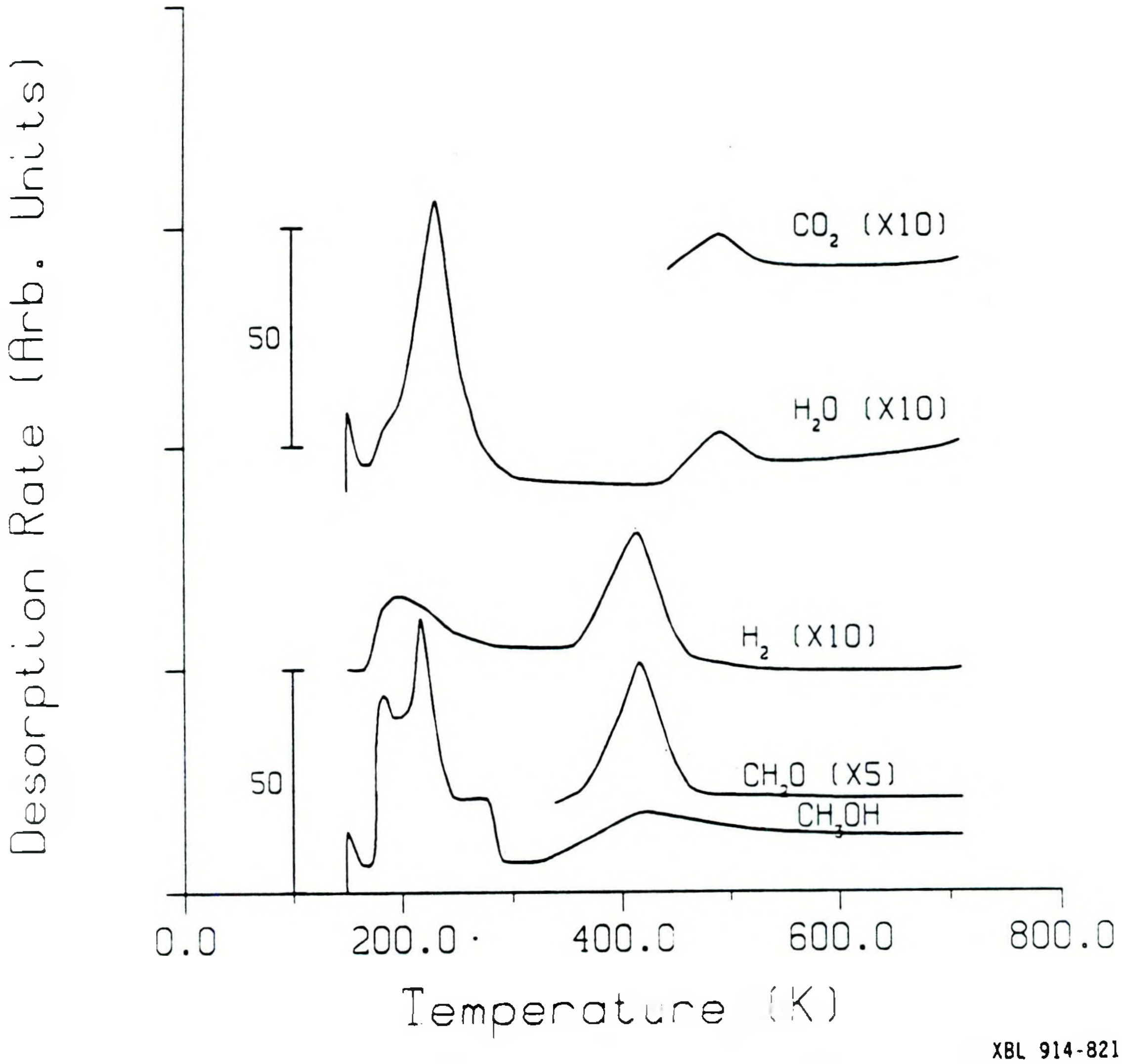

Figure 6.2: Products from 2.0 L methanol adsorption on 0.5 ML oxygen covered Cu(110) (0.5 ML O/Cu(110)) at 150 K. Methanol decomposes to formate and methoxy intermediates. Formate decomposes to CO_2 and H_2O at 490 K and methoxy decomposes to formaldehyde and hydrogen at 410 K.

3) There is a decrease in the amount of $[CH_2O]_{methoxy}/CH_3OH$ production indicating that there are less methoxy parent species chemisorbed than on clean Cu(110).

4) The $[CH_2O]_{methoxy}/CH_3OH$ and $[H_2]_{methoxy}/CH_3OH$ peak decomposition temperature increases from 370 K on clean Cu(110) to 410 K in the presence of 0.5 ML chemisorbed oxygen on Cu(110).

Similar results were obtained by Wachs and Madix [5] who observed simultaneous CO_2, H_2O, and H_2 desorption at T_p=470 K and a shift in the simultaneous CH_2O and H_2 desorption peaks to T_p=390 K for 0.4 ML O/Cu(110). We do not detect H_2 desorption with CO_2 and H_2O desorption at T_p=490 K. We believe this is due to the high H_2 background in our chamber. All the products and their temperatures at peak desorption from methanol adsorption on 0.5 ML O/Cu(110) are summarized in table 6.1a.

The effect of oxygen coverage on Cu(110) for $[CH_2O]_{methoxy}/CH_3OH$, $[CO_2]_{formate}/CH_3OH$, and CH_3OH/CH_3OH production is shown in figure 6.3. Both the $[CH_2O]_{methoxy}/CH_3OH$ and $[CO_2]_{formate}/CH_3OH$ production exhibit a maximum at 0.2-0.3 ML O/Cu(110), in agreement with work by Wachs and Madix [5]. We find that the amount of CH_3OH/CH_3OH production decreases at >0.3 ML oxygen, but Wachs and Madix [5] found a maximum in methanol desorption at 0.2-0.3 ML oxygen. This discrepancy is due to our use of 150 K as the adsorption temperature for methanol rather than 180 K, as used by Wachs and Madix.

We will note that the ratio of the maximum in $[CO_2]_{formate}/CH_3OH$ to $[CH_2O]_{methoxy}/CH_3OH$ production is 1:9 (uncorrected for mass spectrometer sensitivities) in the absence of ZnO_x, and we will see in the next section how this ratio changes in the presence of ZnO_x.

Methanol Decomposition from ZnO_x/O/Cu(110)

Products from methanol adsorption on ZnO_x/0.5 ML O/Cu(110) are shown in figure 6.4. All the desorption temperatures of products from methanol interaction

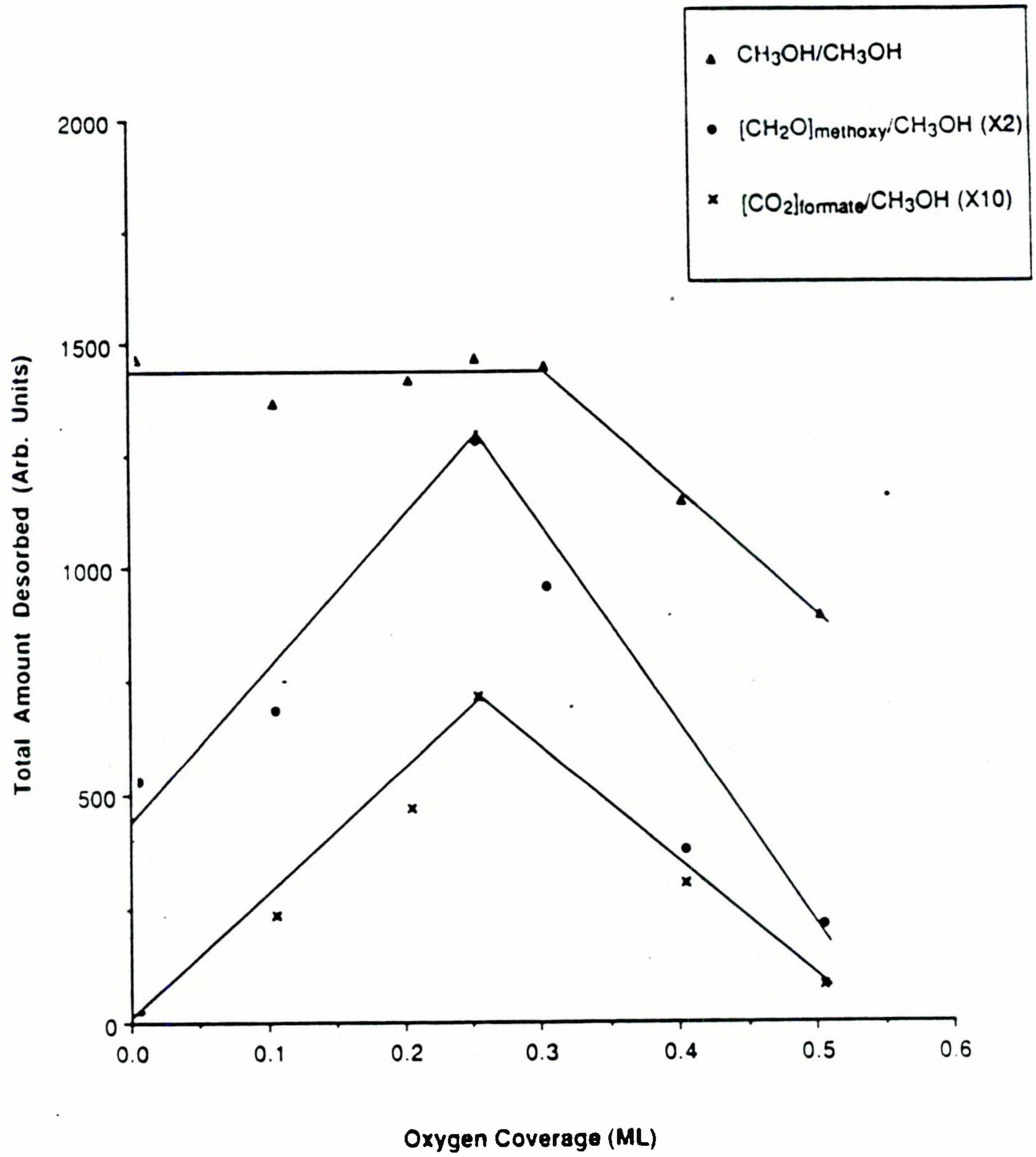

Figure 6.3: The effect of θ_{oxygen} on Cu(110) upon the production of CH_3OH, CH_2O, and CO_2, following 2.0 L CH_3OH exposure at 150 K. To emphasize the relationship between the various species, we have used the notation $[X]_Y/Z$, where X is the decomposed product from intermediate Y, produced by adsorption of Z.

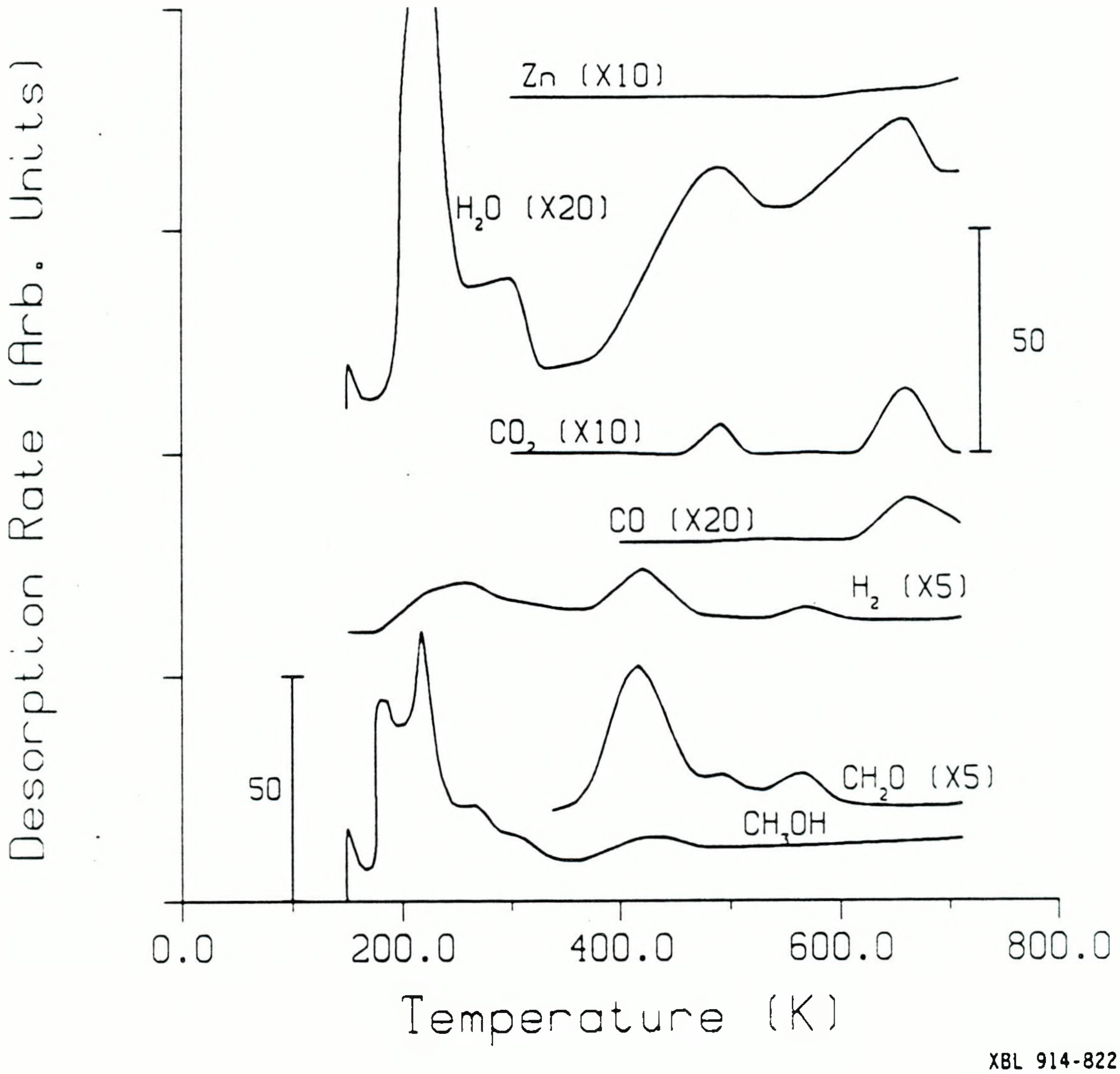

Figure 6.4: Products from 2.0 L methanol adsorption on ZnO_x/0.5ML O/Cu(110) at 150 K. Methanol decomposition on ZnO_x/0.5 ML O/Cu(110) is qualitatively like the addition of methanol decomposition on 0.5 ML O/Cu(110) and ZnO_x. Note that ZnO_x is being reduced as indicated by the detection of $Zn_{(g)}$ beginning at ~600 K.

Table 6.2:
Temperature at peak desorption of species from CH_3OH decomposition on ZnO

Surface	Adsorbed Species	Decomposition Products	T_p	Reference
"2ML" $ZnO_x/Cu(110)$	Formate,	CO_2+CO+H_2O	660 K	this work
	Methoxy	CH_2O+H_2	560 K	this work
Polycrystalline	Formate,	$CO+H_2$	580 K	6
ZnO with large	Formate,	CO_2+H_2O	540 K	6
fraction of polar faces	Methoxy	CH_2O	340 K to 540 K	6
Thin Films	Formate	CO_2+CO+H_2	580 K	7
ZnO(0001)	Formate,	CO_2+CO+H_2O	575 K	8
	Methoxy	CH_2O+H_2	520 K	8
ZnO($10\bar{1}0$) and ($50\bar{5}1$)	Formate	CO_2+CO+H_2	650 K	9,10
ZnO(0001)	Formate,	$CO_2+CO+H_2+H_2O$	750 K	9,10
	Methoxy	$CO+CH_2O+H_2$	670 K	9,10
C-axis oriented	Formate,	CO_2+CO+H_2	635 K	11
ZnO thin films	Methoxy	CH_2O+H_2	585 K	11
ZnO($000\bar{1}$)	Formate	CO_2+CO+H_2	470 K	12
>15ML $ZnO_x/Cu(110)$	Formate,	$CO+CO_2+H_2O+CH_4$	650 K	this work
	Methoxy	CH_2O+H_2	570 K	this work
ZnO_x/Au foil	Formate,	$CO+CO_2+H_2O+CH_4$	670 K	this work
	Methoxy	CH_2O+H_2	620 K	this work

with 0.5 ML O/Cu(110) are essentially unchanged. The desorption products from ZnO_x/0.5 ML O/Cu(110) surfaces are summarized in table 6.1b.

We attribute the simultaneous desorption of formaldehyde and hydrogen at 560 K to methoxy decomposition on ZnO_x islands. The simultaneous desorption of CO, CO_2, and H_2O at 660 K is attributed to formate decomposition from ZnO_x islands. Table 6.2 summarizes the decomposition temperatures of formate and methoxy species from various zinc oxide surfaces. The peak temperatures for formate and methoxy decomposition vary over a wide range, depending on the surface structure of ZnO. It is difficult to compare our zinc oxide overlayer with any particular surface. The products from formate and methoxy decomposition on our zinc oxide overlayer is most like that from ZnO(0001) as reported in [8], but our peak temperatures of decomposition are between those reported in [8] (T_p=575 K for formate decomposition and T_p=520 K for methoxy decomposition) and [9,10] (T_p=750 K for formate decomposition and T_p=670 K for methoxy decomposition).

We have seen in the previous section that changing the chemisorbed oxygen coverage on Cu(110) changes the amount of $[CO_2]_{formate}/CH_3OH$, $[CH_2O]_{methoxy}/CH_3OH$, and CH_3OH/CH_3OH production from O/Cu(110). What is surprising is the dramatic difference in the amount of $[CO_2]_{formate}/CH_3OH$ and $[CO]_{formate}/CH_3OH$ produced from the ZnO_x component of the surface by changing oxygen coverage on Cu(110). This is illustrated in figure 6.5, which shows the amount of zinc, CH_2O, CO, and CO_2 desorbed from a ZnO_x/0.5 ML O/Cu(110) and a ZnO_x/0.2 ML O/Cu(110) surface. Four points should be noted in comparing the ZnO_x/0.2 ML O/Cu(110) surface to the ZnO_x/0.5 ML O/Cu(110) surface:

1) The amount of zinc desorbed from a ZnO_x/0.2 ML O/Cu(110) surface is about fives times greater than the amount of zinc desorbed from a ZnO_x/0.5 ML O/Cu(110) surface.

2) The amount of formate from the ZnO_x component increases while the amount of methoxy from ZnO_x remain the same.

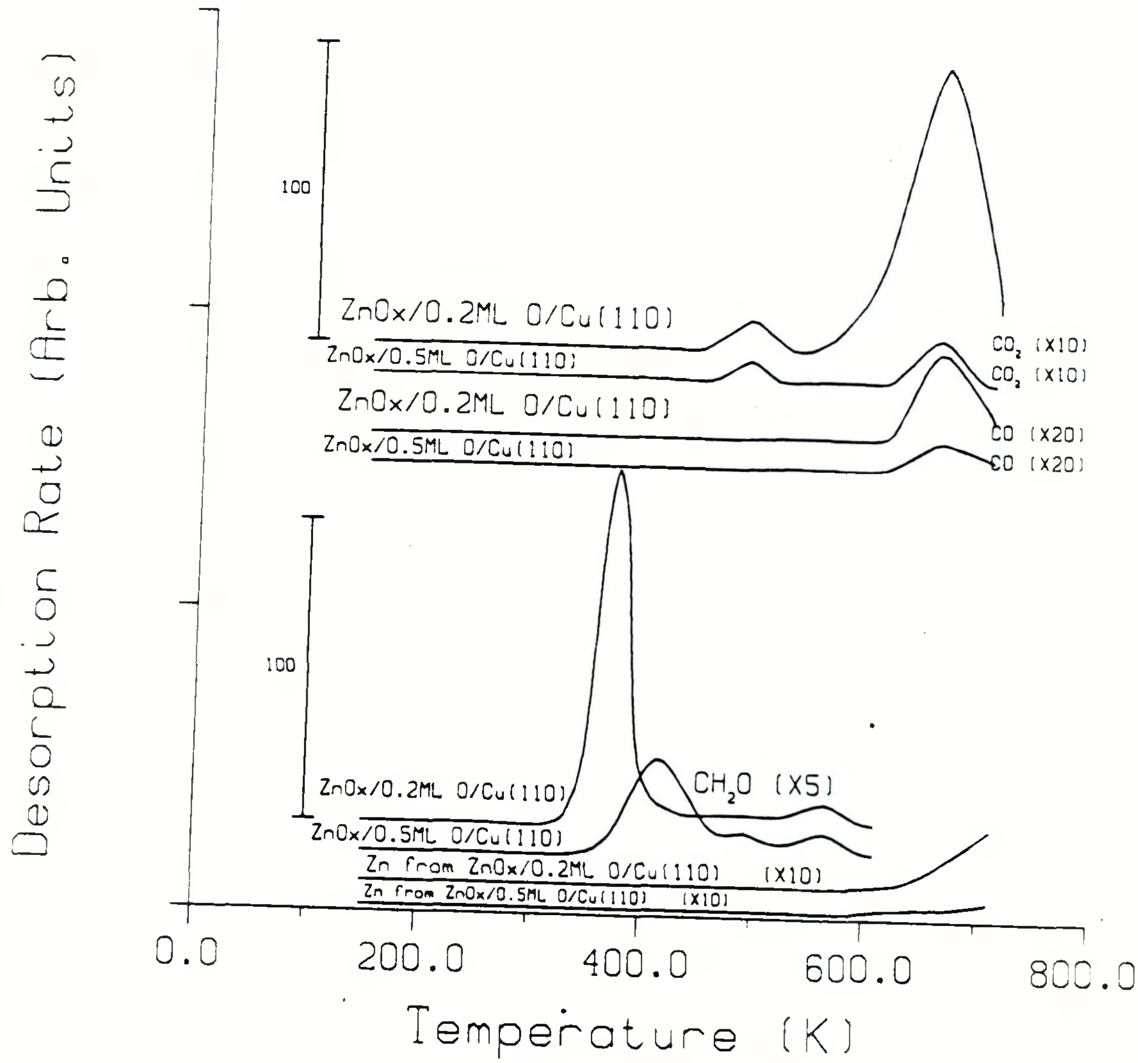

Figure 6.5: The amount of zinc, CH_2O, CO, and CO_2 desorbed from a ZnO_x/0.5 ML O/Cu(110) surface and a ZnO_x/0.2 ML O/Cu(110) surface after 2.0 L exposures of methanol at 150 K.

3) The amount of formate and methoxy from the O/Cu(110) component both increases when changing the oxygen coverage from 0.5 ML to 0.2 ML (similar to O/Cu(110) behavior toward methanol in the absence of ZnO_x).

4) The total $[CO_2{+}CO]_{formate}$: $[CH_2O]_{methoxy}$ ratio increases, suggesting greater formate formation in the case of ZnO_x/0.2 ML O/Cu(110) surfaces.

The following sections will further develop these points.

We noted in the previous section that at 0.2-0.3 ML O/Cu(110), the ratio of $[CO_2{+}CO]_{formate}$: $[CH_2O]_{methoxy}$ was 1:9. We see from figure 6.5 that for ZnO_x/0.2 ML O/Cu(110) surfaces, the $[CO_2{+}CO]_{formate}$: $[CH_2O]_{methoxy}$ ratio has increased to 1:3, indicating an increase in the relative surface formate concentration.

No other thermal decomposition products apart from those shown in figures 6.1, 6.2, and 6.4 were observed; in particular, we searched for, but did not see, methane, methyl formate, methylal, and dimethyl ether. Oxygen does not desorb from the Cu(110) surface until >1000 K. The oxygen from ZnO_x decomposition between 710 K and 1100 K is adsorbed (and absorbed) by the Cu(110) [14].

Effect of O/Cu(110) on ZnO_x Reduction

Figure 6.6A shows the amount of zinc desorbed by 710 K versus the number of methanol TPD experiments for two different ZnO_x/0.5 ML O/Cu(110) surfaces. These surfaces produce a p(2×1) surface structure which slowly diminishes with each methanol TPD experiment, since formate formation and decomposition takes away oxygen from the surface. The initial rise in the amount of zinc reduced for each 2.0 L dose of methanol is due to the depletion of oxygen from the copper component, chemisorbed oxygen on Cu(110) being used to re-oxidize the reduced zinc. After the initial rapid rise in the amount of zinc reduced with each 2.0 L dose of methanol, there is a slow decline in the amount of zinc reduced. This is most likely due to the decrease in ZnO_x left to reduce. (The first ten methanol TPD experiments reduces the original AES zinc signal by 30%.) By AES, the oxygen signal decreased by 35% after the first four methanol TPD experiments, while the zinc signal decreased by only 15%. The oxygen loss is mainly from the copper, as

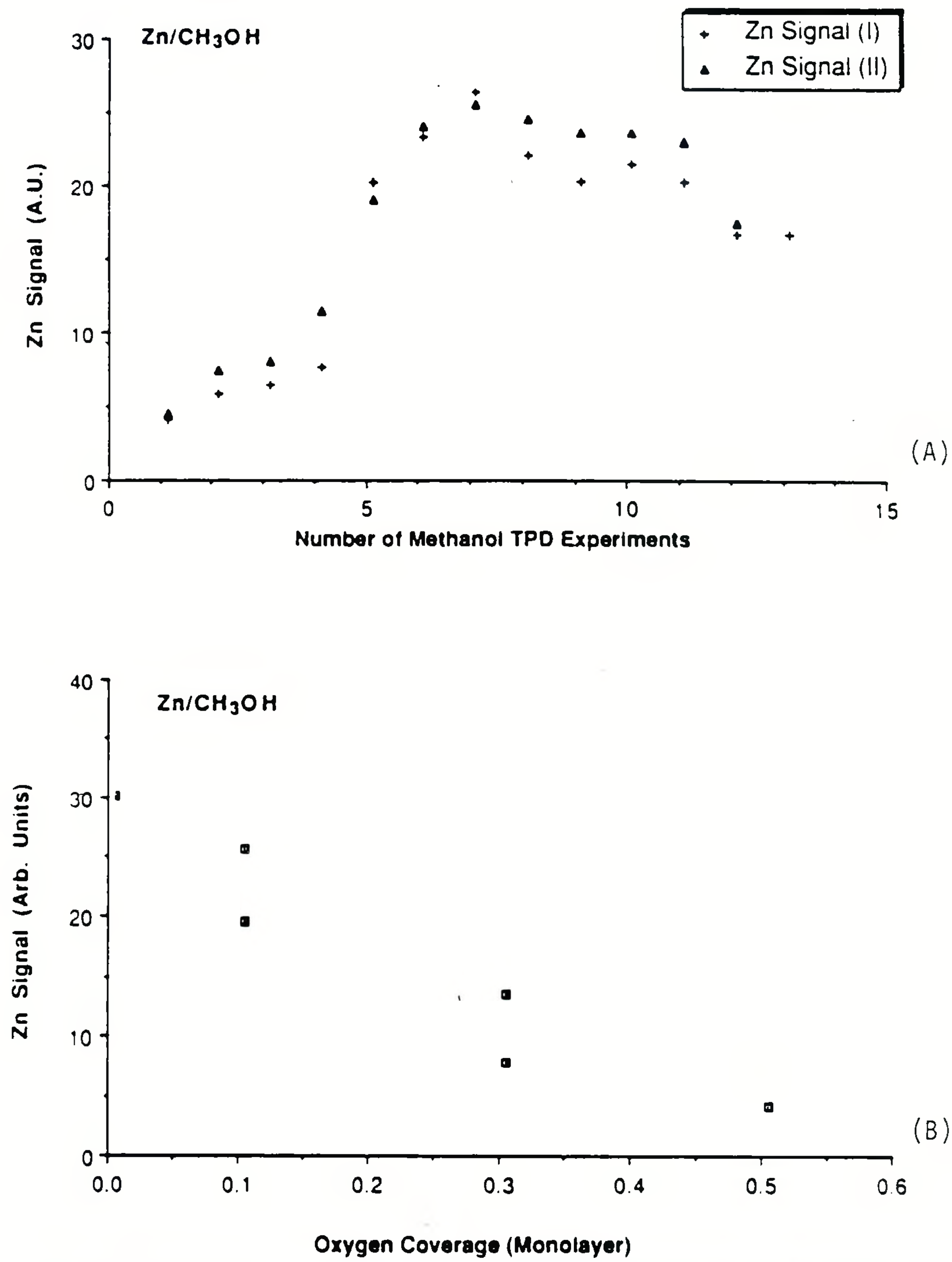

Figure 6.6: (A) Amount of zinc desorbed by 710 K (for each 2.0 L dose of methanol) versus the number of methanol TPD experiments from two separate ZnO_x/0.5 ML O/Cu(110) surfaces. With increasing reduction of the Cu-Zn-O surface (each methanol TPD reduces the surface), the amount of zinc reduced first increases and then slowly decreases. The first ten methanol TPD experiments reduces the original AES zinc signal by 30%. (B) The influence of θ_{oxygen}/Cu(110) on the amount of reduced zinc following 2.0 L CH_3OH exposure at 150 K for ZnO_x/O/Cu(110) surfaces. Oxygen on the Cu(110) part helps keep the ZnO_x islands oxidized.

can be seen by an order in magnitude increase in CO adsorption capacity (due to bare copper), and the transformation of a p(2×1) surface structure, at the beginning of the first methanol TPD, to a (1×1) surface structure, after the fourth methanol TPD.

The effect of O/Cu(110) on the ZnO_x component can be seen in another set of experiments where the amount of zinc reduced is monitored from surfaces with different oxygen coverage on Cu(110) but the same amount of ZnO_x. This is shown in figure 6.6B: Less zinc desorbs because less ZnO_x is reduced with greater θ_{oxygen} on the Cu(110) component. This suggests oxygen spillover from the Cu(110) component to the ZnO_x to keep zinc oxidized. Hence, we see that one of the rôles of chemisorbed oxygen on the copper component is to help keep the zinc oxidized.

Effect of O/Cu(110) on $[CO_2+CO]_{formate}/CH_3OH$ Production from the ZnO_x Component

A more surprising finding is shown in figure 6.7, in which the amount of chemisorbed oxygen on the copper component influences the production of CO_2+CO from CH_3OH decomposition (henceforth denoted $[CO_2+CO]_{formate}/CH_3OH$) on the zinc oxide component. Remember that the amount of CO_2+CO desorbed with T_p=660 K is the amount of surface formate species decomposed from the ZnO_x component of the surface. To determine that this volcano plot is indeed due to the chemisorbed oxygen on the copper component, we performed two sets of experiments, summarized in figures 6.8 and 6.9. With figure 6.8, we show the results of the amount of $[CO_2+CO]_{formate}/CH_3OH$ produced as a function of the number of methanol TPD experiments for three different surfaces - ZnO_x/Cu(110), ZnO_x/0.2 ML O/Cu(110), and ZnO_x/0.5 ML O/Cu(110). Two points should be noted from this figure:

1) the maximum for $[CO_2+CO]_{formate}/CH_3OH$ production from the ZnO_x component of the ZnO_x/0.2 ML O/Cu(110) is four times greater than that produced from the ZnO_x/Cu(110) surface, and

2) the maximum in $[CO_2+CO]_{formate}/CH_3OH$ formation from the ZnO_x component of the Cu-Zn-O surface is reached at about 0.2-0.3 ML oxygen on

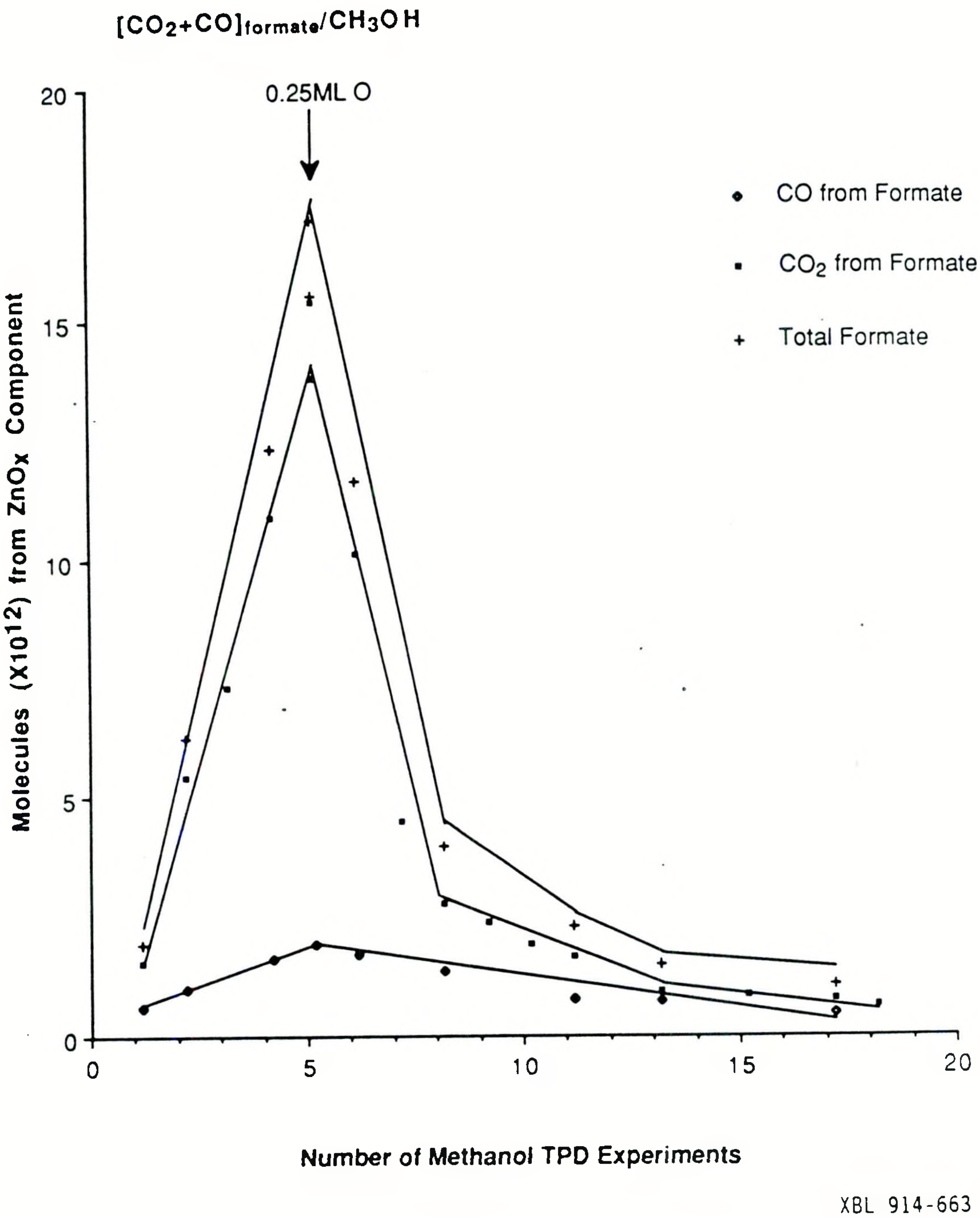

Figure 6.7: Production of CO_2 and CO from the ZnO_x component of a ZnO_x/0.5 ML O/Cu(110) surface for 2.0 L exposures of CH_3OH as a function of the number of methanol TPD experiments.

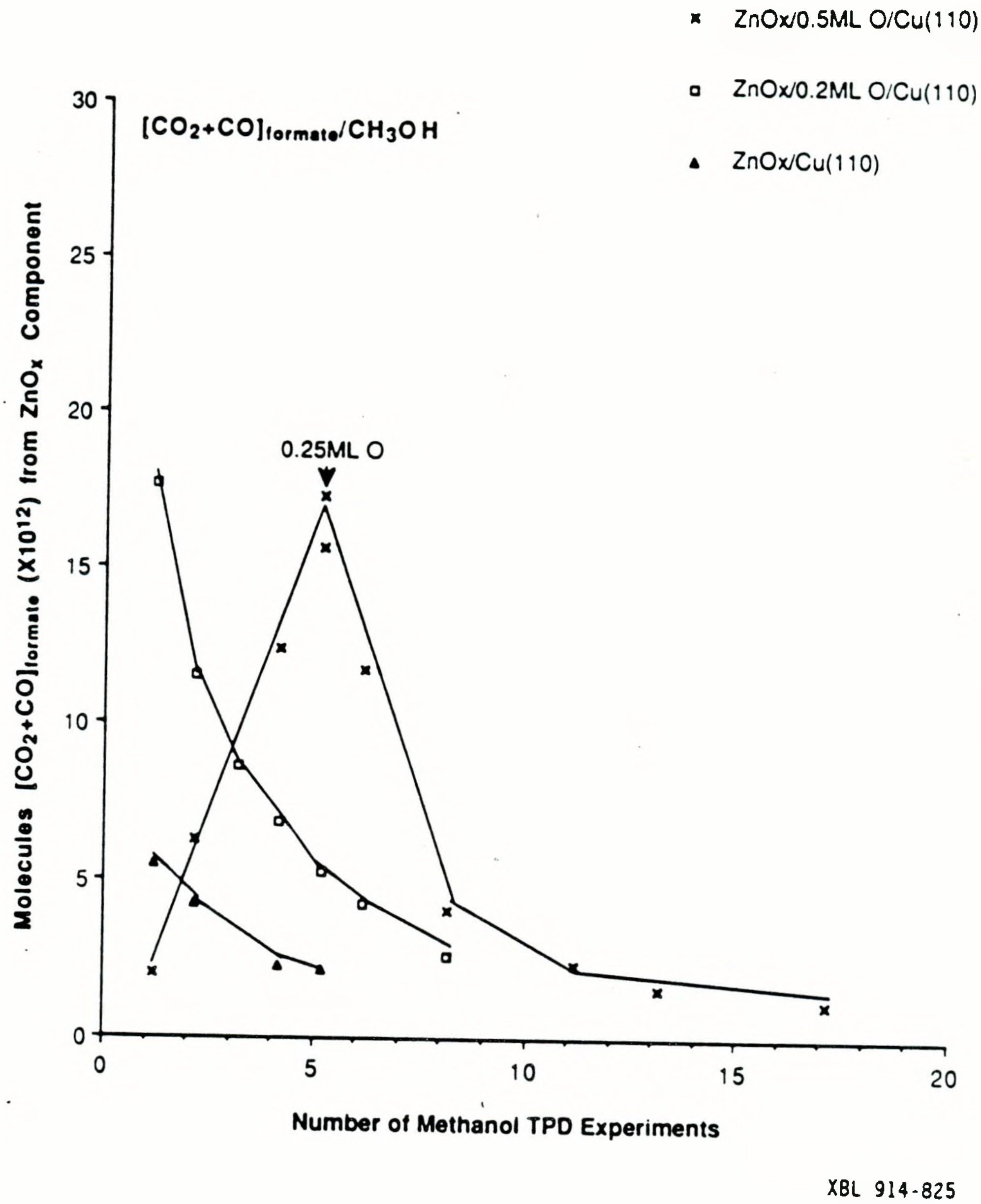

Figure 6.8: The effect of reduction on $[CO_2+CO]_{formate}/CH_3OH$ production for three different surfaces. It does not seem to matter whether we start with 0.2-0.3 ML oxygen on the Cu(110) component of the surface or reach those oxygen coverages by reduction with methanol; in both cases, the maximum amount of $[CO_2+CO]_{formate}/CH_3OH$ production from the ZnO_x component is obtained when there is 0.2-0.3 ML oxygen on the Cu(110) component, producing about 2×10^{13} molecules of $[CO_2+CO]_{formate}/CH_3OH$ from the ZnO_x component. Each CH_3OH exposure was 2.0 L.

the Cu(110) component, regardless of whether one starts with a ZnO_x/0.2 ML O/Cu(110) surface or a ZnO_x/0.5 ML O/Cu(110) surface reduced by methanol to an oxygen coverage of 0.2-0.3 ML.

Multilayers of ZnO_x/Au reproducibly give the same amount of $[CO_2+CO]_{formate}/CH_3OH$ with each methanol TPD. Hence, the amount of chemisorbed oxygen on Cu(110) does indeed influence the amount of $[CO_2+CO]_{formate}/CH_3OH$ production, or formate formation, on the ZnO_x component of our model Cu-Zn-O surface.

In figure 6.9, we show the effect of exposing a ZnO_x/0.2 ML O/Cu(110) surface, that has been reduced by methanol, to oxygen. We begin with ZnO_x/0.2 ML O/Cu(110) surface. The ZnO_x component of this surface produces $\sim 2 \times 10^{13}$ molecules CO_2+CO for a 2.0 L dose of methanol. By the seventh methanol TPD, the ZnO_x component produces only $\sim 3 \times 10^{12}$ molecules $[CO_2+CO]_{formate}/CH_3OH$, and the original zinc AES signal has been reduced by ~20%. At this point, enough oxygen (30 L O_2) to form a 0.5 ML oxygen coverage on the bare Cu(110) part of the surface was introduced into the UHV chamber. After the introduction of oxygen, methanol TPD experiments showed the formation of a volcano plot with regards to the amount of $[CO_2+CO]_{formate}/CH_3OH$ from the ZnO_x component of the surface as a function of the number of methanol TPD experiments. The maximum in this volcano plot occurs, again, when there is 0.2-0.3 ML oxygen on the Cu(110) part of the surface. But this time, the maximum amount of $[CO_2+CO]_{formate}/CH_3OH$ production from the ZnO_x component is 1×10^{13} molecules, half of what was obtained at the beginning of these experiments with the ZnO_x/0.2 ML O/Cu(110) surface. This is most likely due to the smaller amount of ZnO_x left on the surface by the twelfth methanol TPD as compared to the first methanol TPD. (Remember that methanol reduces zinc oxide.) As reference, the amount of $[CO_2+CO]_{formate}/CH_3OH$ from the ZnO_x component of a ZnO_x/0.2 ML O/Cu(110) surface with increasing reduction is shown to continually decline (due to decreasing amounts of ZnO_x).

The effect of oxygen exposure on the various surface areas was determined by CO and CO_2 TPD. Saturation doses of CO_2 before and after the oxygen exposure

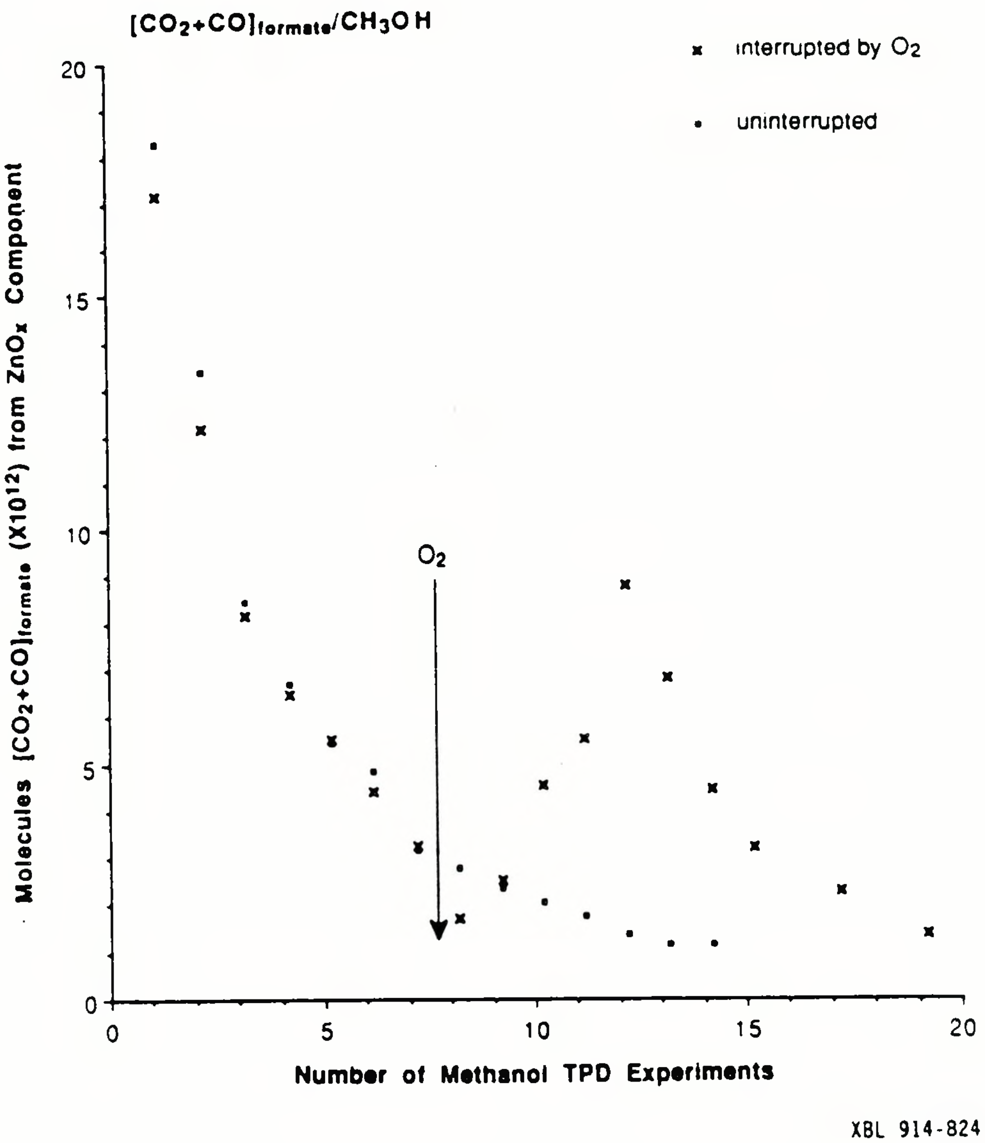

Figure 6.9: Effect of oxygen on formate production from the ZnO_x component of our model Cu-Zn-O surface. Dark square boxes indicate a ZnO_x/0.2 ML O/Cu(110) surface continually reduced with methanol. The x marks indicate a ZnO_x/0.2ML O/Cu(110) surface that was exposed to 30 L O_2 at 150 K after the 7^{th} methanol TPD experiment. CO_2 TPD before and after the introduction of O_2 showed that the ZnO_x component remain unchanged. CO TPD after the introduction of O_2 show that there is a great decrease in exposed Cu(110) area; this along with the formation of a p(2×1) surface structure indicates oxygen adsorption on the Cu(110) component of the surface. Hence, the volcano plot formed after the introduction of O_2 is due to chemisorbed oxygen on the Cu(110) part of the surface.

showed no changes in either the size of the desorption peaks or the desorption temperatures. This suggests that ZnO_x islands remain unaltered. On the other hand, saturation doses of CO after oxygen exposure showed a dramatic decrease in CO adsorption capacity; this along with the formation of a p(2×1) surface structure points to oxygen adsorption on the Cu(110) component. Thus, we conclude that oxygen adsorbed on the Cu(110) component of the Cu-Zn-O surface does affect the amount of $[CO_2+CO]_{formate}/CH_3OH$ from the ZnO_x component of the ZnO_x/O/Cu(110) surfaces.

Effect of ZnO_x Islands on $[CO_2]_{formate}/CH_3OH$ Production from the O/Cu(110) Component

Figure 6.10 shows the amount of CO_2 produced from a 2.0 L dose of methanol at 150 K from the **O/Cu(110) component** in the absence and presence of ZnO_x islands. We see that:

1) The O/Cu(110) component is more quickly reduced in the presence of ZnO_x islands, and

2) The maximum in $[CO_2]_{formate}/CH_3OH$ production is three times greater in the absence of ZnO_x than in its presence.

These observations suggest that oxygen is being taken away from the copper. As there is no oxygen desorption except in the form of formate decomposition, the oxygen is most likely migrating to the ZnO_x islands to re-oxidize the ZnO_x reduced by methanol. Earlier, we had obtained this same conclusion from the change in the amount of reduced zinc as a function of the number of methanol TPD experiments for ZnO_x/0.5 ML O/Cu(110) surfaces. Although the presence of ZnO_x decreases the amount of formate decomposed on the O/Cu(110) component, the amount of formate from the ZnO_x islands is increased by a greater amount in the presence of 0.2-0.3 ML O/Cu(110). We will examine this promotional effect on total formate production in the next section.

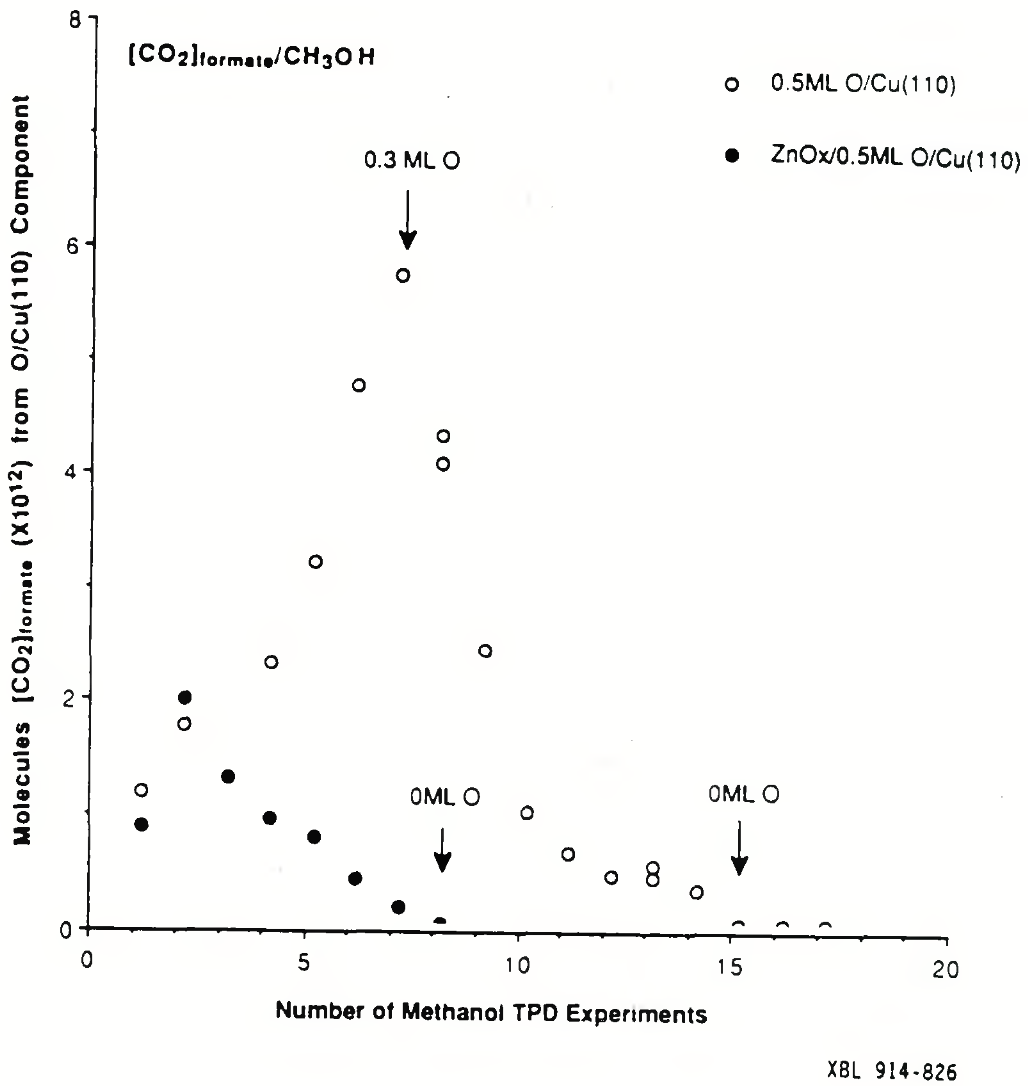

Figure 6.10: Amount of $[CO_2]_{formate}/CH_3OH$ from the **O/Cu(110) component** in the presence and absence of ZnO_x. The O/Cu(110) component is more quickly reduced in the presence of ZnO_x islands and the maximum in $[CO_2]_{formate}/CH_3OH$ production from the O/Cu(110) component is about three times greater in the absence of ZnO_x islands than in its presence. This figure, along with figure 6.6, show that oxygen is transferred from the copper to the ZnO_x component to help keep the ZnO_x oxidized. Note that although the presence of ZnO_x decreases the amount of formate decomposed on the O/Cu(110) component, the amount of formate from the ZnO_x is increased by a greater amount in the presence of 0.2-0.3 ML O/Cu(110).

$[CO_2+CO]_{formate}/CH_3OH$ Production on the Three Component System versus the Addition of the Two Separate Components

We have seen that oxygen on Cu(110) can promote both the amount of $[CO_2+CO]_{formate}/CH_3OH$ produced from the ZnO_x component and the O/Cu(110) component of our model Cu-Zn-O surface. But as the oxygen is taken away from the copper to the ZnO_x component of the ZnO_x/O/Cu(110) surface, less $[CO_2+CO]_{formate}/CH_3OH$ is produced on the O/Cu(110) component in the presence of ZnO_x islands. To determine the overall effect on total $[CO_2+CO]_{formate}/CH_3OH$ production on the O/Cu(110) and ZnO_x components in the presence and absence of each other, experiments were performed on three types of surfaces: O/Cu(110) surfaces in which the oxygen coverage was varied, ZnO_x/Cu(110) surface, and ZnO_x/O/Cu(110) surfaces in which the oxygen coverage was again varied. We show the amount of $[CO_2+CO]_{formate}/CH_3OH$ produced from the components of ZnO_x and O/Cu(110) of the three-component system – ZnO_x/O/Cu(110) – and compare that to the addition of the separate components – ZnO_x/Cu(110) + O/Cu(110) – as a function of the oxygen coverage on the copper component of the surface (as seen by CO titration). The results are plotted in figure 6.11 and show that:

(1) θ_{oxygen}/Cu(110) effect $[CO_2+CO]_{formate}/CH_3OH$ production from both the ZnO_x and O/Cu(110) components of ZnO_x/O/Cu(110) surfaces, and

(2) The maximum for $[CO_2+CO]_{formate}/CH_3OH$ production from the ZnO_x and O/Cu(110) components of ZnO_x/O/Cu(110) surfaces is twice that of the addition of the separate surfaces of ZnO_x/Cu(110) plus O/Cu(110). (The plot in figure 6.11 did not correct for surface area so that the promotional effect seen is a minimum.)

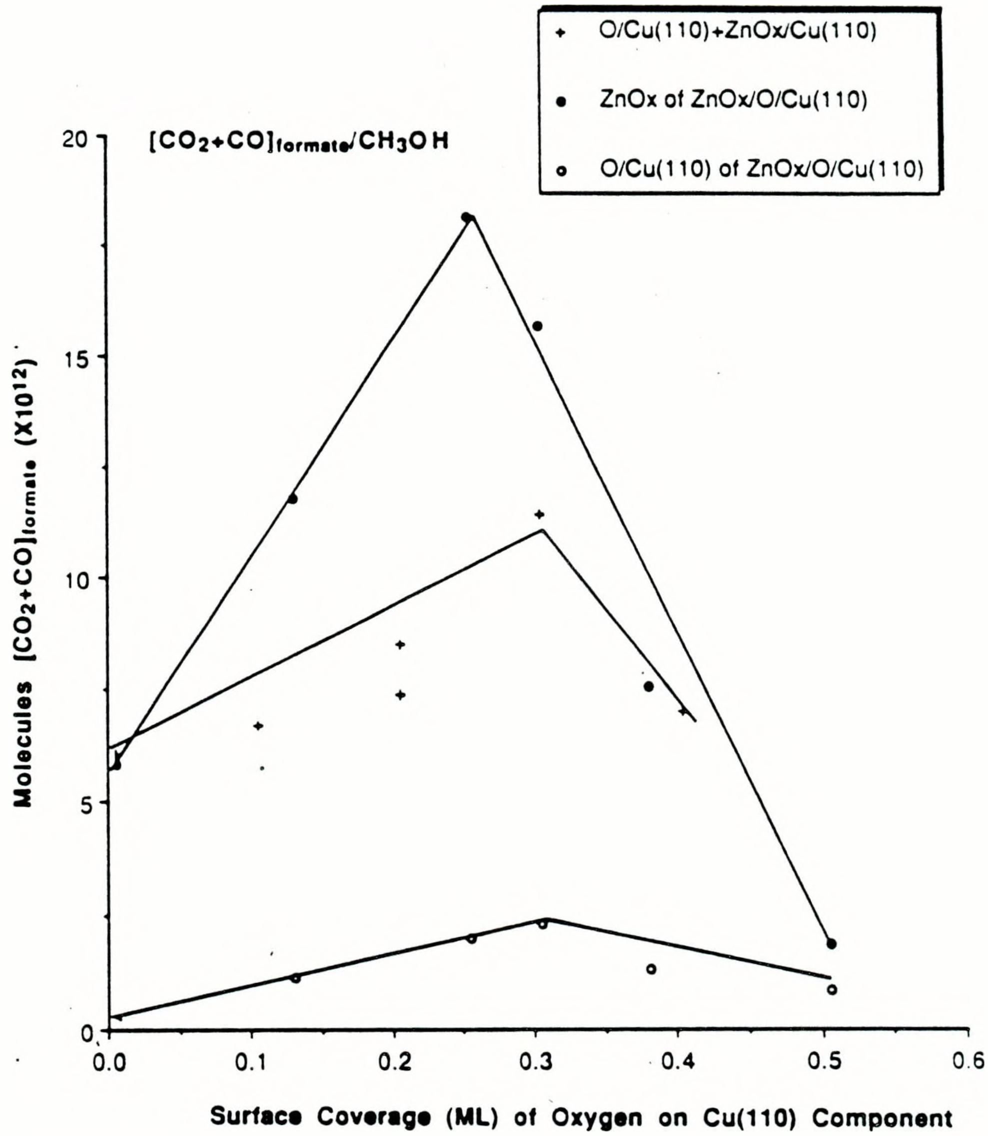

Figure 6.11: The amount of $[CO_2+CO]_{formate}/CH_3OH$ from the ZnO_x and O/Cu(110) components in the three-component system, and the addition of the separate components as a function of θ_{oxygen}/Cu(110). Experiments were done on three different types of surfaces and the amount of $[CO_2+CO]_{formate}/CH_3OH$ from the two separate surfaces of O/Cu(110) and ZnO_x/Cu(110) were added up and compared to the amount of formate from the separate components of the three-component surface. As oxygen-free copper does not produce any $[CO_2]_{formate}/CH_3OH$, the ZnO_x/Cu(110) plus O/Cu(110) has only 20-30% more surface area than the ZnO_x/O/Cu(110) surface. Area was not corrected for in order to obtain the most conservative view of any promotional effect.

$[CH_2O]_{methoxy}/CH_3OH$ Production from the Three Component System versus the Addition of the Two Separate Components

In order to assess the effect of O/Cu(110) and ZnO_x on each other in $[CH_2O]_{methoxy}/CH_3OH$ production, similar experiments were performed to those for the observation of $[CO_2+CO]_{formate}/CH_3OH$ production. We find that for ZnO_x/O/Cu(110) surfaces, the amount of $[CH_2O]_{methoxy}/CH_3OH$ from Cu(110) changes with θ_{oxygen}, but methoxy decomposition from ZnO_x remain unchanged in the presence of O/Cu(110). Comparing the amount of $[CH_2O]_{methoxy}/CH_3OH$ from the ZnO_x and the O/Cu(110) components of ZnO_x/O/Cu(110) surfaces to the addition of the two separate surfaces of ZnO_x/Cu(110) and O/Cu(110), we see that there is no effect of O/Cu(110) and ZnO_x on each other in terms of $[CH_2O]_{methoxy}/CH_3OH$ production. This is best summarized in figure 6.12, which plots $[CH_2O]_{methoxy}/CH_3OH$ production from the ZnO_x and O/Cu(110) components of the three-component system, and the addition of the separate components. In order to make this the same type of comparison as figure 6.11, the amount of $[CH_2O]_{methoxy}/CH_3OH$ from the copper component of the ZnO_x/Cu(110) surface was discarded as $[CO_2+CO]$ is not produced from methanol decomposition on the bare Cu(110) component, while CH_2O is produced; hence, the ZnO_x/Cu(110) + O/Cu(110) data has 20-30% greater surface area than the ZnO_x/O/Cu(110) surface, as in the comparison of figure 6.11. But, unlike figure 6.11, where we saw a promotional effect of a factor of two in $[CO_2+CO]_{formate}/CH_3OH$ production from the three-component system, indicating the promotion of formate formation, we see no promotional effect for $[CH_2O]_{methoxy}/CH_3OH$ production, and hence, no promotional effect for methoxy formation on the three-component system.

Total Methanol Desorption

Comparing figure 6.2 and 6.4, one can see that methanol desorption from ZnO_x/0.5 ML O/Cu(110) is dominated by methanol desorption from oxygen covered Cu(110). (The only difference is an additional desorption peak at T_p=310 K for the ZnO_x/0.5

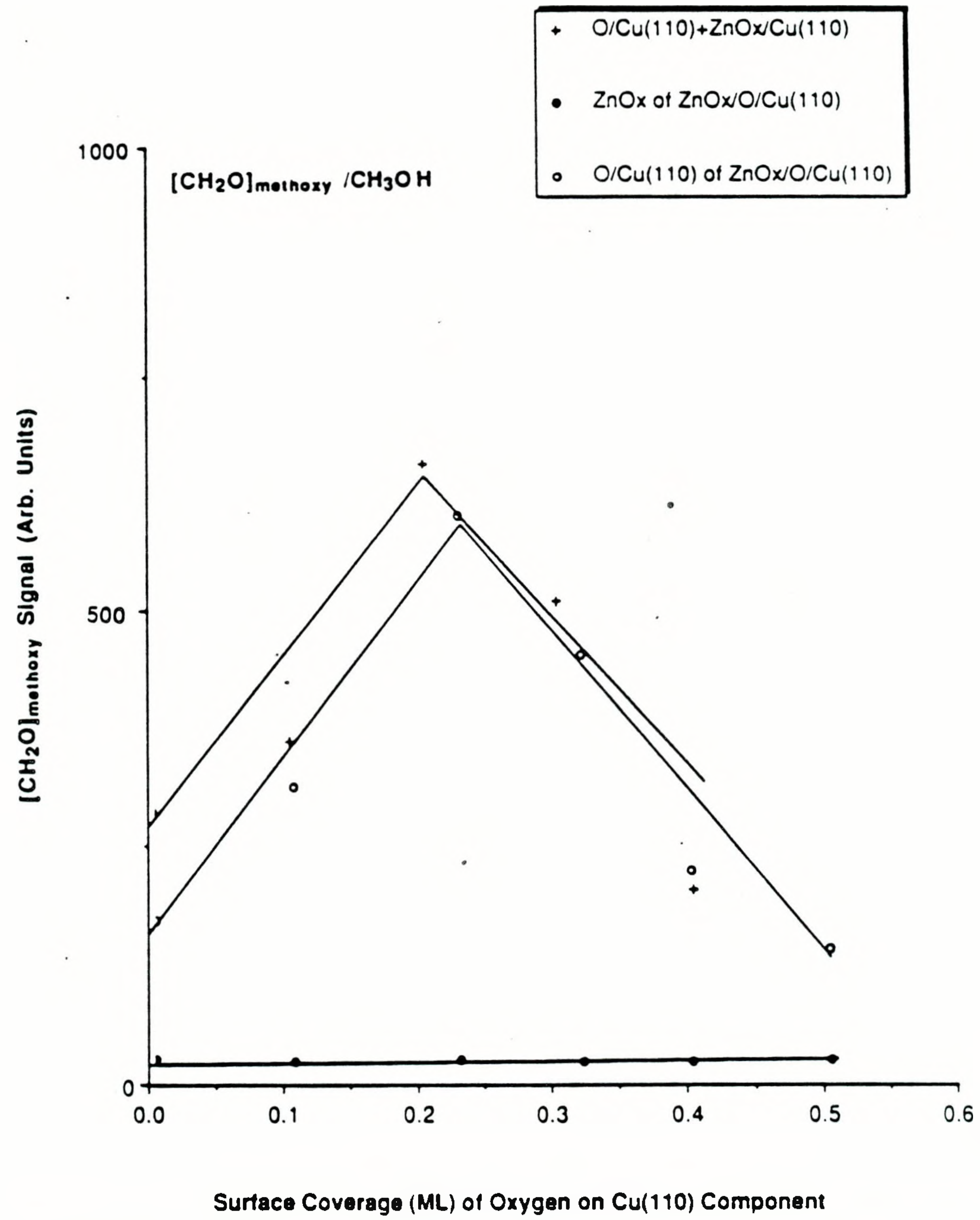

Figure 6.12: The amount of $[CH_2O]_{methoxy}/CH_3OH$ from the ZnO_x and O/Cu(110) components of the three-component system, and the addition of the separate components as a function of the oxygen coverage on the copper component. To make this graph the same type of comparison as figure 6.11, the amount of $[CH_2O]_{methoxy}/CH_3OH$ from the copper component of the ZnO_x/Cu(110) surface was discarded as $[CO_2]_{formate}/CH_3OH$ is not produced from the copper component of ZnO_x/Cu(110) surfaces while $[CH_2O]_{methoxy}/CH_3OH$ is produced.

ML O/Cu(110) surface.) This is consistent with previous studies which have shown methanol to be a minor product in methanol TPD from ZnO(0001) surfaces [9] while methanol has been shown to be a major product from methanol interaction with oxygen modified Cu(110) [5].

Figure 6.13 shows that the amount of methanol desorbed as a function of the number of methanol TPD experiments for both a ZnO_x/0.5 ML O/Cu(110) and a 0.5 ML O/Cu(110) surface is the same, and increases with decreasing amounts of θ_{oxygen}/Cu(110). It is surprising, at first, that the amount of desorbed methanol is the same for the two surfaces. If the amount of desorbed methanol was a function only of the oxygen coverage on Cu(110), then we would expect to see one curve offset from the other on the y-axis, with the ZnO_x/O/Cu(110) surface obtaining the maximum more rapidly due to a faster loss of chemisorbed oxygen on Cu(110). Instead, we have overlapping curves for the two surfaces. The offset is within our 20% error bar for methanol desorption area. Hence, it is difficult to say whether the total amount of methanol desorption changes in the presence of ZnO_x islands.

Source for Surface Oxygen

We used O_2 in our studies to produce surface oxygen. Under industrial conditions, surface oxygen is produced from CO_2, either by

$$CO_2 \rightarrow O_{(surface)} + CO$$

or

$$CO_2 + H_2 \rightarrow H_2O + CO \rightarrow O_{(surface)} + CO + 2H_{(surface)}.$$

Hence, we attempted to oxidize the Cu-Zn-O surfaces with CO_2 and H_2O after reduction of the surface with methanol TPD experiments. ZnO_x/Cu(110) surfaces were annealed at 560 K in 1×10^{-4} Torr CO_2 for 10 minutes. There was an increase in the AES spectrum for both the oxygen and carbon peaks due to carbonate formation. After the surface carbonates had been decomposed by heating in vacuum, methanol TPD indicates that the surface has not been oxidized by CO_2. Heating

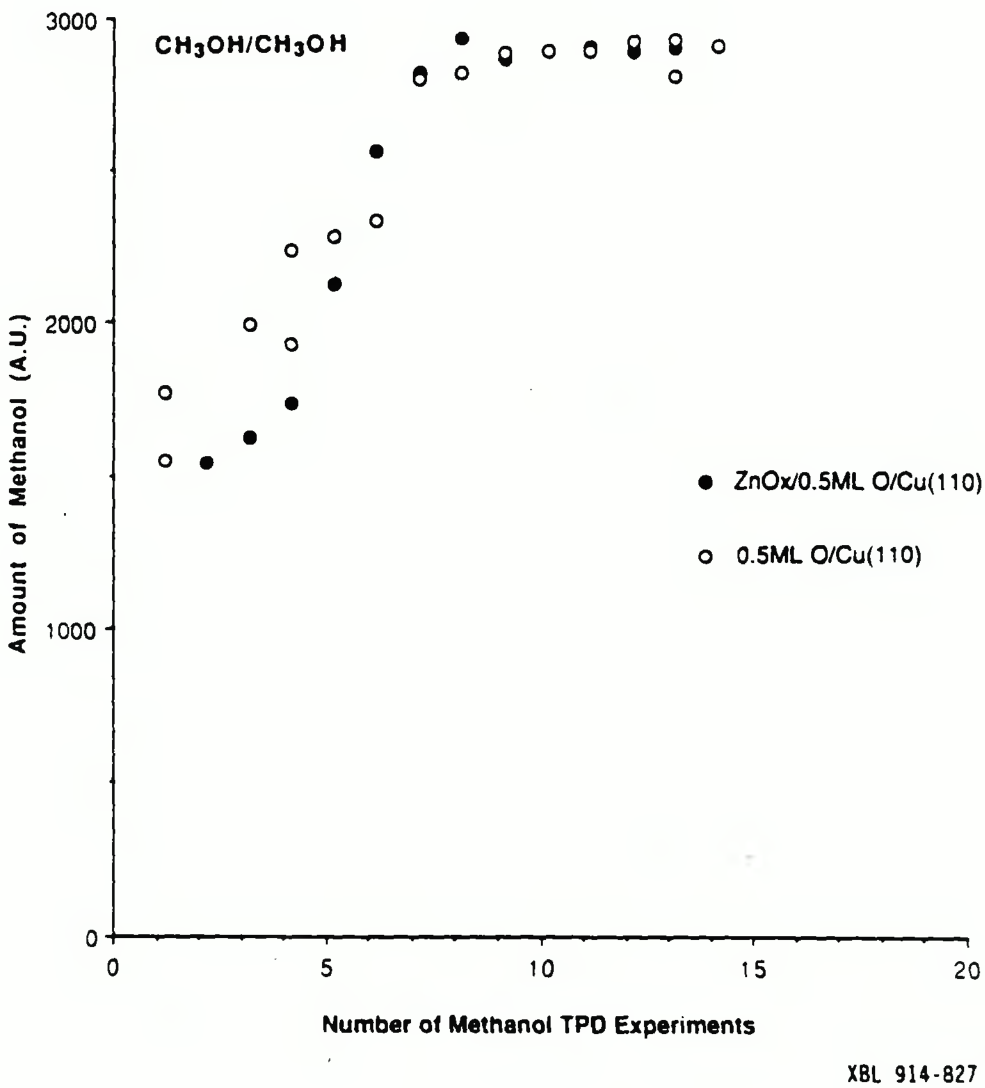

Figure 6.13: Amount of methanol desorbed for each 2.0 L dose of methanol for a ZnO_x/0.5 ML O/Cu(110) surface and a 0.5 ML O/Cu(110) surface as a function of the number of methanol TPD experiments.

the reduced ZnO_x/Cu(110) surface in 1×10^{-8} Torr H_2O at 560 K for 10 minutes produced no change as detected by AES, LEED, and methanol TPD.

We were unable to produce surface oxygen from either CO_2 or H_2O due to our limits to low pressures. It has been shown that under the high pressures used in industry (>20 atm), there is a direct correlation between CO_2/CO feed ratio and the amount of chemisorbed oxygen on the copper surface [4]. Hence, although the source of surface oxygen under industrial conditions is CO_2, we have used O_2 due to the inability of CO_2 to dissociate on ZnO_x/Cu(110) surfaces at low pressures.

6.4 Discussion

Wachs and Madix [5] have shown that $[CO_2]_{formate}$, $[CH_2O]_{methoxy}$, and CH_3OH production from CH_3OH exposure are all affected by pre-adsorbed oxygen on Cu(110). We show in this chapter that for the three-component system of ZnO_x/O/Cu(110), O/Cu(110) affect $[CO_2+CO]_{formate}/CH_3OH$ production on the ZnO_x component as well. In addition to promoting $[CO_2+CO]_{formate}/CH_3OH$ production on the ZnO_x component, the oxygen on the copper component helps to keep zinc oxidized.

By following the decomposition products of CO_2, CO, and CH_2O, we have shown that the three-component system of ZnO_x/O/Cu(110) has a promotional effect on the production of formate species, but not on the production of methoxy species. In addition, the relative ratio of $[CO_2]_{formate}/CH_3OH$ to $[CH_2O]_{methoxy}/CH_3OH$ changes from 1:9 on 0.2-0.3 ML O/Cu(110) to 1:3 on ZnO_x/0.2-0.3 ML O/Cu(110) surfaces, indicating that the three component system has a higher concentration of surface formate. Detailed studies by various investigators [2,15] have shown formate species to be the common and most long-lived intermediate on $Cu/ZnO/Al_2O_3$ catalysts, ZnO catalysts, and polycrystalline copper. They argue that methanol is produced from carbon dioxide and hydrogen reacting to form formate species. These investigators [2], along with others [1], have also found that the more active Cu-Zn-O methanol synthesis catalysts have 30-60% of their copper surface area covered with oxygen after reaction in CO, CO_2, and H_2. Assuming each oxygen atom blocks two copper sites (this is a good approximation in the O/Cu(110) case), these methanol synthesis catalysts are covered with 0.15-0.30 ML of oxygen. We have shown above that the maximum in total formate production ($[CO_2+CO]_{formate}/CH_3OH$ production) on the three-component system occurs when the Cu(110) component contains 0.2-0.3 ML oxygen. Though the maximum in formate production from the addition of the separate components is also 0.2-0.3 ML oxygen on Cu(110), its maximum is only half of the maximum produced in the three-component system. We propose that one of the rôles of oxygen on the copper component is to increase the amount of formate formation. This suggestion is consistent with recent findings that $Cu/ZnAl_2O_4$ catalysts produce 20 times the amount of formate than $ZnAl_2O_4$ catalysts from CO_2+H_2 feed [16]. These $Cu/ZnAl_2O_4$ catalysts were shown to contain chemisorbed oxygen on the copper component. Hence, both the model ZnO_x/O/Cu(110) surfaces and the working $Cu/ZnAl_2O_4$ catalysts show a promotional effect for formate formation with chemisorbed oxygen on the copper component.

We have seen that the other effect of O/Cu(110) is to help keep the ZnO_x component oxidized. This rôle is most likely not a prominent one in the working catalyst as there is bulk ZnO_x to draw surface oxygen from in the industrial catalyst, but this rôle of O/Cu(110) may be important in avoiding Cu-Zn alloy formation which could reduce the active surface area.

6.5 Conclusion

We have shown that the amount of surface oxygen on the Cu(110) part of the catalyst determines the amount of formate produced on the ZnO_x component of the surface as well as the O/Cu(110) component of the surface. The three component system of ZnO_x islands on Cu(110) with 0.2-0.3 ML oxygen on the Cu(110) part produced twice the amount of formate than the maximum reached with the addition of the separate components. In contrast, we saw no promotional effect of the three-component system on methoxy formation. The relative ratio of surface formate to methoxy species increases from 1:9 in the case of 0.2-0.3 ML O/Cu(110) to 1:3 in the case of ZnO_x/0.2-0.3 ML O/Cu(110). In addition to promoting total formate production, the O/Cu(110) helps keep the ZnO_x islands oxidized.

References

1. B. Denise, R.P.A. Sneeden, and O. Cherifi, Applied Catal. 30 (1987) 353.
2. M. Bowker, R.A. Hadden, H. Houghton, J.N.K. Hyland, and K.C. Waugh, J.Catal. 109 (1988) 263.
3. Z.X. Ren, J. Wang, L.J. Jia, and D.S. Lu, Applied Catal. 49 (1989) 83.
4. G.C. Chinchen, M.S. Spencer, K.C. Waugh, and D.A. Whan, J. Chem. Soc. Faraday Trans. I 83 (1987) 2193.
5. I. Wachs and R. Madix, J. Catal. 53 (1978) 208.
6. M. Bowker, H. Houghton, and K.C. Waugh, J. Catal. 84 (1983) 252.
7. D.L. Roberts and G.L. Griffin, J. of Catal. 95 (1985) 617.
8. J.M. Vohs and M.A. Barteau, Surf. Sci. 176 (1986) 91.
9. S. Akhter, W.H. Cheng, K. Lui, and H.H. Kung, Journal of Catal, 85 (1984) 437.
10. W.H. Cheng, S. Akhter, and H.H. Kung, Journal of Catal. 82 (1983) 341.
11. L. Chan and G.L. Griffin, Surf. Sci. 155 (1985) 400.
12. S. Akhter, K. Lui, and H.H. Kung, J. Phys. Chem. 89 (1985) 1958.
13. J.M. Dominquez E., G.W. Simmons, and K. Klier, J. of Molecular Catal. 20 (1983) 369.
14. Sabrina S. Fu and G.A. Somorjai, Surf. Sci. 237 (1990) 87.
15. M. Bowker, H. Houghton, and K.C. Waugh, J. Chem. Soc. Faraday Trans. I 77 (1981) 3023.
16. C. Chauvin, J. Saussey, J.C. Lavalley, H. Idriss, J.P. Hindermann, A. Kiennemann, P. Chaumette, and P. Courty, J. of Catal. 121 (1990) 56.

Appendix A

High Pressure Studies

Throughout this thesis, a number of suggestions have been made concerning the rôle of different copper faces and the rôle of chemisorbed oxygen on the copper component of Cu-Zn-O methanol synthesis catalysts. These suggestions need to be tested under methanol synthesis conditions; high pressure (>20 atm) and 500-570 K.

In order to do this, we attempted high pressure studies in a combined ultra-high vacuum/high pressure (UHV/HP) chamber. The model catalysts were characterized in UHV, and then enclosed in a high pressure cell and heated resistively to reaction temperatures. This approach proved unsuccessful because of the limitations of the existing high pressure apparatus to be tailored to the Cu-Zn-O system. I do believe that is is possible to perform high pressure studies on model copper and Cu-Zn-O catalysts, but not without major changes from the experimental approach I had started with. Below, I discuss the major problems I have encountered while working with this particular catalytic system and some of the possible solutions:

1. In order to resistively heat the sample to 500 K, extremely large currents (100 amps) were required. When such large currents are passed through the sample, then manipulator parts and the high pressure reaction cell and loop are heated, and produce reaction products. Large amounts of current were needed to heat the copper samples due to the low electrical resistivity of copper (1.678 microhm-cm for copper at 293 K) and the high pressures of hydrogen which removed the heat from the copper by thermal conduction. Using resistive heating with 1.0 inch long 20 mil gold support wires, and

10 mil copper foil as the model catalyst, a current of 100 amps was needed in order to reach a sample temperature of 500 K, the point at which methanol production can be detected by gas chromatography. The current required to reach a sample temperature of 500 K could be reduced to 50 amps by using 20 mil gold wires, 0.5 inch long, and copper foil 1.0 mil thick. Clearly, one needs as thick and as short a supporting wire as is experimentally feasible in order to reduce the current needed to heat the sample. However, it became difficult to spot-weld copper to gold once the copper foil was thinner than 1.0 mil and the gold support wires were thicker than 20 mil. Copper support wires at 0.5 inch was as short as experimentally feasible to mount a sample 0.4 inch long. In spite of the reduction in current to 50 amps, manipulator parts and the high pressure loop and cell still produced reaction products on the order of those produced by the model copper catalyst; a clearly undesirable situation.

2. The second problem is that of low surface area and reactivity of the copper surface compared to the high surface area and reactivity of the reaction cell. The stainless steel cell and loop has a total surface area of 250 cm^2. The model catalysts have a surface area $\sim$1 cm^2 and consist of one of the least reactive of metals - copper. In order to minimize the background activity, water cooling lines around the high pressure cell were installed. Cooling the high pressure cell with ice water reduced its activity, but it was not possible to reduce the background activity to an order in magnitude less than that of the sample.

It is evident that resistive heating of copper under high pressures is inappropriate. A more suitable method of heating under these circumstances would be using microwaves. The microwaves would heat up the reactant gases of CO, CO_2, and H_2, which in turn would heat up the copper sample. This method of heating the 1 cm^2 model catalyst should reduce the temperature of the manipulator during reaction. To further reduce reaction on the manipulator parts, the manipulator should be coated with approximately 1 mil gold film.

In addition to reducing the temperature of the manipulator parts during reaction, microwave heating will also enable the use of copper samples thicker than 1.0 mil. This is an essential prerequisite to working with copper single crystals, as it is difficult to polish single crystals thinner than ~10 mil.

Although the use of microwaves should reduce the heating up of manipulator parts, the high partial pressures of hydrogen under reaction conditions will most likely carry significant amounts of heat to the manipulator, and the high pressure cell and loop. In order to reduce the activity of the reaction cell and loop, it is best to use an inert substrate such as glass. I believe that with a glass reactor and the sample heated with microwaves, the formation of methanol under high pressures from small area copper samples can be examined. This will enable the elucidation of the effect of copper structure and ZnO_x overlayers on methanol production under industrial conditions.

Appendix B

Cu-Zn-O Phase Diagram

In this thesis, we examined Cu-Zn-O interaction on the surface of copper single crystals. For comparison to bulk studies, I have reproduced a copy of a Cu-Zn-O phase diagram below. This phase diagram was obtained from Dr. Church at the International Copper Association.

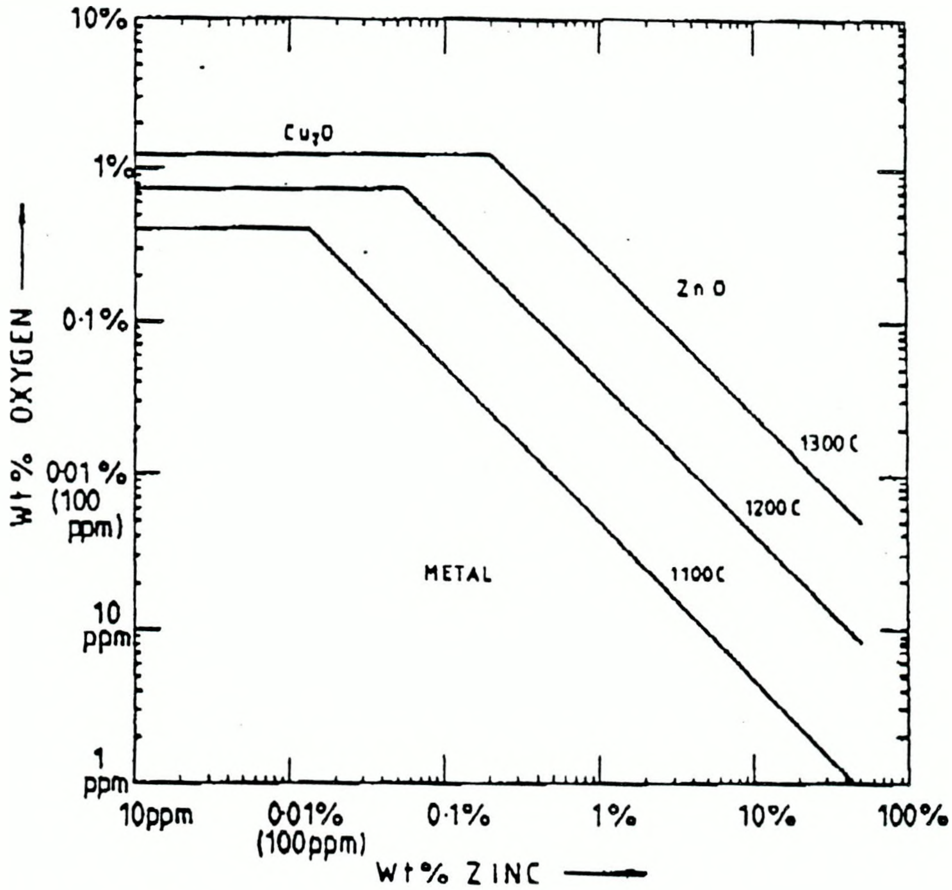

1.20 Solubility limits, Cu-Zn-O.

LAWRENCE BERKELEY LABORATORY
CENTER FOR ADVANCED MATERIALS
1 CYCLOTRON ROAD
BERKELEY, CALIFORNIA 94720